UNIVERSIDADE D
COIMBRA

Bruno Alexandre Coutinho dos Santos

Interfacing Silicon Chips with Printed Inks for Ultra-Stretchable Circuits

Dissertação no âmbito do Mestrado Integrado em Engenharia Biomédica orientada pelo Professor Doutor Mahmoud Tavakoli e apresentada ao Departamento de Física da Faculdade de Ciências e Tecnologia da Universidade de Coimbra.

Novembro de 2020

FACULDADE DE CIÊNCIAS E TECNOLOGIA
UNIVERSIDADE D COIMBRA

Bruno Alexandre Coutinho dos Santos

Interfacing Silicon Chips with Printed Inks for Ultra-Stretchable Circuits

Thesis submitted to the
University of Coimbra for the degree of
Master in Biomedical Engineering

Supervisors:
Prof. Dr. Mahmoud Tavakoli

Coimbra, 2020

This work was performed in collaboration with the project “Add.Additive” (Reference: 59563), co-financed by the European Regional Development Fund (ERDF), through the “Programa Operacional Competitividade e Internacionalizacão” (POCI-01-0247-FEDER-024533). Funding also came from the CMU-Portugal project WoW (Reference: 45913) which had support of European Regional Development Fund (ERDF) and the Portuguese State through Portugal2020 and COMPETE 2020, and the project ”Dermotronics” (Reference: 31784), funded by ”Fundos Europeus Estruturais e de Investimento” (FEEI), through the ”Programa Operacional Regional do Centro”.

Esta cópia da tese é fornecida na condição de que quem a consulta reconhece que os direitos de autor são pertença do autor da tese e que nenhuma citação ou informação obtida a partir dela pode ser publicada sem a referência apropriada.

This copy of the thesis has been supplied on condition that anyone who consults it is understood to recognize that its copyright rests with its author and that no quotation from the thesis and no information derived from it may be published without proper acknowledgement.

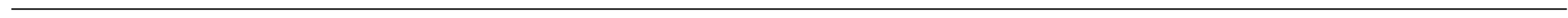

Agradecimentos

Primeiro, gostaria de agradecer ao meu orientador, Mahmoud Tavakoli, pela oportunidade de trabalhar numa área tão interessante e revolucionária, e por me proporcionar um ano cheio de crescimento, aprendizagem, e conselhos que certamente levarei para o futuro.

Agradeço também toda a equipa de laboratório do ISR por me fazer sentir confortável e integrado desde o primeiro dia. A vossa ajuda e colaboração foram extremamente importantes, não só para o desenvolvimento deste projeto, mas também para o meu ânimo e motivação. Em especial, gostaria de agradecer ao Pedro Lopes o apoio que me dedicou durante este ano e que certamente não irei esquecer.

À Carreiró, Inês, e Patrícia, um obrigado por todos os momentos que passámos durante estes 5 anos e que com certeza serão recriados durante muitos mais. Ao Zé, um gigante obrigado por ser a pessoa que é e por me ouvir, apoiar e motivar nos momentos mais difíceis e desesperantes. Agradeço também aos meus pais todo o carinho e apoio incondicional, e por me ensinarem a ser ambicioso e a não descansar até cumprir os meus objetivos. Sem vocês nada disto seria possível.

O último obrigado vai para Coimbra, por todas as amizades, tradições e oportunidades que tanto me fizeram crescer, e que tanta saudade vão deixar!

Resumo

Circuitos eletrónicos convencionais são compostos por materiais rígidos e quebradiços. No entanto, orgãos biológicos são fundamentalmente moles (*soft*). Este desfasamento evidente despertou interesse no campo da electrónica deformável, que se foca no desenvolvimento de materiais e métodos de fabrico para circuitos cujas propriedades mecânicas se assemelham às dos tecidos biológicos. Estes esforços têm sido direcionados para a introdução de novos métodos e técnicas de fabrico de formas deformáveis de elétrodos, conectores e sensores. Porém, a funcionalidade de circuitos deformáveis ainda está dependente da utilização de tecnologias de estado sólido (SST), tais como díodos emissores de luz (LEDs) e circuitos integrados (ICs), para aquisição, processamento e comunicação de dados.

A integração de SST em circuitos extensíveis introduz uma incompatibilidade mecânica no sistema, o que leva à falha prematura e/ou perda de funcionalidade do circuito quando é aplicada uma deformação. Apesar deste ser o maior obstáculo contra o fabrico escalável de circuitos extensíveis, poucos esforços têm sido direcionados para o combater de forma eficiente, já que as soluções apresentadas são geralmente complexas e trabalhosas.

Este trabalho propõe um novo método de interface de componentes rígidos com circuitos deformáveis que lhes permite resistir a um distensão máxima recorde de >600%, 3× superior a qualquer outra técnica publicada. Os circuitos são fabricados através de deposição de uma tinta bifásica inovadora composta por Ag-EGaIn-SIS sobre um copolímero de bloco de estireno-isopreno (SIS). Em seguida, *microchips* SMD são colocados sobre as conexões utilizando uma máquina *pick and place*. Uma técnica inovadora de exposição de vapor de tolueno é depois utilizada para causar uma transição duro-mole tanto no substrato de SIS, como na tinta composta por SIS. O *microchip* consegue então penetrar e aderir à tinta e a estrutura do componente é envolvida na íntegra pelo substrato adesivo. Além de possibilitar a integração de *microchips*, o tratamento de vapor de tolueno melhora a percolação do

compósito condutivo, o que resulta num aumento de 2× na condutividade das pistas do circuito. Exposição ao vapor permite ainda eliminar defeitos como micro-fendas presentes no substrato, possibilitando assim atingir distensões superiores. Para caracterizar a técnica analisou-se um conjunto de parâmetros como a tolerância máxima de distensão e resistência à fadiga. Recorreu-se ainda à microscopia eletrónica de varredura e microscopia ótica para investigar e compreender os mecanismos subjacentes à integração dos components rígidos. Além destas vantagens face ao estado de arte, o método descrito é consideravelmente mais simples que outras técnicas previamente publicadas, constituindo assim um passo importante no fabrico automático e escalável de circuitos deformáveis com integração de *microchips*.

O método foi desenvolvido e demonstrado com sucesso através de um *case-study* que consistiu em desenvolver um circuito extensível para medição da temperatura da pele. Este circuito foi depois transferido para um tecido de modo a formar um máscara *wearable* para medição de temperatura do utilizador.

Palavras-Chave: Eletrónica deformável, Interface de componentes rígidos, Tratamento de vapor de tolueno, Metal líquido, Copolímeros de bloco de estireno-isopreno.

Abstract

Conventional electronic systems are composed of rigid and brittle materials. Biological organs however are mostly made of soft materials. This conspicuous mismatch sparked interest in the field of stretchable electronics, which focuses on materials and methods for fabrication of thin, soft, and stretchable circuits that can interface a host surface, for instance the human epidermis, and keep their functionality despite the dynamic morphology of the host system. Such efforts mostly focused on the introduction of materials and methods for patterning of stretchable electrodes, interconnects, and sensors. However, the ultimate functionality of these systems remains dependent of solid-state technology (SST), from simple light emitting diodes (LEDs), to packaged integrated circuits (ICs) for data acquisition, processing and communication.

Integration of SST into these circuits induces a drastic mechanical mismatch, resulting in premature failure and/or loss of the circuit functionality when strain is applied to the systems. Even though this problem is the main bottleneck against scalable fabrication of stretchable electronics, very few works tried to address it. In addition, the previously presented solutions are complex, labor-intensive and require many fabrication steps.

In this work, we proposed a novel method for interfacing SST components into stretchable circuits that can withstand a record-breaking maximum strain tolerance of >600% of strain, 3× higher than any previously reported technique. Circuits are fabricated by printing a novel biphasic Ag-EGaIn-SIS ink over a Styrene-isoprene block copolymers (SIS) substrate. Then, SMD microchips are placed over the interconnects using a pick and place machine. This is followed by an innovative technique of toluene vapor exposure that provokes a hard-soft transition both in the SIS substrate, and in the SIS-containing ink. Then, the microchip penetrates and adheres to the ink, and the body of the component gets surrounded by the adhesive substrate entirely on all of its perimeter. In addition to the microchip integration, the vapor

treatment improves the percolation of the conductive composite, resulting in a 2× increment in the conductivity of the printed traces. Furthermore, vapor exposure eliminates defects and micro-cracks present in the substrate, allowing for a higher strain tolerance. To characterize the technique, we analyzed a set of parameters, including maximum strain tolerance and fatigue tolerance. SEM and optical microscopy were as well used to inspect the underlying mechanisms that lead to the integration of the rigid components. In addition to these advantages over state-of-the-art, this method is considerably simpler than previously reported methods, thus paving an important step toward scalable and automated fabrication of microchip-integrated stretchable circuits.

An example of application was demonstrated through fabrication of a microchip-integrated stretchable circuit that could measure the skin temperature, or that can be transferred to a textile mask for acquisition and display of the temperature.

Keywords: Stretchable printed electronics, Microchip interfacing, Toluene vapor exposure, Eutectic gallium indium liquid metal, Styrene-isoprene block copolymers

List of Figures

1.1 Technology readiness chart from proof of concept to maturity and market introduction. 2
1.2 Application of electronic artificial skin in biomedical engineering. . . . 5
1.3 Applications of stretchable systems for implanted systems. 6
1.4 Examples of fully stretchable electronic components. 7

2.1 Applications of PDMS and Ecoflex showcasing their excellent properties like conformability and stretchability. 12
2.2 Out-of-plane and in-plane deterministic structures. 14
2.3 Liquid metals - characteristics and features. 16
2.4 Stretchable conductive composites. Graphic of typical behavior of the conductivity of a stretchable composite and schematics of the network of the material. 17
2.5 Ashby graphic with comparisons of different published works – metallic films, liquid metals, conductive composites – in terms of their maximum conductivity and strain at their breaking point. 17
2.6 zPDMS Conductive Film - Schematics and photos of the interconnects. 18
2.7 Patterning techniques for liquid metal interconnects - current and emerging methods. 21
2.8 Direct integration techniques - Ball-stitch bonding. 23
2.9 Indirect integration techniques - FPCB embedded in PDMS. 25
2.10 Indirect integration techniques - Multi-layer circuit with LM interconnects, laser-ablated filled VIAs and FPCBs embedded in PDMS. . 26
2.11 Indirect integration techniques - zPDMS conductive film. 27
2.12 Direct integration techniques - Dual Concentric Islands 28
2.13 Direct integration techniques - Interconnect Micropatterning and Flip-Chip 29
2.14 Direct integration techniques - CMOS/Microfluidic hybrid microsystem. 31
2.15 Direct integration techniques - "Gull Wing" design 32

2.16 Direct integration techniques - HCl Vapor. 33

3.1 Examples of equipment used throughout the development of the dissertation. 38
3.2 Side-view schematics of the integration process through toluene vapor exposure. 41
3.3 Side-view schematics of the encapsulation process using PDMS as the encasing substrate. 42
3.4 Fabrication flow of the stretchable circuit with integrated microelectronics. 43
3.5 Steps for the fabrication of the stretchable circuit with rigid components integrated through the toluene vapor method. 44
3.6 Equipment used in the electromechanical characterization tests. . . . 46
3.7 Preparation of the SIS dog-bone samples for tensile stretching tests. . 46
3.8 Schematics of the dob-bone and circuit track used in the electromechanical characterization tests and corresponding measurement details. 47
3.9 Samples during the cyclic loading tests. 48
3.10 Sample used in SEM analysis for the interface characterization. . . . 50
3.11 Schematics of the circuit track used in the characterization of the printed circuit and corresponding measurements. 51
3.12 Preparation of the ink samples for SEM analysis. 52

4.1 Results of the uniaxial tension test performed at a constant rate of 100 mm/min for each individual sample. 56
4.2 Tears appear on the samples during the uniaxial tensile loading tests. 57
4.3 Maximum stretchability comparison between the results obtained with the developed method and other state-of-the-art techniques. 58
4.4 Cyclic loading test carried out with a 10 Ω resistor, interfaced through toluene vapor. 59
4.5 Representation of electrical resistance variation over the displacement cycles. 60
4.6 Top pictures of the process for integration of a surface-mount 49.9k in a sample. 61
4.7 Side-view pictures of a surface-mount 49.9k integrated in a stretchable circuit. 62
4.8 Bottom pictures of a sample with a surface-mount 49.9k resistor integrated in a stretchable circuit. 63

4.9 Top images of the integration site after an extreme toluene treatment. 64
4.10 Resistance measurements of the samples tested in the electrical characterization. 65
4.11 Cross-section schematics showing the rearrangement of the composite's components during the toluene treatment. 67
4.12 Images of a thin layer of ink deposited through spray coating, before and after toluene vapor treatment. 68
4.13 Images of a layer of ink deposited through stencil printing, before and after toluene vapor treatment. 69
4.14 Cross-section images of a layer of ink deposited through stencil printing, before and after toluene vapor treatment. 70
4.15 Conductivity calculations from previously determined resistances. . . 71
4.16 Cyclic loading test of 5 cycles without a rigid component. 72
4.17 Results of the uniaxial tension test performed to treated and untreated samples. 73
4.18 Images of a SIS layer deposited using the thin film applicator, before and after toluene vapor treatment. 75

5.1 Machines used in the fabrication process of the stretchable temperature patch. 78
5.2 The circuit can withstand some strain and can also be deformed without loss of conductivity and function. 79
5.3 Stretchable temperature patch placed over the forearm. 79
5.4 Side-view schematics of the transference process to the cloth mask through the toluene vapor treatment. 80
5.5 Mask with attached temperature system. 80

A.1 Pictures of latex substrate after toluene treatment. 90
A.2 Substrate samples before and after toluene treatment. 91

Acronyms

SST Solid State Technology

LED Light Emitting Diode

IC Integrated Circuit

SMD Surface-Mount Device

SMT Surface-Mount Technology

EMG Electromyography

ECG Electrocardiography

EEG Electroencephalography

PDMS Polydimethylsiloxane

sEMG Surface Electromyography

SNR Signal-to-Noise Ratio

AgNW Silver Nanowires

EES Epidermal Electronics System

STS Stretchable Temperature Sensor

SPS Stretchable Pressure Sensor

PLED Polymer LED

SEM Scanning Electron Microscope

DNTT Dinaphtho[2,3-b:2',3'-f]thieno[3,2-b]-thiophene

SIS Polystyrene-block-polyisoprene-block-polystyrene

EGaIn Eutectic Gallium-Indium

OPS Out-of-Plane Structures

IPS In-Plane Structures

LM Liquid Metal

PCB Printed Circuit Board

FPCB Flexible Printed Circuit Board

IC Integrated Circuit

CMOS Complementary metal-oxide-semiconductor

NMOS N-type Metal-oxide-semiconductor

PVC Polyvinyl Chloride

PMMA Poly(methyl methacrylate)

PI Polyimide

SEM Scanning Electron Microscopy

Contents

List of Figures xv

1 Introduction **1**
1.1 Proof-of-Concept Devices . . . 3
1.2 Motivation . . . 7
1.3 Goals . . . 8
1.4 Thesis Overview and Contributions . . . 8

2 State of the Art **11**
2.1 Materials . . . 11
2.1.1 Elastic Polymers as Substrates . . . 11
2.1.2 Conductive Interconnects . . . 13
2.2 Fabrication Methods . . . 19
2.2.1 Fabrication of Elastic Polymers as Substrates . . . 19
2.2.2 Patterning Techniques - Liquid Metals . . . 19
2.3 Integration Methods . . . 22
2.3.1 Indirect Integration . . . 23
2.3.2 Direct Integration . . . 27
2.3.3 Progress Over State-of-the-Art . . . 34

3 Materials and Methods **35**
3.1 Materials and Equipment . . . 35
3.2 Novel Interfacing Method . . . 39
3.2.1 Film Preparation . . . 39
3.2.2 Printed Circuit Fabrication . . . 39
3.2.3 Toluene Vapor Treatment . . . 40
3.2.4 Encapsulation . . . 41
3.3 Interface Analysis . . . 45
3.3.1 Electromechanical Characterization . . . 45

a) Maximum Stretchability Tests 47
b) Cyclic Loading Tests 47
3.3.2 Interface Microscopy 49
3.4 Printed Circuit Characterization 50
3.4.1 Improvement of Electrical Conductivity After Treatment . . . 50
3.4.2 Improvement of Strain Tolerance of the Stretchable Circuit After Treatment 53

4 Results 55
4.1 Interface Analysis 55
4.1.1 Electromechanical Characterization 55
a) Maximum Stretchability Tests 55
b) Cyclic Loading Tests 58
4.2 Interface Microscopy 61
4.3 Printed Circuit Characterization 65
4.3.1 Improvement of Electrical Conductivity After Treatment . . . 65
4.3.2 Improvement of Strain Tolerance of the Stretchable Circuit After Treatment 73

5 Case Studies 77
5.1 Stretchable Temperature Patch 77

6 Conclusions 83
6.1 Limitations and Future Work 84

Appendices 87
A Substrate Choice 89

Bibliography 93

1

Introduction

Biological systems like the human skin and organs are soft and irregularly-shaped, while conventional electronics are made of materials that are fundamentally rigid, hard and bulky [1]. This mismatch in properties between both structures leads to a poor integration of conventional electronics in biological systems, thus hindering their performance in the field of wearable devices [1, 2].

This problem sparked interest in the development of devices that could fully conform to irregular structures like the human organs and skin and maintain their performance during mechanical deformations, such as bending, stretching and twisting [3]. Hence, over the last few decades, constant progress in materials and fabrication techniques have enabled stretchable electronics to cross over from science-fiction to reality, with the field quickly becoming an emerging area of biomedical engineering due to its potential medical value.

Stretchable circuits are composed of mechanically soft and flexible materials, thus allowing the overall system to remain electrically functional while strained and also to return to its original state soon after the external load is removed [4]. This endows these technologies with the unique ability of matching the compliance, elasticity, and density of the human tissue [4]. Therefore, systems built with stretchable electronics will be more robust overall and will provide more sensitive recordings of human motions and physiological signals [3, 4].

In addition to being of great value for biomedical applications, soft and stretchable circuits are versatile enough to be employed in several different fields [5]. These materials offer the foundation for flexible devices involved in energy conversion and storage like stretchable solar cells [6], supercapactiors [7], batteries [8], and also stretchable strain sensors [9], actuators [10], and even soft display screens [11], opening up new possibilities in various fields, such as energy, robotics, defense, and multimedia.

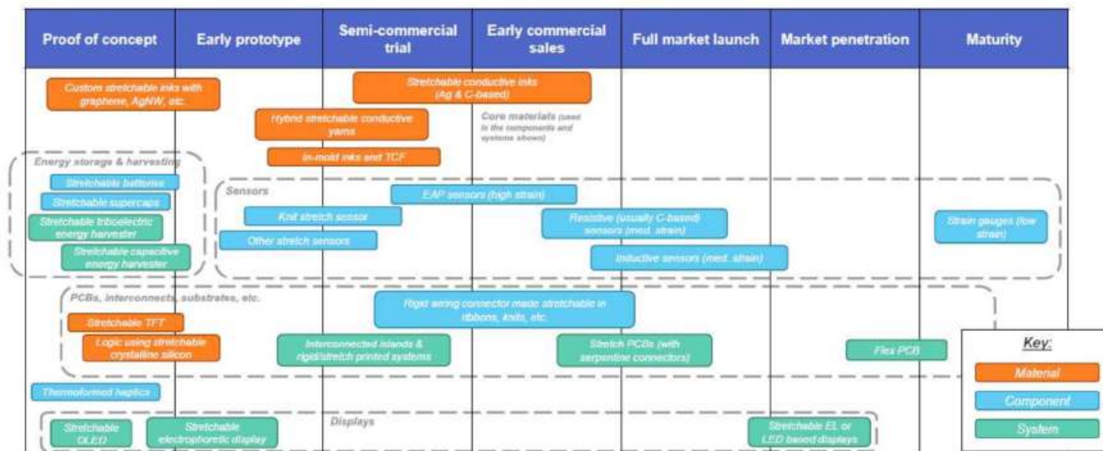

Figure 1.1: Technology readiness chart from proof of concept to maturity and market introduction (from [12]).

Stretchable electronics represent a thriving area that is currently delivering strong value in multiple applications, at times as an enabling technology [12]. It can be seen in Figure 1.1 that strain gauges are already fully commercial nowadays with some other technologies nearing market launch (e.g. inductive and resistive sensors). Others, like stretchable batteries and energy harvesters are still in lab development and are expected to remain in this early stage for the next 10 years.

The high attention and demand for stretchable electronics are expected to create a surge in this market from a small base today to around $500 million in 2029 [12]. In the healthcare industry, wearable devices are emerging as very powerful systems that have potentially transformative impact, with monitoring, diagnostics and prediction of certain medical conditions being some of the main applications of focus in the area [13].

1.1 Proof-of-Concept Devices

In recent years, the rapid evolution of materials and fabrication techniques has led to significant progress in the development of new proof-of-concept stretchable wearable devices in the biomedical field. This constant development throughout the last decades has granted flexible electronics the potential to achieve widespread use in the healthcare industry.

Flexible biosensors capable of detecting biological parameters like pH [14] and glucose [15] have been successfully designed and tested. Stretchable electrode patches that collect electro-physiological data, such as electroencephalograms (EEG) [16], electrocardiograms (ECG) [17], and electromyograms (EMG) [18], are also among the applications of wearable electronics. In fact, rapidly deployable and disposable wearable patches for measuring physiological data have been developed by Leal and colleagues [13]. In order to achieve this, the team integrated hydrogel electrodes with AgInGa interconnects and an Ag_2O-Zn battery (Figure 1.2a,b). The device was functional in the collection of EMG data and had an incorporated stretchable battery with an energy autonomy of nearly 5 days.

Sensors designed to measure physical parameters like the strain [19], proximity [20], and pressure [21] on the human body have also been developed. Stretchable electronics, like the prototype reported by Yan *et al.* [22], can also be used to measure the body temperature. The team built an innovative temperature sensor based on conductive AgNW electrodes and a resistive graphene detection channel, exhibited in Figure 1.2c,d. This device was tested to measure temperatures of up to 100°C and it was able to maintain its functionality in the 0 - 50% strain range (Figure 1.2e). Temperature sensing might even be employed on some devices in order to achieve more complex tasks. Hattori Y. and colleagues [23] designed an epidermal electronics system (EES) that is capable of producing real-time records of the temperature and thermal conductivity of skin tissue to achieve precise monitoring of cutaneous wound healing in a clinical setting. The developed system can measure and map the skin temperature with an accuracy comparable to that of a high-end infra-red camera. This allows for capturing the inflammation phase of the healing process. Furthermore, the equipment is able to determine the thermal conductivity of the wound site which is an aspect that strongly correlates to the hydration state, important in wound care. The prototype showed negligible temperature reading changes when elongated to 15% of its size.

Some more advanced projects can likewise benefit from the incorporation of soft electronic systems. A complex equipment consisting of a soft prosthetic hand with an electronic skin embedded on its digits has recently been achieved by Tavakoli and colleagues [24], allowing for an increased sense of touch and a smoother operation of the equipment by the amputee (Figure 1.2f,g). Because of its enhanced functions and high performance, smart artificial skin as a multifunctional sensing platform (Figure 1.2h) has been increasingly more used in the developing fields of smart prosthetics [5, 25]. Another example is the recently developed e-skin composed of tattoo-like ultrathin film electronics which has been demonstrated to perform well in health monitoring tasks [26].

In addition, flexible and stretchable electronics can also be designed to integrate seamlessly with dynamic and soft biological systems, such as organ-machine interfaces [3]. Power-harvesting throughout the macroscale displacement cycles associated with natural movements of organs like the heart and lungs (Figure 1.3a,b) has already been achieved, opening up an opportunity for batteryless implantable biomedical devices (e.g. pacemakers, neural stimulators) [27].

Applications of soft materials in health have become increasingly more advanced and complex with one research team developing soft interfaces that mimic the shape and the mechanical behaviour of the dura mater [28]. The implant (named e-dura) is able to deliver electrochemical spinal modulation that reportedly restored locomotion after paralyzing spinal cord injuries (in lab mice). This application of the device is illustrated in Figure 1.3a and the equipment can be seen in Figure 1.3b.

From the cases presented, it is clear that stretchable electronics are capable of endless application on the biomedical field. Because the field is still relatively recent, it is expected that the functionalities of these devices become even more powerful in the near future with the development of new materials and fabrication techniques.

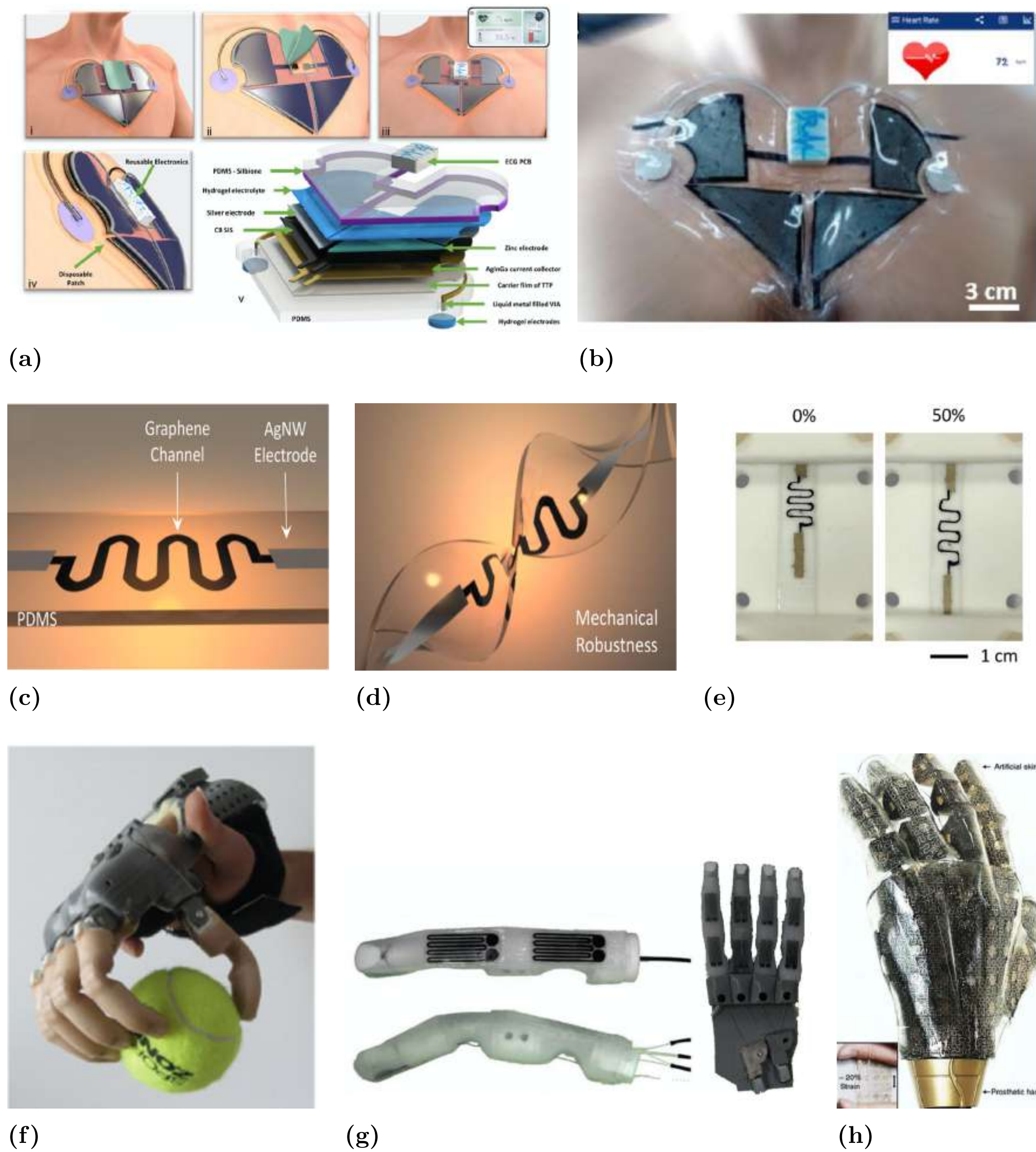

Figure 1.2: Application of electronic artificial skin in biomedical engineering. (a) Disposable patch with integrated Ag_2O-Zn battery, hydrogel electrodes, and electrical interconnects. Adapted from [13]. (c,d) Temperature sensor based on conductive AgNW electrodes and a resistive graphene detection channel. Schematic representations of the stretchable graphene thermistor at relaxed and twisted (360°) states. (e) Images of the device at 0% and 50% strain. Adapted from [23]. (f,g) Soft prosthetic hand with integrated electronic skin. Adapted from [24]. (h) Smart artificial skin integrating a strain sensor, STS, SPS, humidity sensor, electroresistive heater, and tensile multiple electrode arrays. Adapted from [25].

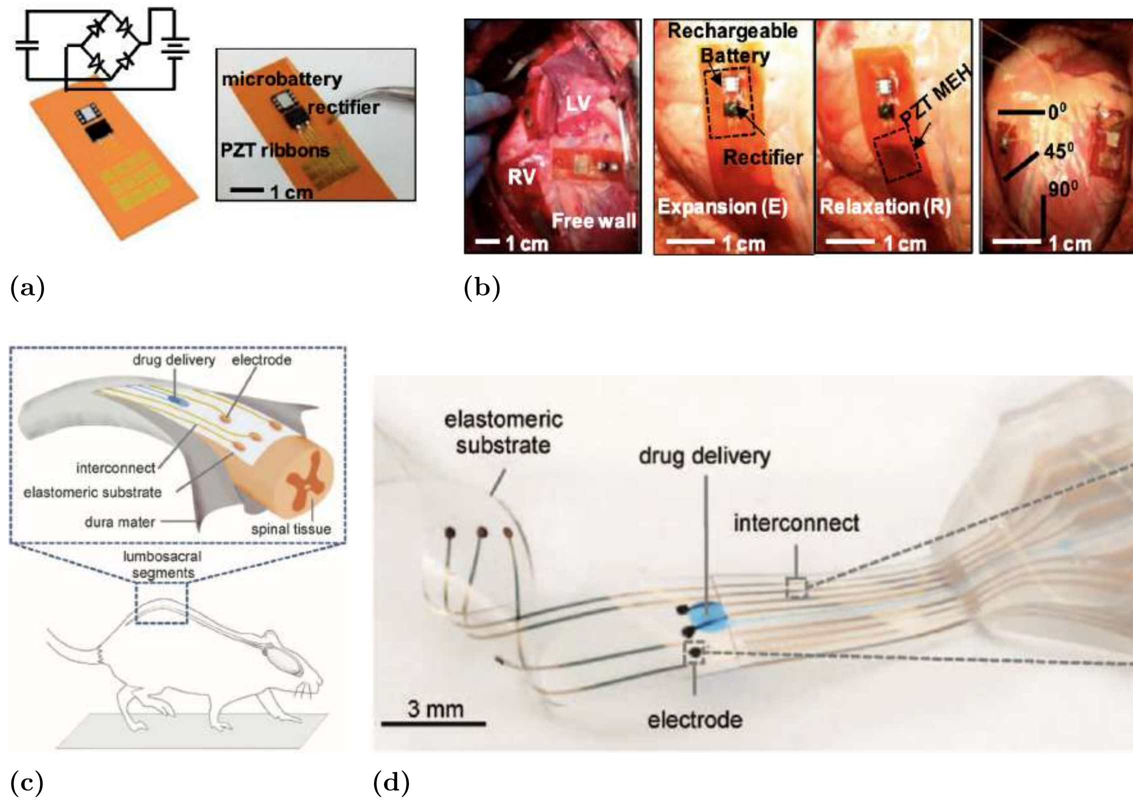

(a) (b) (c) (d)

Figure 1.3: Applications of stretchable systems for implanted systems. (a) Illustration of the piezoelectric mechanical energy harvester used in the collection of energy from the natural movements of organs. (b) Operation of the device in the collection of energy on the walls of a bovine heart. Adapted from [27]. (c) Illustration of the localization of the e-dura implant in the spinal subdural space of mice. (d) Optical image of the implant used. Adapted from [28].

1.2 Motivation

In the last decade, rapid advances were made in materials and methods for fabrication of stretchable circuits, including interconnects, sensors, and antennas. Nevertheless, the ultimate functionality of these circuits is still dependent on the use of silicon-chips. In fact, most applications that were described before benefit from rigid-soft interfacing.

Nowadays, it is possible to produce fully stretchable interconnects, electrodes and LEDs [29]. Even though the first steps have been taken in order to fabricate flexible components like transistors [30] and capacitors [31], these technologies are still no match for their solid-state counterparts in terms of reliability, speed, computational performance and ease of fabrication. Furthermore, many electronic components like microprocessors and resistors are still not available in flexible form.

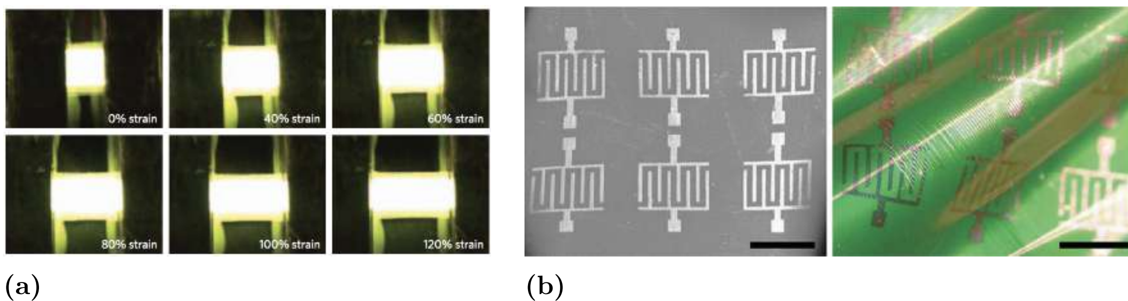

Figure 1.4: Examples of fully stretchable electronic components. (a) Stretchable electroluminescent polymer LED (PLED) with AgNW-PUA electrodes under operation from 0%-120% strain (from [29]). (b) SEM (left) and 3D optical microscope images of stretchable transistors, achieved by combining Au electrodes with DNTT and organosilicone dielectric (from [30]).

Even though the integration of solid-state microelectronic components in soft electronics is still unavoidable, methods for interfacing these rigid microchips into stretchable circuits are still underdeveloped. This is odd given that integration of the such components is usually the motive behind premature failure and/or loss of functionality of devices [32].

Due to the fundamental differences in materials used in stretchable electronics and traditional PCBs, current methods (such as soldering techniques) cannot be used to integrate microchips into stretchable circuits.

Furthermore, the integration of two materials with different mechanical properties results in a region of mechanical stress accumulation. Therefore, when the system

is under strain, this soft-rigid interface is often the starting point of failure of the whole structure.

Creating a reliable interface between packaged integrated circuits (ICs) and soft circuits is probably the biggest challenge in the wearable electronics field and, even though efforts towards developing fabrication methods for stretchable interconnects keep on increasing, the problem of microchip interfacing is rarely addressed by researchers.

1.3 Goals

The main objective of this dissertation is to develop a fabrication technique that allows for a simple integration of silicon chips, including SMD components, into stretchable circuits. The developed method should create reliable interfaces that are able to withstand considerable amounts of strain before failure. In addition, the proposed technique should also be durable, easy to replicate, fast to apply and scalable in the industry.

The developed technique will be electrically and mechanically characterized, and its potential for widespread application in the stretchable electronics field will be assessed.

1.4 Thesis Overview and Contributions

The ideal integration method should respect the different properties described in the last section. However, most of these requirements are not easy to mutually achieve and a technique that combines them is still yet to be reported.

This work presents, for the first time, a rigid-soft interfacing technique for integration of rigid microchips in stretchable circuits that can withstand over 550% uniaxial strain, which is clearly above the results of previously reported techniques ($\leq 200\%$ strain). Furthermore, the technique is extremely easy and fast to reproduce and works with microchips of different sizes and architectures, thus making the method ideal for scalable industrial production.

The proposed technique, based on exposure of the printed circuit to a solvent vapor, not only allows for the efficient "soldering" of rigid components, but it is also able to smooth the polymeric substrate used and improve the electromechanical properties of the overall circuit.

In addition to a comprehensive electromechanical characterization of the interfacing method, microscopy and SEM (Scanning Electron Microscopy) analysis were performed in order to discover its underlying mechanisms of action. Besides, it is also demonstrated that this method improves the percolation of the metallic fillers of the conductive ink, therefore increasing its electrical conductivity and strain tolerance, even prior to integration of SMD chips.

The rest of the dissertation is organized in the following way: in Chapter 2 a brief literature review of the materials used for fabrication of stretchable circuits and interfacing techniques will be provided; the proposed method will be presented and explained in Chapter 3, as well as all the techniques used in its characterization; Chapter 4 will concern the results of characterization tests; a case-study will be presented in Chapter 5; and lastly, the final conclusions and limitations will be addressed in Chapter 6.

2

State of the Art

Typically, electronic modules comprise of a stretchable polymeric substrate embedded with conductive stretchable interconnects. In order to achieve the desired properties of the electronic device, the choice of substrate and conductive interconnects is fundamental.

In this chapter, previously reported materials and methods for fabrication of stretchable electronics are investigated and discussed. This includes:

1. Materials typically used for implementation of stretchable electronics, including elastic polymers that are used as substrates and sealing layers; and stretchable conductive materials, such as thin metal films, conductive composites, and liquid metals;
2. Methods for printing/patterning liquid metal in the fabrication of stretchable circuits;
3. Previously reported techniques for integration of silicon chips into stretchable circuits.

2.1 Materials

2.1.1 Elastic Polymers as Substrates

Materials with intrinsic stretchability like elastomers are usually the choice for substrates in stretchable electronics as the low stiffness and the elastic behavior of these polymers enables a great conformation to biological systems.

Due to its attractive characteristics, the most popular material for the fabrication of stretchable electronics is PDMS (Figure 2.1a). This elastomer is chemically inert, stable over a wide range of temperatures, optically transparent, and has variable and well-researched mechanical properties [33]. On top of that, its commercial

availability makes it a very convenient material [34]. The Young Modulus of PDMS typically ranges from 0.1 to 3 MPa which makes this material highly flexible and easily stretched by mechanical forces while its volume stays relatively constant [4, 35].

Natural rubber (latex) also makes up a great substrate for stretchable systems as it exhibits high strength with outstanding resistance to fatigue and high resistance to cutting and tearing [36]. As opposed to PDMS, this material is not generally inert which enables it to adhere better to some conductive inks. The Young modulus of latex is relatively low, ranging from 10-100 MPa [35].

Other options have also been explored like Ecoflex rubbers (Figure 2.1b) which are commercial platinum-catalyzed silicones. This material is very soft, flexible and is safe to the skin, on top of being resistant to stretching and tearing [37]. Previously conducted tests have shown that this material can withstand strains of up to 800%, which is adequate for application in stretchable electronics [38].

Other elastomers have also been employed when manufacturing flexible electronic systems such as polyurethane (PU), styrene butadiene rubber (SBR) and ethylene-propylene-diene monomer (EPDM), which can all reversibly endure high deformations (200%) [39].

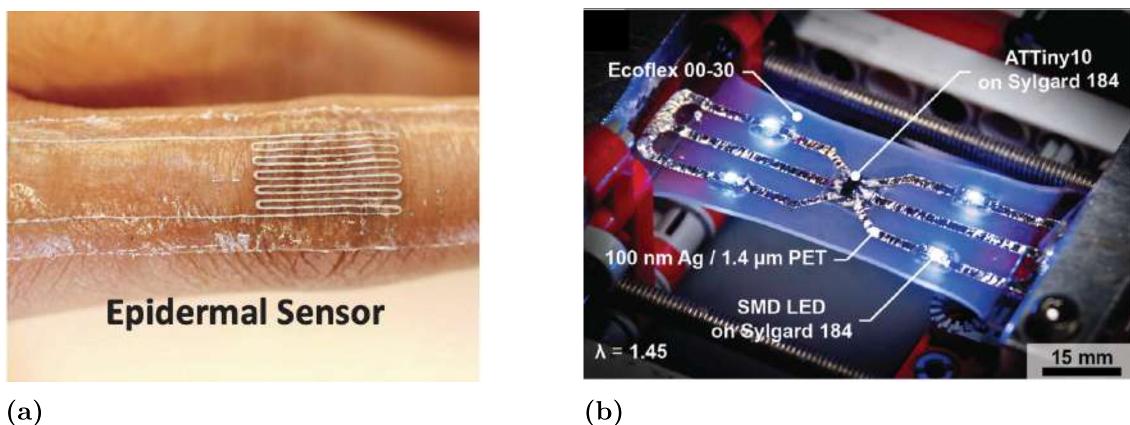

(a) **(b)**

Figure 2.1: Applications of PDMS and Ecoflex showcasing their great properties like conformability and stretchability. (a) Stretchable strain sensor attached to the skin made of PDMS, displaying the conformability of the material (from [40]). (b) Electronic circuit with an ecoflex substrate being strained to 50% of its original size (from [41]). The circuit incorporates rigid materials like LEDs and a microprocessor.

2.1.2 Conductive Interconnects

Soft electronics typically incorporate stretchable interconnects on a polymer matrix, with the substrate representing the bulk of the device. In spite of this, the interconnects are equally important in influencing the performance of the stretchable systems.

These constitute the surface where electrical interconnections will be established, hence good conductivity must be an ubiquitous concern. Furthermore, and more importantly, soft interconnects must be able to maintain their conductivity under variable amounts of strains, which will depend on the final application of the device. For over-the-skin patches, for example, materials should be resistant to 20% - 30% strains [42], however, other applications (like the wearable sensing of the human joint) might require them to go over 100% strain.

Thus, traditional rigid materials for interconnecting, such as metal thin films, need to be replaced by flexible options [43]. The most commonly used alternatives are deterministic structures, liquid metals and conductive composites.

- **Deterministic Structures**

Rigid conductors like gold, copper and aluminum cannot endure strains higher than 2% without breaking [4]. However, the design of these materials can be changed in architectures with "acquired stretchability" that can be classified as out-of-plane (OPS) or in-plane structures (IPS) [44]. These designs allow the metals to deform by bending and twisting, instead of stretching, keeping local strains minimal and preserving their electrical conductivity.

OPS usually consist of wrinkled metallic thin films on an elastomer substrate [4]. Several procedures have been reported in order to achieve this. Wang X. and colleagues [45] used a technique consisting of coating a pre-stretched elastomer with copper and then releasing the elastomer, allowing it to return to its original state and buckling the metal in the process. The schematic illustration of this method is displayed in Figure 2.2a. This produced stretchable conductors able to withstand 300% strain.

Recently, other interesting out-of-plane architectures have started to emerge. Iwata *et al.* [46] used a technique known as folding deformation, to achieve a stretchable conductive substrate, that can be seen in Figure 2.2b. The material proved itself very promising, as its shape allowed it to be stretched in both x and y directions.

IPS, on the other hand, represent designs that are tangent to the planar substrate, rather than structures with a 3D configuration [44]. This can be achieved using multiple designs, but the most popular one seems to be the serpentine architecture [4]. The horseshoe design particularly, seems to be the serpentine architecture that yields the best results because of its large uniaxial strain resistance [47]. Using a multi-track version of the horseshoe design (displayed in Figure 2.2c), Brosteaux and his team [48] were able to increase the maximum elongation of their samples from 20% (uni-track) to 55%. Some authors, however, have reported devices that could reach 300% strain using serpentine architectures [8].

Out-of-plane and in-plane structures have proved very efficient, with good flexibility and excellent conductivity. However, high flexibility usually requires sophisticated patterns, thereby increasing wire resistance and process complexity [49]. Because of this, intrinsically stretchable materials like liquid metals or conductive composites are usually preferred.

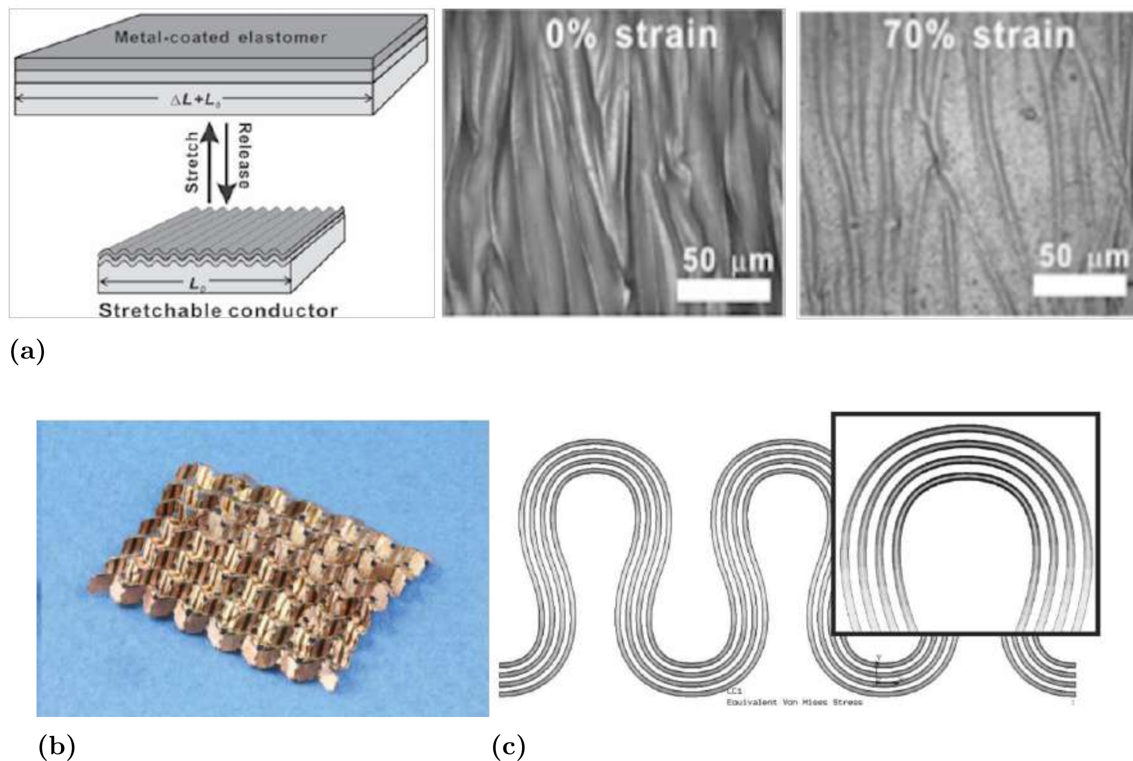

Figure 2.2: Out-of-plane and in-plane deterministic structures. (a) Schematic illustration of the fabrication of the stretchable conductor and optical microscopy images of the surface morphology of the buckled copper (with and without any strain applied). Adapted from [45]. (b) Stretchable conductive substrate made of copper, achieved through folding deformation. Adapted from [46]. (c) Horseshoe split into 4 different tracks in order to achieve higher elongations. Adapted from [48].

- **Liquid Metals**

Liquid metals are one of the most promising and compelling alternatives to deterministic structures, as these materials are liquid at room temperature and exhibit the best combination of conductivity and stretchability among the available options [50].

One of these metals is Mercury (Hg), but even though mercury is electrically conductive and has a wide range of applications, this metal is toxic which limits its utilization in stretchable electronics [51]. Ga-based alloys such as eutectic gallium-indium ("EGaIn", 75% Ga 25% In) and gallium indium tin ("Galinstan", 68% 22% In 10% Sn) are viable alternatives to Hg, having melting points of 15.8 °C and -19 °C, respectively [52, 53]. These substances show very similar properties - negligible vapor pressure and low toxicity - but, just like Hg, both show a high surface tension.

These GA-based alloys typically form a passivating layer when in contact with the oxygen from the air. This thin oxide layer behaves like an elastic material and allows for the lowering of the surface tension [51]. This characteristic enables the liquid metal to adhere to surfaces and adopt shapes that would not be possible if the surface tension was not stabilized (Figure 2.3a) [50].

Liquid metals make up "intrinsically stretchable" electrical conductors with mechanical properties usually defined by the encasing elastomer [50]. This means that these materials are able to be stretched to extreme strains while maintaining metallic conductivity. M. D. Dickey [50] reports that, when encasing liquid metal in elastomeric fibers, strains as high as 800% can be achieved (Figure 2.3b). Alternatively, by encasing LM on thermoplastic elastomers, other authors reported that an elongation of 600% can be reached [54] (Figure 2.3c).

Liquid metals seem like the optimal materials to create stretchable conductive traces in stretchable electronics, albeit its usage can bring a few disadvantages. They display lower conductivity compared to solid metals (even though it is just for one order of magnitude) and when used in electrical devices they need to be completely encapsulated in sealed elastomers to prevent any leakage [55]. Furthermore, despite recent advances on patterning methods for liquid metal, scalable fabrication remains yet to be demonstrated.

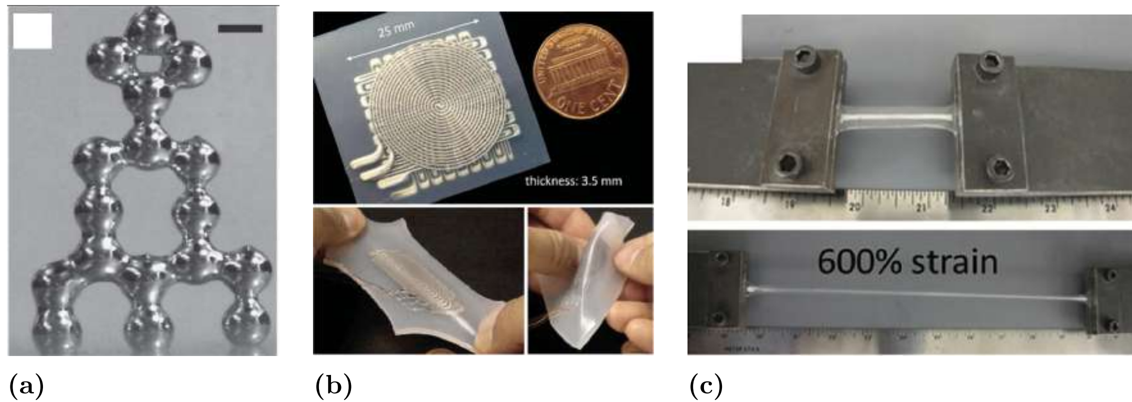

(a) **(b)** **(c)**

Figure 2.3: Liquid metals - characteristics and features. (a) 3D structure made of LM droplets, possible due to oxide layer that is formed on the surface of the metal (from [56]). (b) LM in elastomeric microchannels. Adapted from [57]. (c) LM encased in a thermoplastic elastomer (PDMS) being strained to 600% of its original size. Adapted from [54].

- **Conductive Composites**

An alternative to liquid metals are conductive composites, which are mixtures of conductive fillers with elastic polymeric substances. The goal of this blend is to create a composite with the stretchable properties of the polymer and the conductive attributes of the filler [4]. Microparticles (μPs) or nanoparticles (NPs) [58] , flakes [59] and nanotubes [60] are some of the fillers that are nowadays being used.

The conductivity and stretchability of the final composite is greatly affected by the volume fraction of conductive fillers introduced. In fact, this volume fraction must always exceed a percolation threshold to successfully form continuous electrical pathways in a given polymer matrix [55]. This behavior is illustrated in Figure 2.4.

These composites typically exhibit a lower conductivity than LM and, because of this, they are only good alternatives to the latter on certain occasions [50]. However, research on this area has shown that conductive composites can exhibit unique properties like self-healing, shape-memory and conductive sensing, that might be interesting for some applications [55].

The maximum conductivity and strain of thin metallic films, deterministic structures, liquid metals, and conductive composites is summarized in the graphic shown in Figure 2.5 [4].

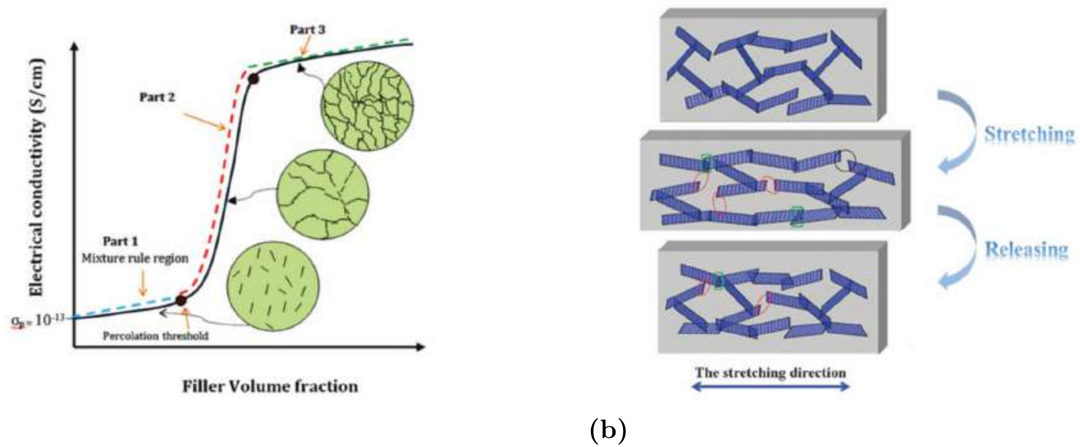

Figure 2.4: Stretchable conductive composites. (a) Typical behavior of the conductivity of a stretchable composite with the volume of filler used (from [61]). Percolation threshold needs to be achieved in order to have a steady increase in conductivity. (b) Schematics illustration of the changes in a graphene network during stretch-releasing cycles (from [4]). These cycles allow for a better the reconstruction of some mechanical pathways and the destruction of others.

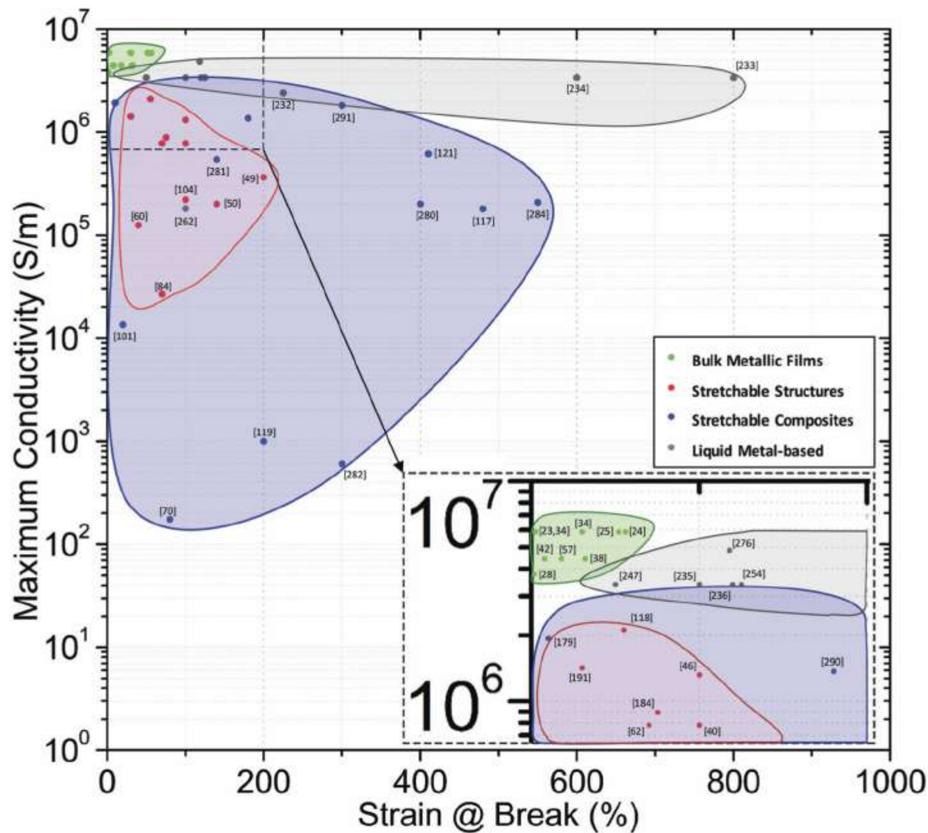

Figure 2.5: Ashby graphic with comparisons of different published works – thin metallic films; deterministic structures; liquid metals; and conductive composites – in terms of their maximum conductivity and strain at their breaking point [4].

Typically, silver is the traditional filler for synthesis of conductive composites [4]. However, alternatives like LM nanocomposites have been recently achieved either by suspending LM nanoscale droplets within a soft polymer matrix, or by mixing them with metallic nanoparticles to form a biphasic composition in which the LM functions as the continuous matrix phase [62]. In spite of still being in early development, LM nanocomposites have already shown great promise for application in stretchable electronics due to their high thermal conductivity and decent maximum strain at failure (120%).

- **zPDMS Conductive Film**

zPDMS is a conductive elastomer that can be used as an alternative to conventional interconnects for rigid chip interfacing [63]. To fabricate it, PDMS is blended with conductive nanoparticles and, while it cures, the mixture is exposed to a magnetic field to magnetically align the particles, making the elastomer conductive in only one direction. Vertically oriented nanoparticles can therefore be achieved to create percolating networks that only show conductivity through the thickness (z-axis) of the elastomer (Figure 2.6). Ag coated Ni nanoparticles are examples of materials that have already been used to create these conductive films.

This technique allows for the integration of SMD chips in circuits through electrical vias that show no risk of leakage and that do not need any alignment, thus bypassing the direct interfacing between rigid components and a conductive interconnect [63].

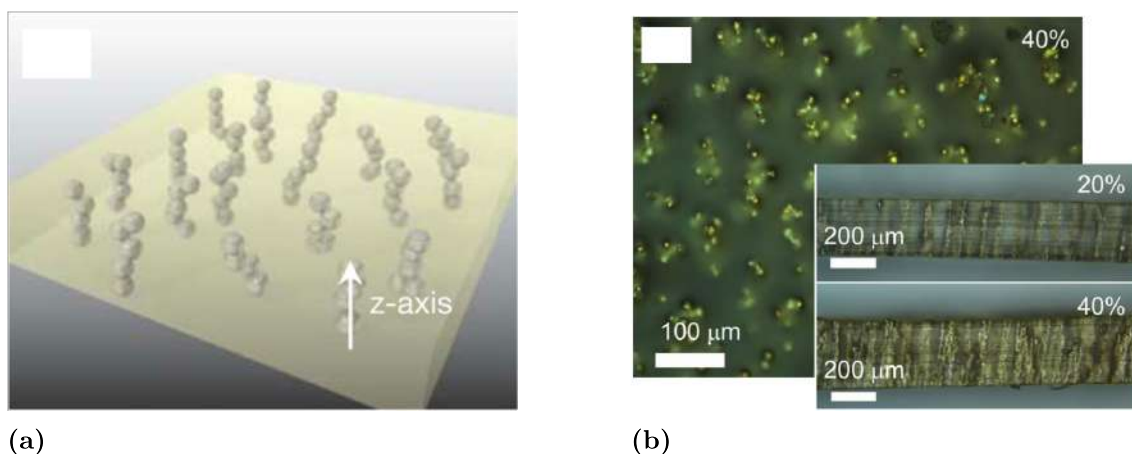

(a) **(b)**

Figure 2.6: zPDMS Conductive Film. (a) Schematics of the film with conductive nanoparticles embedded on an elastomer and supporting conductivity through the thickness of the material. (b) Top and side views of the film where the magnetically aligned columns of nanoparticles can be observed. Adapted from [63].

2.2 Fabrication Methods

In this section, methods for fabrication of stretchable electronics are provided, including techniques for producing elastic polymers and for liquid metal patterning.

2.2.1 Fabrication of Elastic Polymers as Substrates

Methods for fabrication of substrate polymers range from spin-coating and moulding to patterning through a thin-film applicator. In all cases, a viscous pre-polymer is used to build the final polymer layer. The shape and thickness of this material can be created and controlled through one of the abovementioned methods. Once polymerized, the pre-polymer turns into a solid elastic membrane that can be used as a substrate or a sealing layer in stretchable electronics.

Some of these polymers, such as PDMS and Ecoflex™ are fabricated using 2 different components – a monomer and a catalyzing agent [37, 64]. Mixing these reagents quick starts the polymerization process. Other polymers like latex and SIS only need to cure at a high temperature to become rigid elastomers. Some of the mixtures, like Ecoflex™, might need to be degassed to eliminate entrapped air.

2.2.2 Patterning Techniques - Liquid Metals

When compared to other alternatives, LM shows the best combination of conductivity and stretchability, as can be seen in Figure 2.5 [4]. Conductive composites typically suffer from hysteresis and low electromechanical stability – electrical resistance progressively increases over the number of cycles [4]. On the flip side, LM-based interconnects usually benefit from a smaller gauge factor, and exhibit low electromechanical hysteresis, making them more appropriate for applications that undergo large strains [4].

For these reasons, and because a LM-based ink was used throughout the development of this dissertation, only patterning techniques for LM will be provided in this segment.

Because of their low viscosity, the easiest and simplest way to pattern liquid metals is by injection into microfluidic chambers, which can easily be achieved using a syringe [65]. Another simple and effective patterning technique is stencil lithography (Figure 2.7a). The stencil is patterned through laser ablation and lightly glued on top of the desired substrate. Then, the LM is spread on the stencil using a spatula or a roller. The stencil needs to be quickly removed to prevent the oxide from binding

too much to the material. This allows LM to be transferred to the substrate and be subsequently cured. Even though these methods are effective, they often involve multiple manual steps and can be labour intensive, and thus recent researching efforts have been focused on developing digital fabrication methods for automated LM printing [4].

Laser ablation is a fairly simple subtractive technique that consists on the deposition of LM on the surface of a substrate followed by a selective removal of the metal, leaving only the desired pattern of the LM behind (Figure 2.7b) [66]. Techniques based on the direct deposition of LM are also being employed for rapid prototyping of stretchable circuits [4]. For example, a ballpoint pen filled with LM and a controlled force tapping technique has been used to produced complex LM patterns [67]. Other approaches like the deposition of LM droplets through a soft PDMS needle with a hemispherical tip have also been successfully demonstrated [68].

Inkjet printing is a popular direct printing method that has several advantages: potential for automation, manufacturing speed, and high resolution [69]. However, this technique is limited to colloidal suspensions of LM droplets, due to the surface oxide and large surface tension of LM [50]. Even though the surface oxide is problematic on some applications, it enables 3D printing of LM, with the structures being stabilized by the oxide itself (Figure 2.3a) [56].

New lithography-enabled patterning techniques are emerging like the "lift off", where a negative photoresist is spin-coated and then patterned by conventional photolithography to open an area that will be wet by LM (Figure 2.7c) [50, 70]. The LM is casted onto the surface of the photoresist layer and adheres to the substrate in the exposed regions of the material. The photoresist is then dissolved with acetone, along with the LM deposited on top of it, leaving behind the metal that adhered to the surface of the substrate.

Interconnects can also be created by freezing EGaIn and encapsulating these frozen components within an elastomer in a technique known as freeze casting (Figure 2.7d) [71]. Other approach consists of selectively wetting the surface of an elastomer using a mask that only allows for the deposition of LM [72].

M. D. Dickey describes a new promising and interesting approach to conductive interconnects called biphasic conductors [50]. The procedure consists in depositing liquid metal on top of solid metal traces like Au traces. The liquid metal is coated by physical vapor deposition using a stencil mask onto lines of microcracked Au. These microcracks grant great elasticity to the Au and the deposited liquid metal

allows the system to maintain conductivity at large strains. During the deposition, Au and Ga form a solid phase alloy. In order to create the liquid part of the biphasic conductor, a new layer of liquid metal is deposited on top of the alloy.

The created traces are less likely to leak when cut or deform substantially when pressed. The biphasic lines created must then be encased in elastomers to create stretchable interconnects (Figure 2.7e).

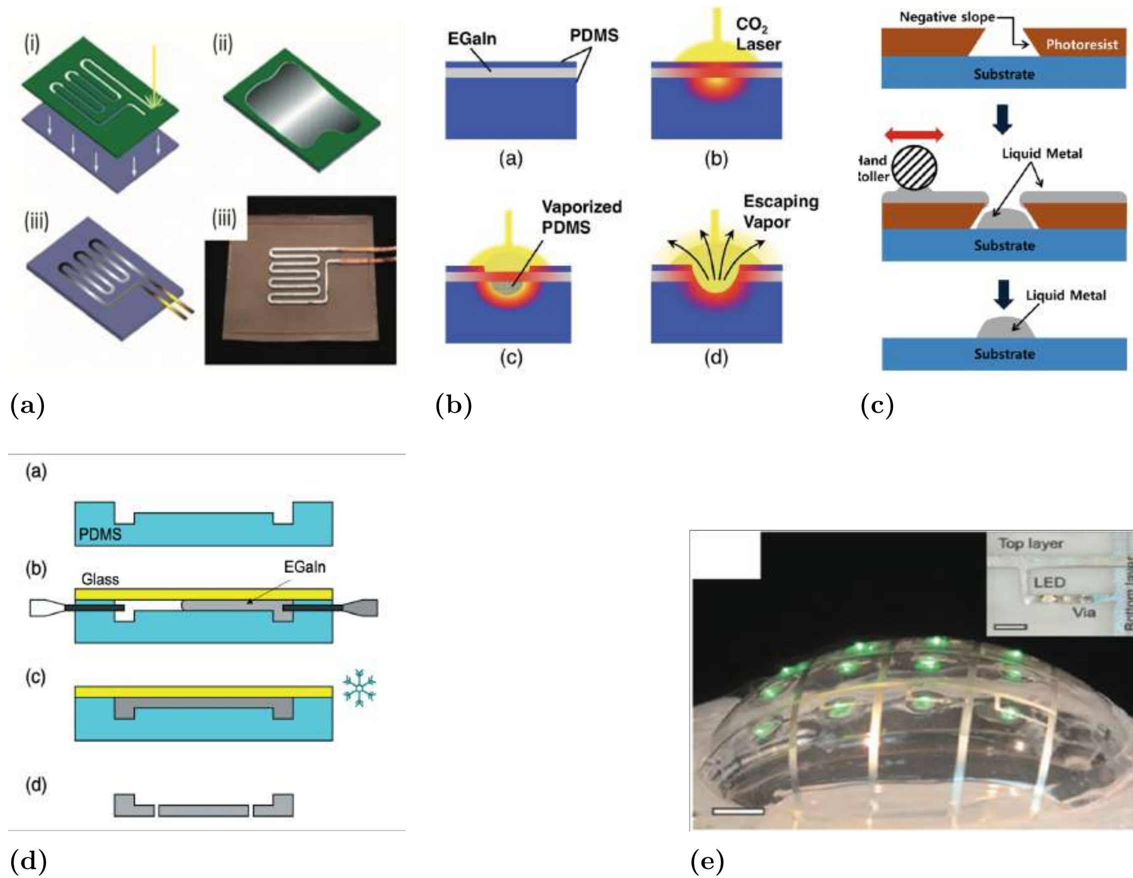

Figure 2.7: Patterning techniques for liquid metal interconnects - current and emerging methods. (a) Schematics of the stencil printing technique (from [50]). (b) Schematics of the laser ablation technique, in which the heat vaporizes the substrate, leading to the escape of the LM (from [66]). (c) Schematics of the lithography-based patterning process (from [70]). (d) Schematics of the process that leads to the formation of EGaIn interconnects through freezing (from [71]). (e) Device created using biphasic lines encased in a soft elastomer (from ([50]).

2.3 Integration Methods

Conventional techniques for direct integration of rigid components in electronic systems have been available for decades and are still widely used in the industry nowadays. In traditional rigid PCBs, wire bonding, flip-chip and soldering are the preferred methods as they are generally cost-effective, quick to perform, reliable and versatile [73].

In wire bonding, a metal wire (usually gold or copper) is used to connect the microcomponent with the pads of the circuit, creating a metallurgic bond between the components [74]. There are 2 types of wire bonding: ball-stitch bonding (Figure 2.8) and wedge bonding. These techniques usually require the use of heat and/or ultrasonic energy [74].

The flip-chip technique consists of flipping a microelectronic component at the end of its manufacturing process and applying solder dots on its pads. When mounting the flip-chip, the solder dots need to be carefully aligned with the pads of the external circuitry and the solder is usually remelted to establish the electrical connection and ensure the component is completely glued to the desired interconnect [75].

Alternatively, solder can be directly applied on the desired areas of the circuit through a paste or by melting a solder alloy [76]. Electrical glues and adhesives are composed of conductive particles and, therefore can also be used to establish the contacts between the microcomponents and the external circuit. These are especially useful when using electrical components that are sensible to temperature and that cannot be integrated through normal soldering procedures [77].

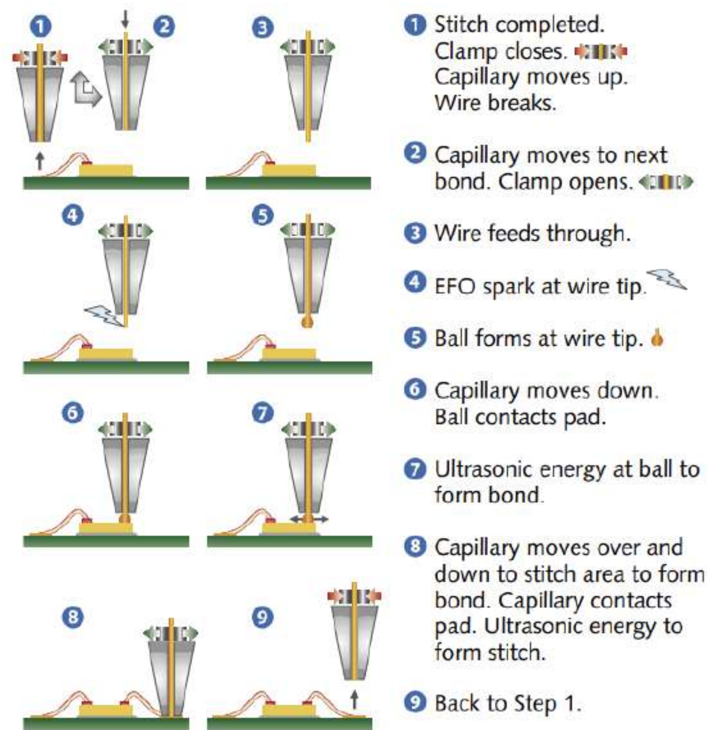

Figure 2.8: Ball-stitch bonding, one of the wire bonding techniques. A ball of metal is placed on top of the microcomponent and the rest of the wire creates the connection to the pad of the circuit. Adapted from [74].

Even though these techniques usually perform well in rigid electronics, their use in stretchable circuits is limited to those that utilize metal thin films or deterministic structures as interconnects. Comparatively, liquid metals and conductive composites provide a superior performance, but traditional integration techniques are usually not compatible with these interconnects due to accumulation of stress in the connection sites. Because of this, researching efforts are now being directed towards developing reliable integration techniques for incorporation of solid-state microelectronics in intrinsically stretchable systems.

In this section, a detailed study of these state-of-the-art methods will be reported, with the analysis being divided in 2 integration categories - direct and indirect.

2.3.1 Indirect Integration

Indirect integration techniques are those that do not require the direct contact between the rigid components and the interconnects. This is usually achieved by incorporating other elements in the system that will indirectly connect the chips and the conductive traces.

- **Printed Circuit Board (PCB)**

One strategy to solve the interfacing problem is to include rigid component islands (PCB-like) across the surface of an elastomeric substrate with stretchable interconnects linking them together [78]. Each of these islands will hold a single or multiple components and act as an interface between the ICs and the stretchable interconnects.

This technique allows for the reduction of the number of unreliable rigid-soft interfaces as all the ICs will be connected to the circuit board, which is generally embedded in the elastomer itself [78]. In spite of this, electrical failure is still observed on these systems due to concentration of strain on the interface between the large rigid islands and the substrate, that ultimately disrupts the interconnects linkage.

Nevertheless, because the only component on the system that will need to be linked to the circuit is the PCB, the amount of interconnects needed for establishing the connections is small, which generally enables simpler designs and integration [79].

Cheng *et al.* [79] developed a variant of this technique by using a flexible printed circuit board (FPCB) made of small pieces of laminates to create a flexible antenna. Conventional rigid ICs and passive components were assembled and soldered to the top of the board. PDMS was filled with galinstan using microfluidic injection and the FPCB was embedded and soldered to the elastomer. Each contact pin of the flex foil was plugged into an opening of the microfluidic channel, thereby contacting with the liquid galinstan alloy and establishing the connections. The schematics of the integration can be observed in Figure 2.9.

PDMS droplets were poured on the most fragile regions (close to the FPCB) in order to create localized stiff cells in which the stress will be lower because of the increased thickness of the area. This allows the flexible circuit board to be isolated to a certain extent of the intense stress distributed over the system. The final device was able to be stretched to 15% of its original size, both in x and y-axis.

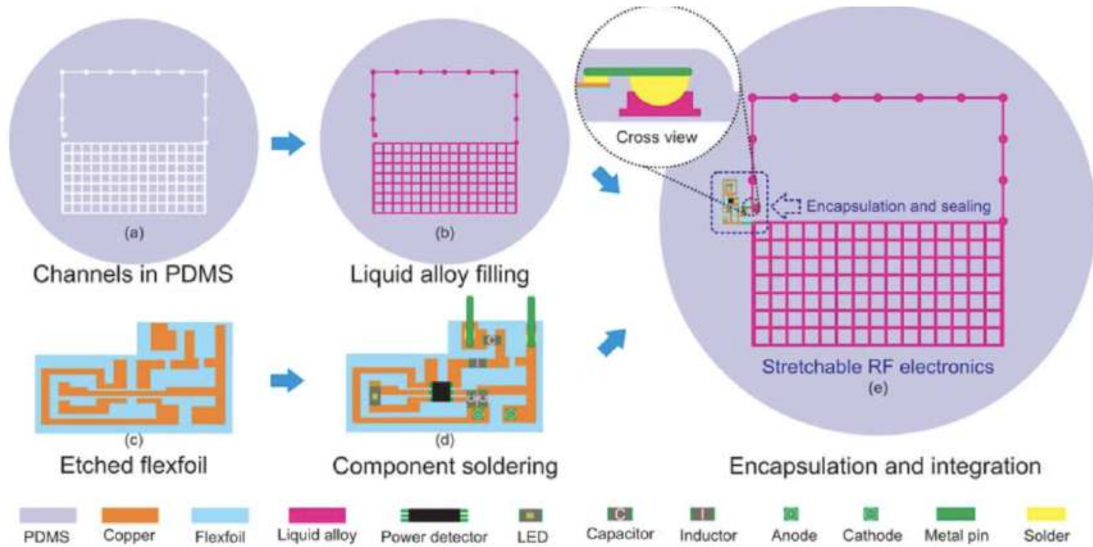

Figure 2.9: Schematics of the FPCB and rigid components integration into the soft circuit (from [79]).

The FPCB concept can be pushed further with more sophisticated circuit designs that allow for a more durable and resistant integration of ICs. In 2019, our lab [32] achieved this by producing a multi-layer circuit based on LM interconnects and laser-ablated EGaIn filled VIAs.

First, polyimide-copper flexible islands (FPCBs) populated with silicon chips were embedded on PDMS. Then, 3 different variations of the processing steps were shown. The simplest method to access the rigid island was by laser ablating part of the enclosing PDMS layer, followed by spray coating EGaIn on top of the elastomer, thereby filling the formed VIAs with LM. The connection between the Cu pads of the FPCB and the EGaIn is therefore established and the circuit can be encased in another layer of PDMS. This method is exhibited in Figure 2.10.

In order to test the electrical resistance of the interface during the application of strain, a surface-mount 0-ohm resistor was interfaced with the FPCB and two EGaIn traces linked both ends of the sample to the Cu pads of the circuit board. Most of the specimens could reach an elongation of 80% before electrical failure occurred due to elastomer rupture at the center of the samples. Furthermore, the system was able to withstand a mechanical loading test of 1000 cycles at 40% strain and 0.4 Hz without significant proof of electrical deterioration.

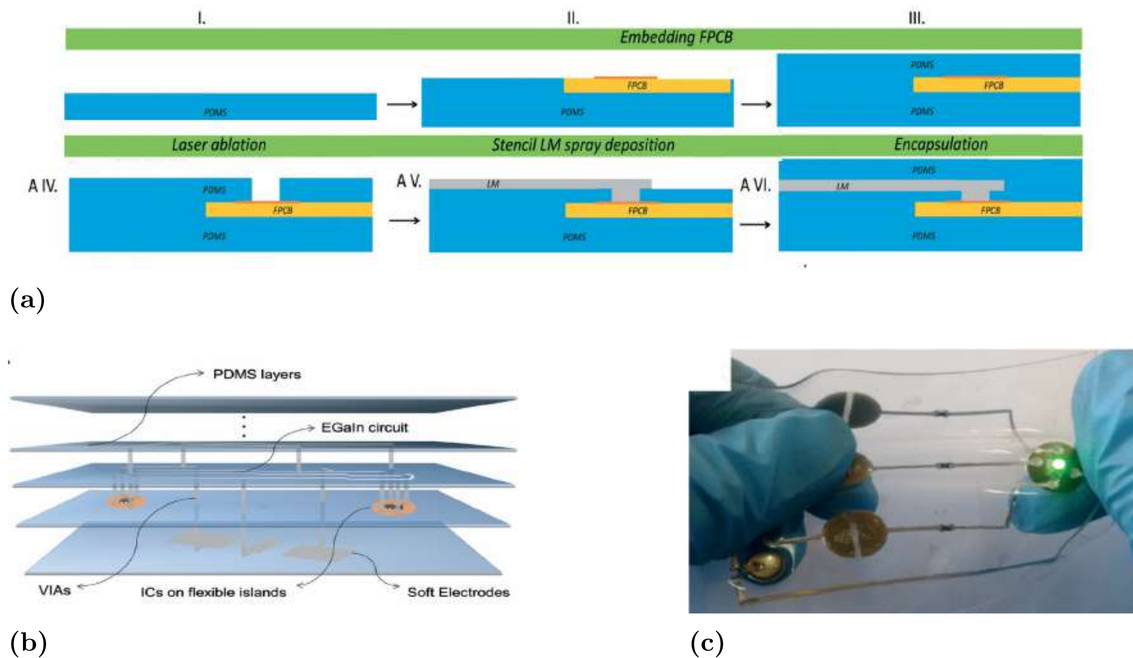

(a)

(b)

(c)

Figure 2.10: Schematics of the multi-layer method developed. (a) Model of one of the processes used to interface the FPCB with the LM. (b) Exploded view of the layers and all the components in the circuit. (c) Stretchable circuit created with this method, with a RGB LED soldered to the FPCB. Images adapted from [32].

- **zPDMS Conductive Film**

As it was described in section 2.1.2, zPDMS is a mixture of PDMS and conductive particles that, when magnetically aligned, establishes columns that function as electrical vias through the thickness of the elastomer.

zPDMS can act as an interface between stretchable interconnects and the pins of rigid ICs. According to Lu *et al.* [63] surface mounted components can be directly placed on top of the zPDMS film, establishing connections with LM circuit terminals embedded on the elastomer (Figure 2.11). The devices created can be encapsulated with an extra layer of PDMS to increase the robustness of the system. External contacts are done through conductive paper.

Mechanical strain tests on samples with a surface-mounted LED reveal that the LED was functional until 110% strain, even though substrate delamination started to occur at approximately 60% elongation. This behavior was only observed for the samples that had an extra layer of PDMS, as the remaining failed at around 30% strain due to delamination.

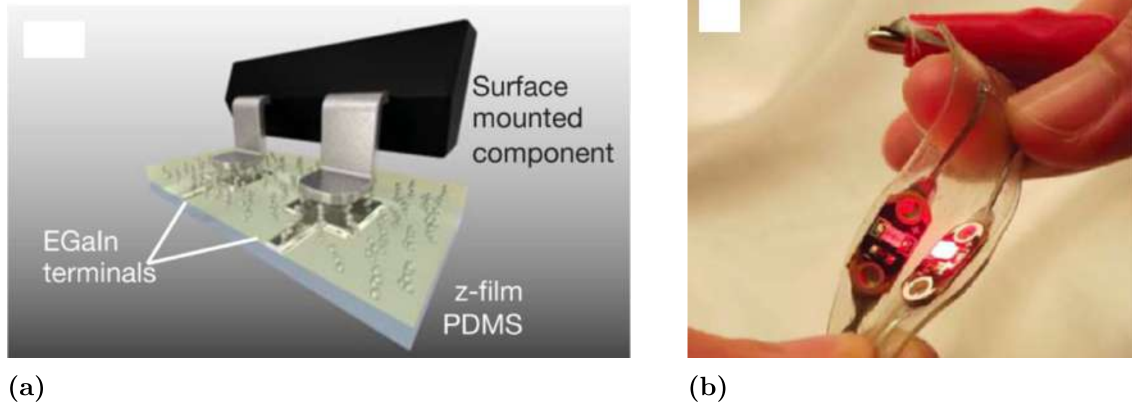

(a) (b)

Figure 2.11: zPDMS conductive film. (a) Schematics of the interfacing between a surface mounted component and a zPDMS conductive film. Vertical vias establish the connections between LM circuit terminals and the pins of the IC. (b) zPDMS employed in the development of a functional circuit with integrated rigid components. Images adapted from [63].

2.3.2 Direct Integration

In direct interfacing techniques, the contacts pins of rigid ICs are directly interfaced with the stretchable interconnects from the soft system. This is achieved by changing the architecture of the system to better accommodate the rigid elements, or by employing chemical methods to establish the connections between both elements.

- **Dual Concentric Islands**

Direct interfacing techniques might be focused on developing compliant circuit designs that allow the stress to be distributed over more flexible segments of the system.

Robinson *et al.* [80] proposed a design where stiff disks are embedded within an elastomeric substrate in order to stabilize the area directly above them. To achieve this, the team embedded two concentric polyimide rigid disks on PDMS (Figure 2.12) - one smaller (5 mm) upper disk positioned towards the PDMS surface and a second disk with a bigger diameter (8 mm) embedded deeper in the PDMS membrane.

The top disk enables the creation of a 0 strain zone on the PDMS directly above it and the bottom one ensures that the surface strain is 0 across the surface area of the top disk. This design guarantees that, when the system is stretched, none of the disks bend significantly and the top surface of PDMS is stabilized. The surface mount components were placed on top of the rigid islands and soldered to Au wiring

using silver paste.

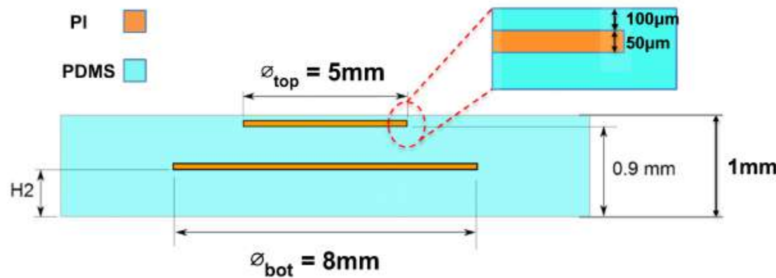

Figure 2.12: Schematic cross section of the model created with the dual-disk approach (adapted from [80]).

Even though both designs incorporate rigid-islands, this method is not similar to the FPCB technique because, in this case, the ICs are directly interfaced with the interconnects. Rigid-islands are only used to ensure that the area where the chips are applied remains stable under strain.

Mechanical strain tests suggested that there was a gradual cracking of the gold interconnects with the increase of strain from 0% to 20%. This was expected as the gold interconnects are not intrinsically stretchable. In fact, after 1000 cycles of mechanical loading up to 20% strain the cracks grew so significant that they were enough to lead to electrical failure of the device.

- **Interconnect Micropatterning and Flip-Chip**

A process that combines the simple flip-chip technique and custom-made interconnect micropatterning was demonstrated by Hu *et al.* [81] to be very effective. The technique consists of creating serpentine-shaped interconnects (encapsulated in PI) that connect gold pads with openings that allow electrical contact and bonding through the flip-chip method.

First, the team spin-coated a PMMA layer on a silicon substrate and created holes on the the PMMA using a shadow mask and a low power etch. A layer of PI was then spin-coated on top of the system, filling the PMMA holes all the way to the silicon. The contact points serve as anchors to prevent the interconnect from drifting off the substrate. A gold layer was patterned on top of the PI using photolithography, and another layer of the polymer was spun over the whole system (Figure 2.13a).

A silicon oxide layer was deposited to protect the bottom PI and a layer of photoresist was patterned on top. The PI is etched down all the way to the gold interconnect to expose the site of contact to the pads of the microelectronics. This way, the whole

topographic surface of the interconnect will perfectly fit the contacts of the rigid material.

The interconnect was transferred to a a stretchable substrate using an adhesive and the now obsolete PMMA layer was dissolved. The authors coated the entire bottom-side of LEDs with anisotropic conductive film and then used a flip-chip bonder to align and attach the contact pads to the gold interconnects.

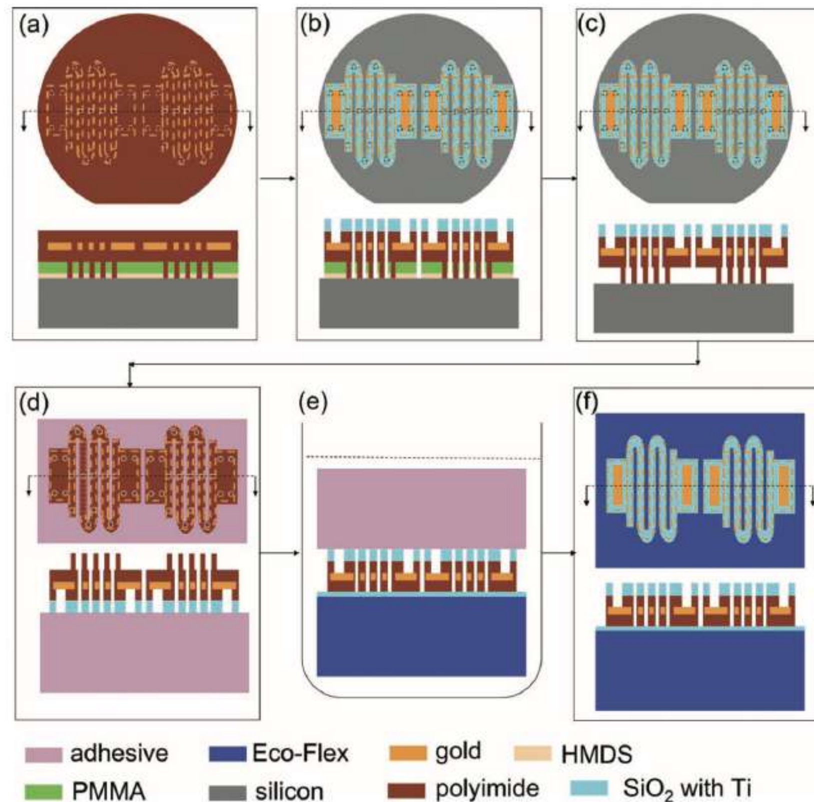

Figure 2.13: Schematic illustrations of the fabrication process of the interconnect micropatterning and flip-chip technique. (a) Patterning of the gold contact pads and serpentine-shaped interconnects and encapsulation in PI. (b) Etching of the circuit according to the topography of the microcomponents. (c) Sacrificial PMMA layer is dissolved. (d) System is picked using an adhesive. (e) Structure is transferred to an ecoflex substrate. (f) Removal of the adhesive tape. Images adapted from [81].

An entire stretchable LED array was created through this technique and the electromechanical results showed that the system could withstand strains of up to 200% of its original size. Fatigue was not a problem as the array endured 5000 stretching cycles loading up to 200% strain. Fracture of the serpentine interconnects near the contact pads was identified as the failure mechanism in all cases.

Even though this method provided great results, the process includes many steps

and becomes complex as it requires that the interconnects are micropatterned according to the bottom topography of each individual electronic component. Therefore, the technique might be hard to scale and might become very expensive and time-consuming when incorporating multiple different components (as most circuits do).

- **CMOS/Microfluidic Hybrid Microsystem**

Another example of how circuit designs can lead to a more durable integration is the model developed by Zhang and colleagues [82] where a NMOS transistor was created by applying a novel strategy for integration of solid state IC electronics in soft systems (Figure 2.14a).

In order to achieve it, a system with 2 PDMS layers was fabricated: a top microfluidic layer and a bottom layer encasing a CMOS die with its connection pins still exposed. Then, the microfluidic channels of the top layer were accurately aligned with the contact pads of the CMOS die embedded in the bottom layer (Figure 2.14b). The channels were injected with Galinstan, establishing the connection of the CMOS die with the rest of circuit. A separate microchannel is used for delivery of LM to the sensor region of the CMOS.

The Young modulus of silicon is much higher than that of PDMS, and the system effectively exploits this as most of the strain will be concentrated in the PDMS and LM regions (Figure 2.14c), which endows the NMOS device with a stable performance under stretching conditions. Hence, with a very simple design, the transistor was able to remain functional under uniaxial strains of up to 15%, while the drain currents exhibited a change of only 0.5% in the aforementioned conditions.

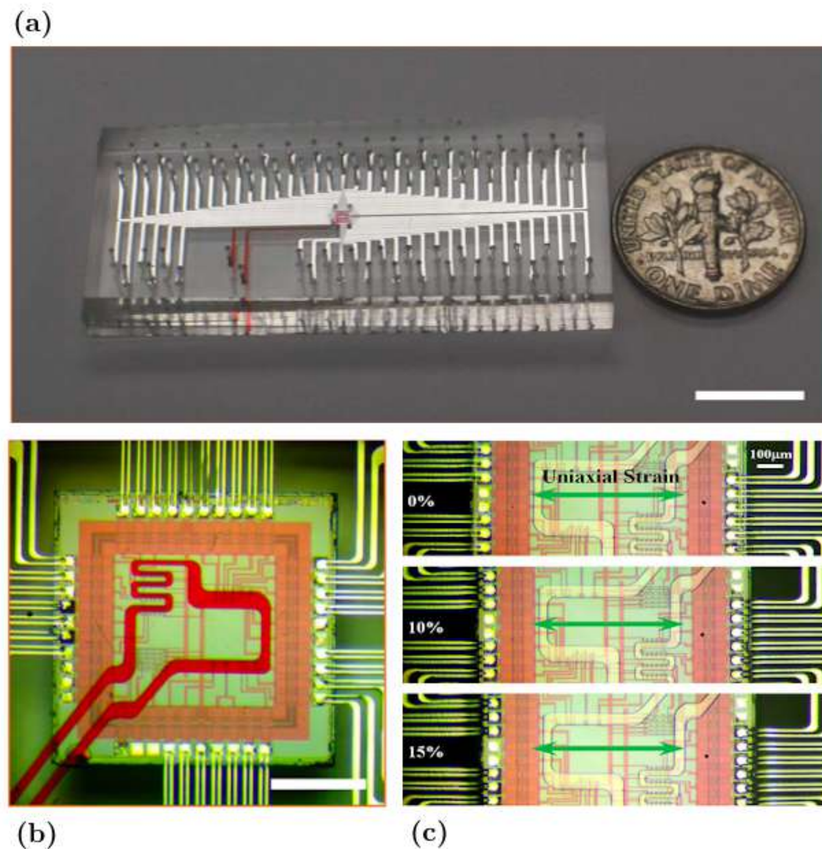

Figure 2.14: CMOS/Microfluidic hybrid microsystem. (a) Optical image of the packaged CMOS/microfluidic hybrid microsystem. (b) The microchannels are filled with LM and exactly aligned with the contact pads of the CMOS die. The sample delivery channel that connects to the sensor area filled with red food dye. (c) Uniaxial strain tests performed on the NMOS transistor. Most of the strain is concentrated on the stretchable regions - PDMS and liquid interconnects. Images adapted from [82].

- **"Gull Wing" Design**

Wang and colleagues [83] attempted to fabricate a circuit with a "gull wing" design in order to better accommodate rigid ICs and provide a more stable interfacing.

An EGaIn alloy was patterned on the surface of a PVC film (primary substrate) to create a functional circuit. Then, the circuit was coated with a layer of PDMS that encased the LM circuit printed before. The PDMS was cured and served as the secondary substrate of the circuit. The system was cooled down below the melting point of the LM, which allowed the PVC to be peeled off and the PDMS to hold the original shape of the LM as the temperature increased to room levels.

Afterwards, the surface-mount electronics were positioned on the circuit pads, which

had previously been strengthened with trace amounts of EGaIn. The described process is exhibited on the schematics in Figure 2.15. Finally, the final system was encapsulated in another layer of PDMS. The design of the circuit combined with the added EGaIn on the connections allowed for a mechanical and electrical enhancement of the bonds between the ICs and the pads.

The potential of the technique was demonstrated by developing a remotely-controlled temperature sensor module with multiple micro control units. Even though strain tests were not presented, the device could be bent, switched and twisted without any signs of electrical failure.

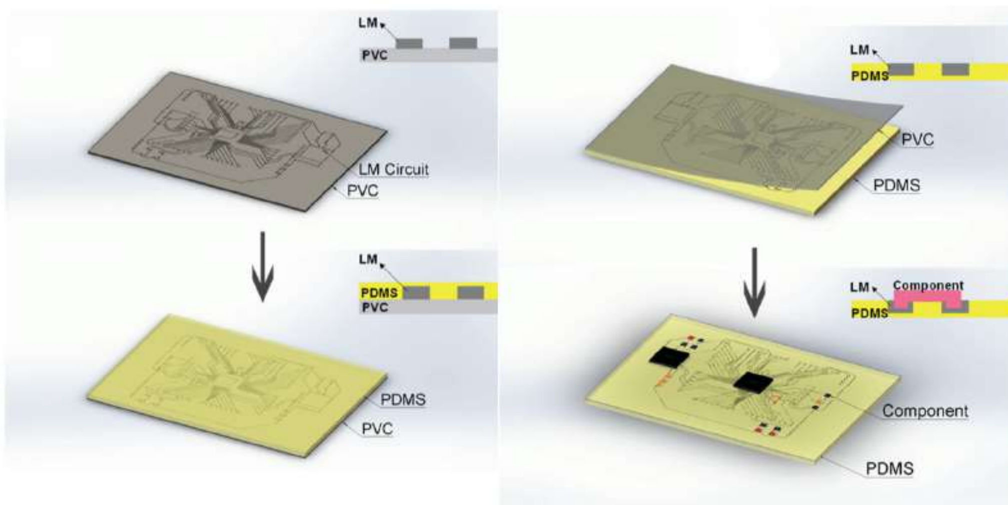

Figure 2.15: Schematic illustrations of the fabrication process of the ”gull wings” circuit developed by Wang and colleagues [83]. After this, an extra layer of PDMS was used to encapsulate the rigid components.

- **HCl Vapor**

Ozutemiz *et. al.* [84] reported, in their 2018 study, a method that achieves reliable soldering of silicon chips to LM interconnects using HCl vapor. The team combined laser ablation and biphasic conductors to create a Cu pattern on PDMS, on which LM was selectively deposited (Figure 2.16).

The microelectronics components were placed on the desired locations of the circuit and HCl vapor was applied in order to ”solder” the metal pins of the chip to the LM. After the vapor treatment, the Gallium oxide around the LM patterns is dissolved, thus causing the LM to reshape and surround the component pins, increasing the interfacial contact area and producing a reliable mechanical connection between LM and the chip. In addition to this, if the component is misaligned, the vapor

exposure will create a self-alignment of the component with respect to the contact pads, eliminating the need for precision component placement tools. After vapor exposure, the whole system was encapsulated with a top layer of PDMS.

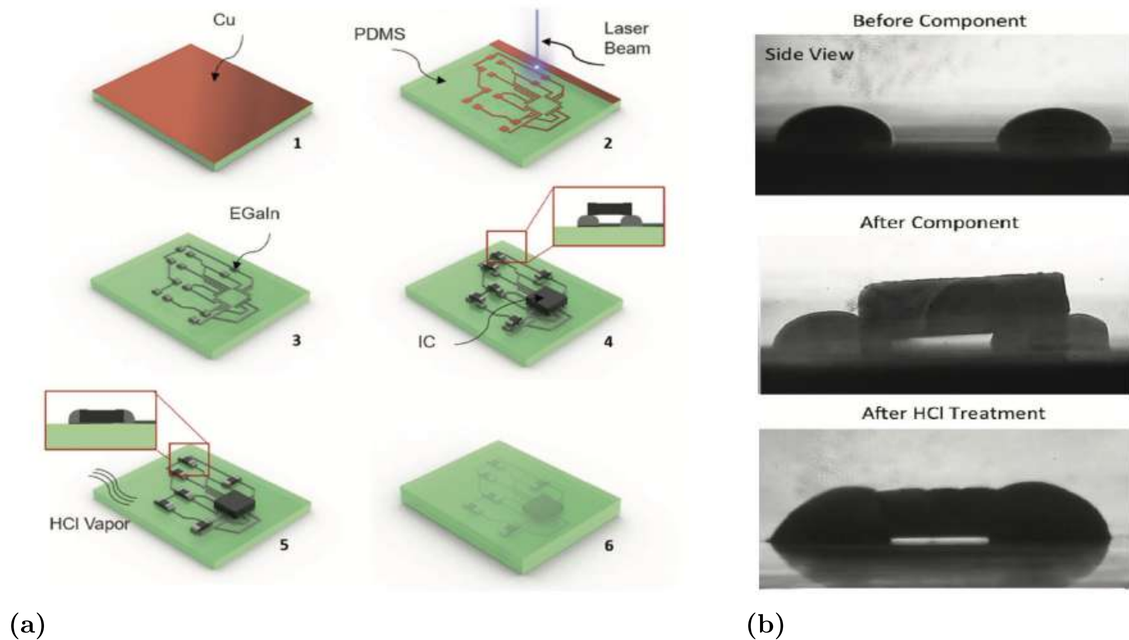

(a) (b)

Figure 2.16: Integration through HCl vapor. (a) Schematic illustrations of the fabrication process of circuits with reliably integrated microelectronics through the use of HCl vapor. (b) Side view of the integration of the rigid component before and after HCl vapor treatment. HCl vapor considerably reduces the misalignment of the component with respect to the contact pads. Images adapted from [84].

Samples treated with the HCl vapor could all withstand 60% strain before the interface between the LM and the pins teared, with some of them reaching 80% strain before electrical failure. Furthermore, the circuit could withstand a mechanical loading test of 2000 cycles from 4% to 40% strain at 0.1 Hz cyclic rate.

Even though this technique provided excellent results, it is limited to packaged components that are not sensitive to short-term application of corrosive vapors. Multi-layer circuit fabrication is also not possible using this method with the devices being limited to one-layer systems.

2.3.3 Progress Over State-of-the-Art

Some techniques described require a complete overhaul of otherwise simple systems to accommodate rigid microelectronics like most indirect methods and interconnect micropatterning. Others are only compatible with some components (e.g. CMOS die and "Gull Wing" Design). The HCl Vapor method is promising, but unusable if packaged components are sensitive to corrosive vapors. More conventional techniques like solder paste require the circuit to be heated to temperatures that might damage common substrates (e.g. PDMS and Latex), and are unreliable when incorporated with soft interconnects.

Hence, the intent is to develop and characterize a technique that tackles the problems with existing methods. This means that the developed method needs to be relatively easy to replicate, fast to apply and fairly compatible with multiple silicon components.

To do so, this work will focus on methods for integration of silicon chips on printed stretchable circuits that are produced using a Gallium-based ink, previously produced by ISR [85]. As it will be shown here, a simple method based on vapor exposure of printed circuits results in highly stretchable integrated circuits, capable of withstanding >550% strain, which is roughly 3 times higher than any work reported till date.

3

Materials and Methods

Throughout the progress of the dissertation, several materials and equipment were utilized in order to reach the experimental results that led to the development of a consistent integration technique.

In this chapter, the materials and equipment used are briefly described and their overall role in the dissertation is outlined. An interfacing method based on toluene vapor is described, along with its interaction with a conductive SIS-based ink. Finally, techniques for characterization of the attachment of the rigid components to the flexible structure are introduced and explained.

3.1 Materials and Equipment

The following materials and equipment were directly involved in the development of the interfacing method that is presented afterwards.

Materials

- Styrene-Isoprene-Rubber Solution – Aldrich (solution produced at ISR)

  Prepared by solubilizing the block copolymer with toluene. The process can be done with different toluene to SIS ratios, as different applications often require the solution to have certain levels of viscosity.

  Used in the fabrication of the stretchable conductive ink and as a substrate in the integration method.

- Silver Flake Material 071 – Technic Inc.

  Used in the fabrication of the stretchable conductive ink.

- EGaIn Liquid Metal – produced at ISR

  Ga and In are poured onto the same container in the solid state. Then, the metals are heated above their melting points overnight. After this process, the resulting alloy is able to remain liquid at room temperature.

  Used in the fabrication of the stretchable conductive ink.

- Toluene – CHEM-LAB

  Used to prepare the SIS solution and to create toluene vapor in the integration method.

- Transfer Paper – Ruspepa

  The transfer paper is coated with a thin layer of silicone that prevents other substrates from strongly adhering to its surface.

  Used as a substrate in the integration method.

- PDMS – Sylgard® 184, Dow Corning Corporation

  Prepared by mixing the base elastomer and the curing agent in a 10:1 ratio.

  Used as an encasing substrate.

Equipment

- VLS3.50 Desktop Laser Cutter (Figure 3.1a) – Universal Laser Systems

  The laser cutter was used to pattern stencils, and cut shapes in cured elastomers. The machine is composed of an arm equipped with a 10.6 μm CO_2 50W laser that can be moved in the x and y directions, and a platform that can be lifted and lowered in the z-direction. Speed and effective power of the laser can be controlled depending to the properties of the material being cut.

- Thin Film Applicator (Figure 3.1b) – Zehntner

  This equipment controls the thickness of substances in a 50–3000 μm range, allowing for the fabrication of thin films that can be used as substrates or encapsulating layers. It was used to create thin films of SIS and PDMS.

- ARE-250 Mixer (Figure 3.1c) – Thinky

  This machine allows for the fabrication of the conductive ink and multiple elastomers with precise control of the process. Mixtures are blended through centrifugation at fixed speeds to achieve homogeneous solutions. Degassing can also be employed to remove entrapped air bubbles in elastomer solutions.

- Drying Oven SLN 115 (Figure 3.1d) – Pol-Eko Aparatura

  The oven was used to fabricate LM, cure the ink and elastomers in samples and accelerate the toluene vapor method. The oven is able to reach temperatures of 300 °C with an accuracy of 0.1 °C.

- Weighing Scale – Kern PCB

  All weighing measurements were done through this equipment.

- INSTRON 5900 Series Universal Testing Instruments

  The INSTRON was used to perform tensile strain and cyclic loading tests with very accurate precision and reliability. It can be also used for other mechanical loading tests like compression, shear and bend tests.

- Stereoscope - Leica S9D

  Used to take microscopic pictures of samples and components.

- SEM Microscope – from Universities of Coimbra and Porto

  Used to acquire high resolution images of the surface of the materials and of the attachment between soft and rigid components.

- Voltera V-One Printer – Voltera

  The machine is able to automatically print circuits. Used for printing the circuit shown in the case studies.

- Pick and Place Machine eC-placer – Eurocircuits

  Used to accurately position rigid chips in their correct positions in the circuits.

The following elements are materials that were used to assist the experimental work, or that were used as secondary equipment throughout the development of the dissertation before achieving the final interfacing method.

Additional Materials and Equipment

- Latex (Form-X), Ecoflex™ 00-30, PMC™-744, Dragon Skin™, Ecoflex™ Gel (all from Smooth-On);
- Spatula, tweezers, scissors;
- Adhesive Stencil;
- Aluminum and copper tape;
- Absorbing paper;
- Multimeter;
- Beaker, pipette, syringe.

(a)

(b)

(c)

(d)

Figure 3.1: Examples of equipment used throughout the development of the dissertation. (a) Laser Cutter (Universal Laser Systems). (b) Thin Film Applicator (Zehntner). (c) Mixer (Thinky). (d) Drying Oven (Pol-Eko Aparatura).

3.2 Novel Interfacing Method

In this section, the method that was developed during this dissertation for interfacing rigid components with stretchable circuits is described. The technique consists of applying a toluene vapor treatment that will act on the substrate and the ink of the circuit, resulting in a transition in consistency of these materials from rigid to soft. This change ultimately leads to the establishment of both an electrical and a mechanical connection between the circuit and the rigid components.

The workflow of the circuit fabrication consists of 3 main steps: preparation of the elastomeric substrate, circuit printing, and integration of the microchips through the toluene treatment technique, first introduced in this work. After fabrication, the circuit can be transferred to other substrates and/or encapsulated. A thorough explanation of these steps will be provided in the following segments.

3.2.1 Film Preparation

Initially, transfer paper is placed on top of a glass with its silicone surface facing upwards. SIS is poured on top of the paper and a SIS layer of 600 μm is created with the thin film applicator (Figure 3.4a). Toluene is left to evaporate at room temperature for 30 minutes in order to achieve a consistent film with minor defects. Because toluene comprises of a big portion of the SIS solution used, the final layer of elastomer will be thinner ($\sim$ 400 μm) due to evaporation of the solvent in the curing process. Transfer paper is used to prevent the rigid component from binding to the glass after the treatment. Moreover, the SIS substrate adheres less to the paper which eases the future lifting of the system.

In order to create a system that can be placed in the toluene vapor treatment, all the materials used for the fabrication of the substrate must not react with this substance in ways that hinder the whole process. The experimental process that led to the choice of materials suitable for use in the treatment is explained in Appendix A.

3.2.2 Printed Circuit Fabrication

A conductive stretchable ink was provided by ISR for circuit fabrication. The ink was previously synthesized and optimized for stretchable conductive circuits, and contains various metallic fillers (Ag, In, Ga) and a polymeric matrix (SIS) [85]. The exact preparation method for the ink is not revealed in this work.

In order to fabricate the circuit, a stencil was previously designed according to the required shape and then patterned using the CO_2 laser. This stencil was then glued to the surface of the SIS substrate. One layer of LM ink was spread homogeneously through the patterned stencil (Figure 3.4bi). After this, the stencil is removed, leaving the desired circuit printed on the SIS substrate which is cured at 60 °C for 10 minutes.

The circuit can also be directly printed through printing extrusion, using the Voltera^{TM} V-One Extrusion Printer (Figure 3.4bii). This device allows for the selective dispensing of the conductive ink through a nozzle in a completely automated fashion, therefore achieving higher printing resolutions than those of the stencil method. After printing, the ink is cured at 60 °C for 10 minutes.

Alternatively, laser ablation can be employed when circuits require printing with even higher resolutions. In this method, the LM ink is spread over the cured SIS substrate. The ink is then placed in the oven at 60 °C for 10 minutes. After this, a laser beam removes unnecessary ink, leaving behind only the patterned conductive traces that make up the desired circuit (Figure 3.4biii). However, this method can sometimes lead to short-circuits due to LM that fails to be removed by the laser between conductive traces.

3.2.3 Toluene Vapor Treatment

The rigid electronic components are carefully aligned on their respective pads of the circuit with tweezers or with a pick and place machine (Figure 3.4c). Absorbent paper is soaked with liquid toluene and placed inside a glass capsule. Afterwards, the circuit is placed inside this container where toluene will quickly evaporate due to its volatility, forming a small vapor chamber (Figure 3.4d). In order to increase the vapor pressure, and therefore increase the amount of vapor in the chamber, the system is heated to 60 °C for around 45 minutes.

Inside the chamber, toluene will evaporate until its gaseous form reaches a saturation limit. At this point, small droplets of toluene will start to condensate and an equilibrium between the vaporization of the liquid and the condensation of the gas will be met.

The process that leads to the integration of the chip in the stretchable circuit is shown in Figure 3.2. Initially, the toluene vapor softens the SIS substrate, causing the ink to ”sink” in the elastomer due to the weight of the rigid component. As the treatment progresses, the SIS overflows the region that is descending and partially

encapsulates the SMD chip. Because the printed circuit is composed of a SIS-based ink, the vapor is able to soften it and the component slightly penetrates the interconnect.

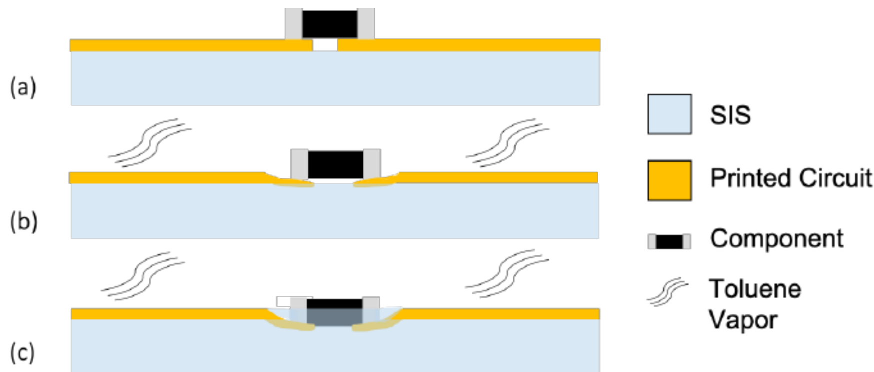

Figure 3.2: Side-view schematics of the integration process through toluene vapor exposure. (a) Component placed on top of the pads of the interconnect (before treatment). (b) Initial stage of the treatment. The conductive interconnect starts to "sink" in the soft SIS elastomer. (c) Final stage of the treatment. The microchip is partially encapsulated in SIS.

Once the treatment is complete, the circuit is placed inside the oven at 60 °C for 5 minutes to re-cure the ink and SIS. This creates a very strong mechanical attachment to the rigid component due to the adhesive nature of the elastomer. After curing, the system regains its firm structure and is ready for encapsulation. The circuit can then be peeled from the transfer paper and be directly placed on glass (Figure 3.4e).

3.2.4 Encapsulation

If the circuit is to be employed in biomedical applications, there cannot be any leakage of LM and/or smearing of the ink onto the body. Because of this, the system needs to be encapsulated in another elastomer to be fully ready to use. However, the circuit can still be utilized without an encapsulation layer for other types of applications.

PDMS was the chosen elastomer due to its incredible stretchable properties and see-through nature (Figure 3.3). After the system is removed from the toluene vapor treatment and is cured for the final time, a 400 μm thick film of PDMS is created on its surface with the thin film applicator. The circuit is then cured in the oven for 1 hour at 60 °C.

The SIS substrate adheres to the PDMS while the latter cures, which makes it possible to lift the whole circuit after the PDMS is ready (Figure 3.5g,h). To fully encapsulate the SIS, another 400 μm layer of PDMS can be deposited on the backside of the stretchable circuit.

This technique allows for the full encapsulation of the circuit with a very stretchable elastomer, at the same time it gives robustness and strength to the bulk of the system. Other elastomers like Ecoflex^{TM} and Latex were also tested with success.

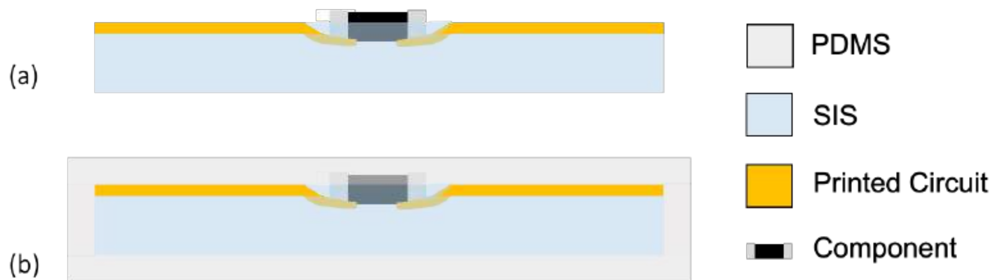

Figure 3.3: Side-view schematics of the encapsulation process using PDMS as the encasing substrate. (a) Stretchable circuit after toluene vapor exposure. The component is encased by the SIS substrate and penetrates the conductive interconnect. (b) Top and bottom encapsulation of the circuit using PDMS.

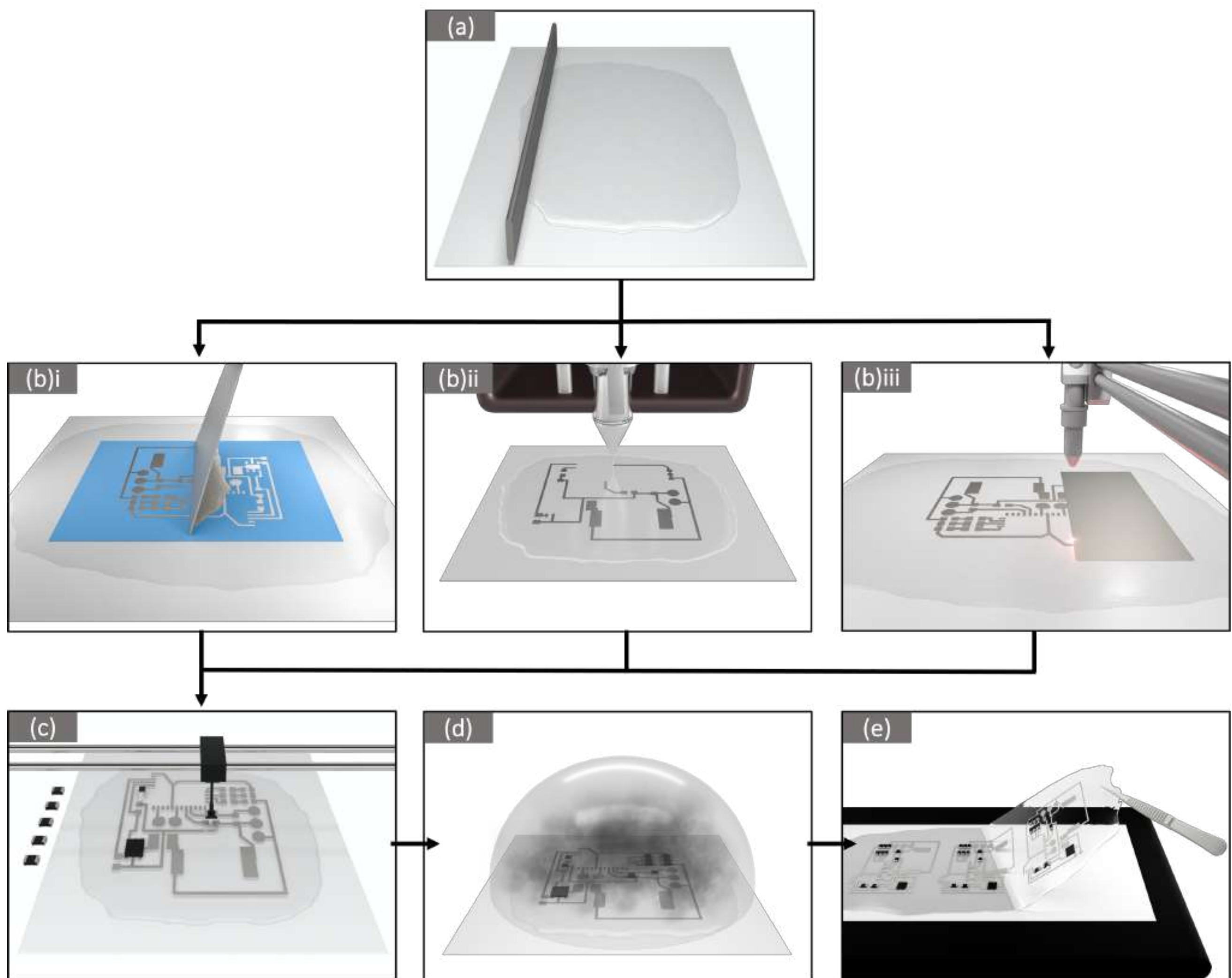

Figure 3.4: Fabrication flow of the stretchable circuit with integrated microelectronics. (a) Creation of a SIS substrate layer on transfer paper using the thin film applicator. (b) Printing of the stretchable circuit through (i) stencil printing, (ii) printing extrusion, and (iii) laser ablation. (c) Placement of the rigid chips on the desired locations of the circuit using a pick and place machine. (d) The printed circuit is exposed to toluene vapor, leading to the integration of the rigid components. (e) After the treatment, the circuit is placed inside an oven. Once cured, the circuit can be peeled from the transfer paper.

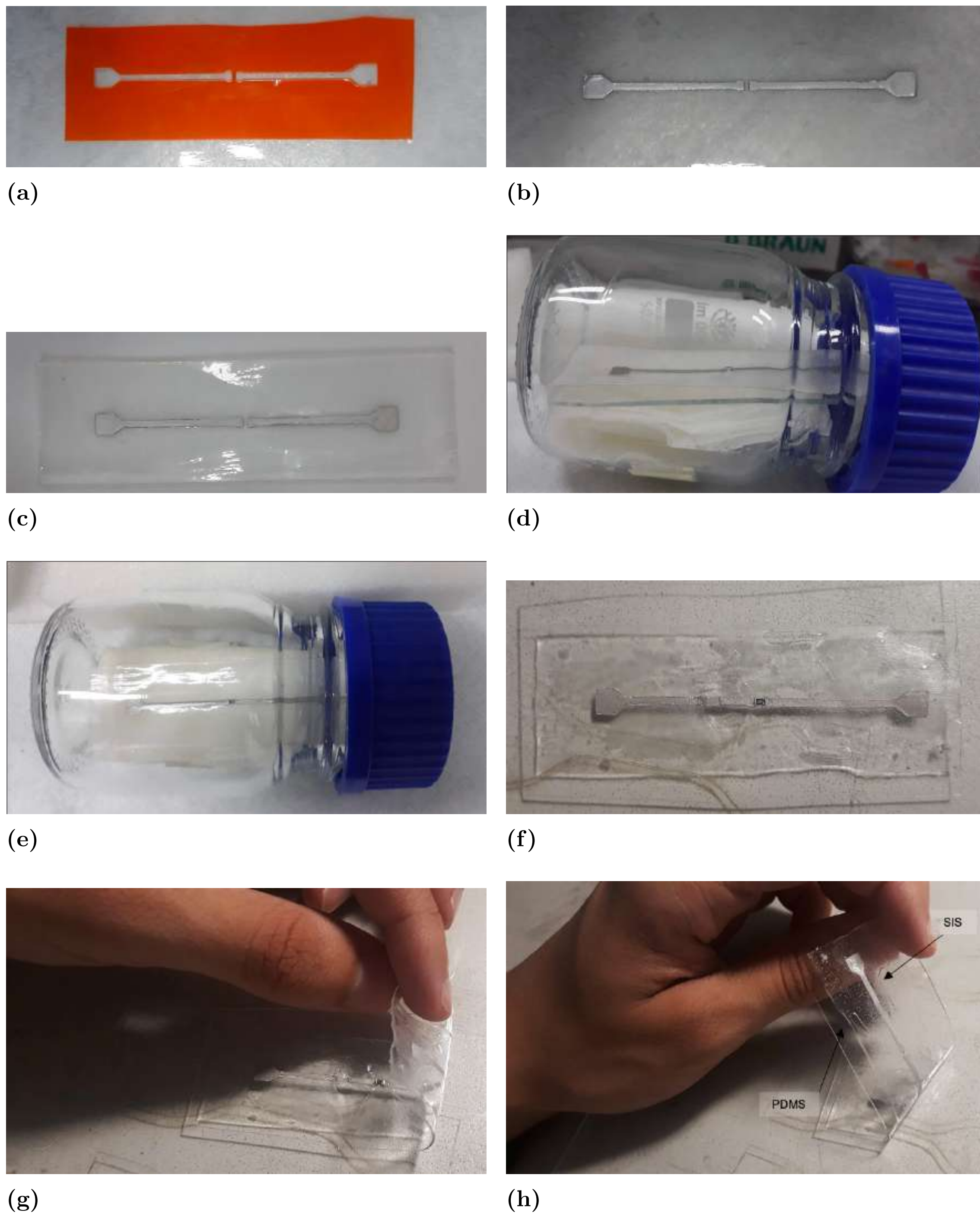

Figure 3.5: Steps for the fabrication of the stretchable circuit with rigid components integrated through the toluene vapor method. (a) Stencil glued over the SIS substrate before circuit printing. (b) Circuit printed through stencil printing. (c) SIS and transfer paper are cut to fit the vapor chamber. (d) Side-view of the circuit with component in the vapor treatment chamber. (e) Top-view. (f) Encapsulated circuit after the vapor treatment procedure and after curing. PDMS was poured over the whole system to encapsulate the circuit. (g,h) Lift-off of the fabricated circuit. PDMS is cured over the system and adheres to the SIS substrate.

3.3 Interface Analysis

This section is focused on the electromechanical characterization of the attachment between the rigid chip and the stretchable circuit, created through the toluene vapor technique. Additionally, the connection site is visually inspected through microscopic images to understand the underlying mechanisms that lead to this integration.

3.3.1 Electromechanical Characterization

It is extremely important to understand the electromechanical behavior of the circuits composed of SMD chips and liquid metal interconnects. Several tests were conducted to provide a quantitative assessment and demonstrate the performance of the developed interfacing method. In this section, these tests will be introduced and described.

Tensile tests were performed to characterize the attachment of the rigid component to the flexible system. Using these techniques, it is possible to investigate the behavior of the samples in stretching conditions and assess if the developed method is fit for biomedical use. For uniformity purposes, all the treated samples were subject to 45 minutes in toluene vapor.

As was mentioned before, tensile tests were conducted through INSTRON 5900 (Figure 3.6), with the Bluehill Universal software. The equipment consists of two pneumatic grips that hold a sample and prevent it from moving during the procedure. As the machine stretches the exemplar, it measures and registers its elongation and electrical resistance with the support of a multimeter.

To avoid tampering the final results, the specimens tested do not have encapsulation layers. By not encapsulating the circuits, it is ensured that the results of the attachment of the rigid component to the soft system are entirely due to the toluene vapor.

Dog-bone shaped specimens were cut using the CO_2 laser and used in all uniaxial tension tests conducted (Figure 3.7). This shape is recommended in this type of tests as it reduces the influence of stress concentrations induced by the loading grips of the INSTRON, thus promoting redistribution of the strain over the whole sample [86]. Details of the dog-bone exemplar used can be seen in Figure 3.8a. This shape and corresponding measurements were adapted from die C, ASTM D412 [87, 88].

Electrical resistance was measured and continuously monitored through strips of copper tape that connected to the top and bottom pads of the samples. Aluminum

tape was used to glue the copper tape to the SIS dog-bone (Figure 3.7). After removal from the transfer paper, the sample is ready for testing.

Figure 3.6: Equipment used in the electromechanical characterization tests. INSTRON 5900 and supporting multimeter used in the tests and closeup of the grips of the INSTRON machine where the sample is immobilized and stretched.

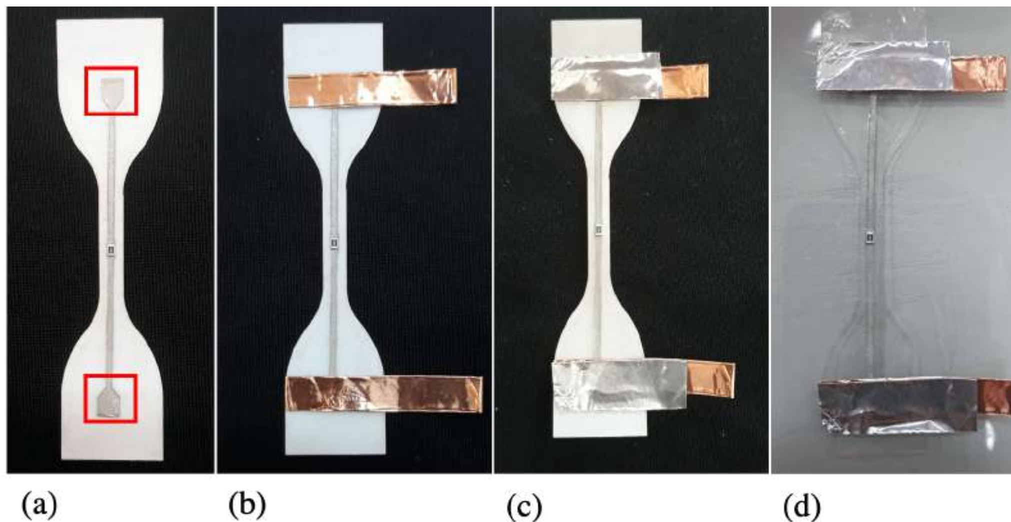

Figure 3.7: Preparation of the SIS dog-bone samples for tensile stretching tests. (a) The paper+SIS system is cut into a dog-bone shape. The top and bottom pads through which the connection to the multimeter is achieved are highlighted in red. (b) Copper tape is connected to the pads. (c) Aluminum tape is glued on top of the copper. (d) SIS is peeled from the transfer paper. This is done last to avoid putting unnecessary pressure on the samples when handling them.

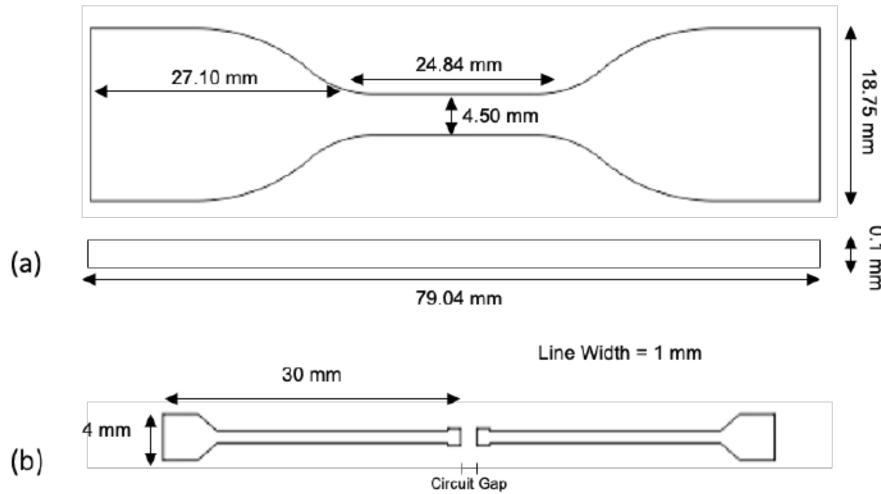

Figure 3.8: Schematics of the dob-bone and circuit track used in the electromechanical characterization tests. (a) Top and side-view schematics of dog-bones used in tensile strain tests and corresponding measurement details. (b) Top schematics of the circuit track and corresponding measurement details.

a) Maximum Stretchability Tests

Break tests were done to determine the maximum elongation the samples could withstand, which corresponds to the amount of strain that leads to mechanical or electrical breakdown of the system. These are the result of substrate rupture or component disconnection, respectively. The samples must be able to withstand at least 20% uniaxial strain so that the method can be employed in biomedical applications.

In order to obtain these measurements, a set of 7 dog-bone-shaped samples with a simple circuit consisting of an ink track with an 1 mm gap (Figure 3.8b) and a 49.9 kΩ surface-mount resistor (±0.5%, 0805, 2.0 mm×1.2 mm×0.45 mm) were stretched until failure with a constant elongation speed of 100 mm/min. The electrical behavior of the samples was monitored while each sample still showed conductivity.

The 49.9 kΩ resistor was preferred over a 0 Ω resistor to avoid measuring results from short-circuits that could form in the fabrication phase or during the tensile tests. A single layer of SIS (400 μm) was used in the production of the samples.

b) Cyclic Loading Tests

In biomedical applications, stretchable circuits applied on the skin or textiles are constantly being mechanically deformed through micro-cycles of strain. Therefore, these systems need to be resistant to fatigue and electrical degradation. Cyclic

loading tests are essential to determine if the interfaces created by the method remain reliable and functional while enduring a high number of displacement cycles.

The designed test consisted of putting a sample through 1000 cycles, each one of them loading up from 0% to 40% strain at a cycle rate of 1.8 cycles/min. The primary goal was to determine if the component remained attached to the sample after 1000 cycles. The electrical behavior of the specimen was recorded throughout the endurance test. Over-the-skin applications need to be functional up to 20% strain, and as such, a maximum strain of 40% was chosen by adding a safety factor of 2.

The circuit used was the same as in the previous break tests (Figure 3.8b), but this time the resistor used was of 10 Ω (±0.5%, 0805, 2.0 mm×1.2mm×0.45mm). Since the multimeter shows a low resolution for high resistances, a component of lower resistance was preferred so that the variations in conductivity could be accurately depicted. Because of the high number of displacement cycles, a layer of SIS with 800 μm in thickness was used in the fabrication of these samples to avoid fatigue and gradual tearing of the substrate.

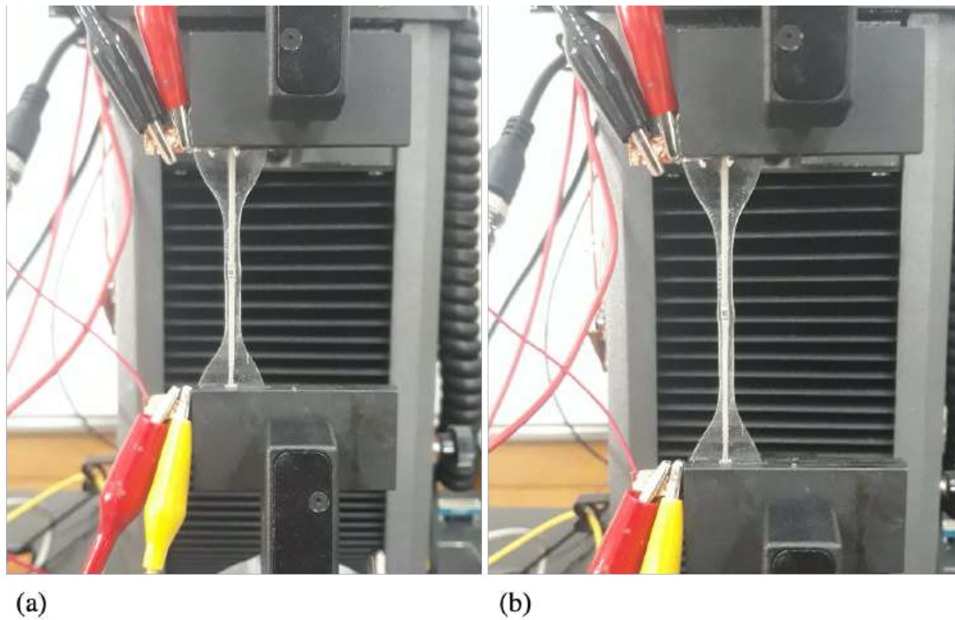

Figure 3.9: Samples during the cyclic loading tests. (a) Initial position of the sample (0% strain). (b) Sample stretched to 40% strain in one of the cycles of the test.

3.3.2 Interface Microscopy

After proving the potential of the technique through the electromechanical characterization tests, it became important to exactly understand the underlying mechanisms that lead to the integration of the rigid chips in the designed circuit. Therefore, the contact between the ink interconnects and the component pins was visually inspected with the Leica S9D Stereoscope.

A sample with a track similar to that shown in Figure 3.8b was exposed to toluene to integrate a 49.9 kΩ surface-mount resistor (±0.5%, 0805, 2.0 mm×1.2 mm×0.45 mm). Microscopic photographs of the top, side, and bottom of the sample were taken before and after the toluene vapor treatment. The objective was to compare the photos from both moments and understand if the changes in the samples proved the initial concept.

SEM (Scanning Electron Microscopy) is a technique that uses a focused beam of electrons over a substrate to create an image [89]. The electrons interact with the components of the substrate and generate signals that give information about the composition and topography of the samples. This technique allows for the creation of images of higher quality, magnification and resolution than those produced by digital microscopes.

SEM images were taken from the interfacing site to better understand the attachment in extreme situations (+45 minutes treatment). To do this, ink was deposited on a SIS substrate as a square shape and a gap was created in the middle of the sample using the laser, exposing the SIS that was previously underneath the ink.

A 2.0 mm×1.2 mm×0.45mm resistor was then placed on top of the ink gap in a way that only its pads contact with the ink to mimic what happens in an actual circuit (Figure 3.10). The sample was placed inside the toluene chamber and was removed after 1h30 to cure at room temperature. The specimen was cut close to the interface to create a small sample that would fit the SEM specimen stage.

A holder that puts the sample at a 90° angle was used in the specimen stage. Signals using secondary electrons were captured and an image was produced to inspect the attachment site of the rigid component.

Figure 3.10: Sample used in SEM analysis for the interface characterization. In this case, 2 resistors were interfaced with the ink over the gap created with the laser. The samples were then cropped over the ink close to the interface to produce small specimens with individual components.

3.4 Printed Circuit Characterization

Toluene vapor exposure of the printed circuit provokes a rigid-soft transition in the conductive ink and SIS substrate. Besides these macroscopic changes, the toluene is also responsible for changing the properties of these materials.

This section aims to study and evaluate the variation in properties of the conductive ink and the SIS substrate and link them to changes in the morphology of the materials' microstructure that take place during vapor exposure.

3.4.1 Improvement of Electrical Conductivity After Treatment

Toluene vapor atmospheres are harsh environments that soften both the conductive trace and the SIS substrate. Because of these modifications, some of the conductive ink and SIS might blend, modifying the concentration of the components that make up the conductive interconnects, and thus possibly increasing the electrical resistance of the printed circuit.

However, during the execution of the project, it was found that the vapor procedure actually improved the electrical resistance of the printed traces. To characterize this change, a set of resistance measurements was executed to 6 samples using a multimeter. The electrical resistance of the specimens was measured at 3 different moments: before the toluene treatment, after a 45 minutes toluene treatment, and after 5 displacement cycles loading up from 0% to 40% strain.

The thickness of the samples was of 400 μm and the circuit used in these tests consisted of a continuous track of ink as the conductive interconnect (Figure 3.11). A double layer of ink was used to obtain more robust and consistent electrical resistance measurements.

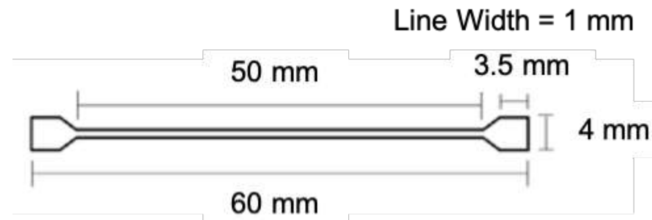

Figure 3.11: Schematics of the circuit track used in the characterization of the printed circuit and corresponding measurements.

To understand and explain the changes in electrical resistance observed, the morphology of the ink's microstructure was analyzed through SEM, before and after the toluene treatment. The preparation of the ink samples went along the following steps:

1. Deposition of a 300 μm layer SIS layer on transfer paper with the thin film applicator. The layer is cured at room temperature for 30 minutes.
2. Deposition of another layer of SIS with 300 μm in thickness on top of the current layer. The new layer is cured at room temperature for another 30 minutes. The final substrate has around 400μm in thickness after curing both layers.
3. Small squares of ink (15mm x 15mm) are printed on the surface of the SIS substrate (Figure 3.12). The ink cures for 1 hour at room temperature.
4. The samples are placed in the toluene vapor treatment for 45 minutes (same time as in the usual treatment for rigid components).
5. The samples are removed from the vapor chamber and cure at room temperature for 1 hour.
6. The SIS around the small squares is cut using scissors.

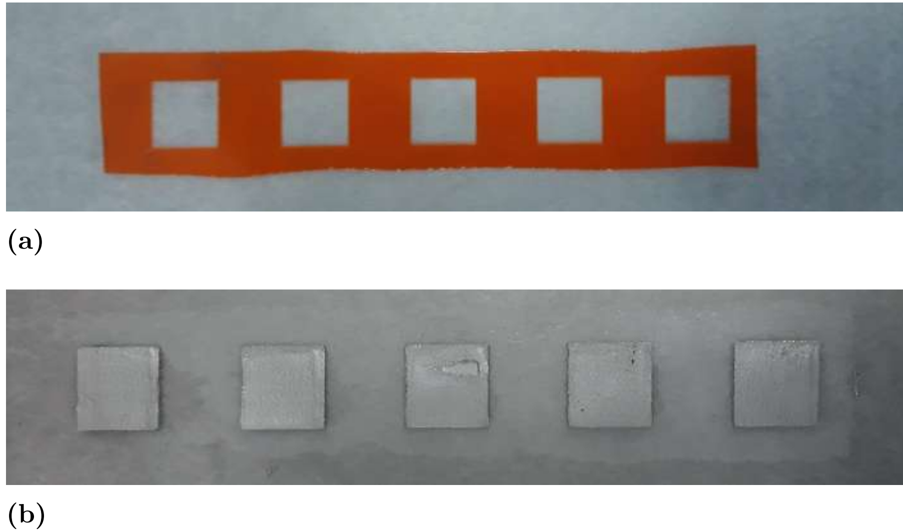

Figure 3.12: Preparation of the ink samples for SEM analysis. (a) Stencil used for printing the ink glued on the SIS substrate. (b) Small squares of ink printed on the SIS substrate.

The samples were prepared keeping in mind the requirements of the SEM procedure. The deposition of the substrate was done in two different iterations of thinner layers to reduce bubble entrapment that could cause the sample to move under high vacuum. Curing under room temperature also showed to be very effective to reduce the amount of bubbles in the substrate. Small squares of ink were printed so that the samples would fit the specimen stage of the SEM equipment without cutting through the ink, which would expose LM to the surface of the samples. Cross-section images of the conductive trace were acquired by freezing the samples in liquid nitrogen and firmly cutting them over the ink composite.

Signals using secondary electrons and back-scattered electrons were captured and the images were created to characterize the organization of the constituents of the materials, before and after the treatment.

Then, the electrical conductivity of the 6 initial samples, before and after vapor exposure, was determined according to Equation 3.1. This was done after analyzing the composite's morphology because the calculation required the determination of its thickness, which could only be achieved through inspection of the SEM micrographs. The trace measurements used for the conductivity calculation are exhibited in Figure 3.11.

$$\sigma = \frac{\ell}{RA} \tag{3.1}$$

Where σ is the conductivity of the trace, ℓ is the length of the specimen (5 mm), R is the electrical resistance of the trace, and A is the cross-sectional area of the specimen – thickness × line width (1 mm).

Finally, a sample without a component was used in a cyclic loading test of only 5 displacement cycles loading up from 0% to 40% to characterize the behaviour of the ink under repeated strain.

3.4.2 Improvement of Strain Tolerance of the Stretchable Circuit After Treatment

In order to understand if the toluene treatment has any influence in the maximum strain that can be reached by the SIS substrate, 6 specimens (3 treated and 3 untreated) were stretched until loss of conductivity or substrate rupture. Similarly to the circuit from the previous section, these also consisted of a continuous ink track as the conductive interconnect (Figure 3.11).

All the samples used in electrical tests were fabricated using a single layer of SIS (400 μm). The samples were cut into dog-bone shaped specimens and electrical conductivity was continuously measured through copper tape and a multimeter in a similar to the other electromechanical tests.

To explain the conclusions obtained through this test, treated and untreated SIS samples were observed under SEM. The fabrication procedure was very similar to the one enumerated in Section 3.4.1, only skipping step number 3. The changes in the morphology of the SIS substrate after the toluene treatment were identified and linked to the results from the strain tolerance test.

4

Results

In this chapter, extensive electromechanical tests are presented in order to evaluate and characterize the attachment of the surface-mount components to the overall system. Furthermore, the interface between the rigid and soft materials will be studied based on visual inspection. The changes in the properties and microstructure of the conductive ink and SIS substrate after vapor exposure will also be investigated and studied.

4.1 Interface Analysis

This section focuses on the characterization and study of the connection between the rigid component and the stretchable circuit, which is established through the toluene vapor treatment.

4.1.1 Electromechanical Characterization

Electromechanical tests were carried out to demonstrate and characterize the attachment of the rigid components to the stretchable printed circuit. This included tests for maximum stretchability and cyclic loading. The procedure leading up to each individual experiment was previously described in Section 3.3.1. For uniformity purposes, all the treated samples were subject to 45 minutes in toluene vapor.

a) Maximum Stretchability Tests

Maximum stretchability tests were performed to obtain a quantitative measurement of the maximum stretchability that the samples could withstand before electrical or mechanical failure. For each sample, a single 49.9 kΩ resistor was interfaced over a 1 mm gap in an ink track. This resistor was used instead of a 0 Ω component to avoid the misinterpretation of short-circuits as viable results.

A set of 7 different samples was treated with toluene vapor to integrate the surface-mount resistors. The specimens were then subject to an uniaxial tensile loading test to demonstrate the performance of the interfacing method. The electrical resistance was monitored during the application of strain and the results obtained are exhibited in Figure 4.1. When the contact with the component is lost the electrical resistance shoots up to very high values. This point is marked on the graph with a square for each individual specimen.

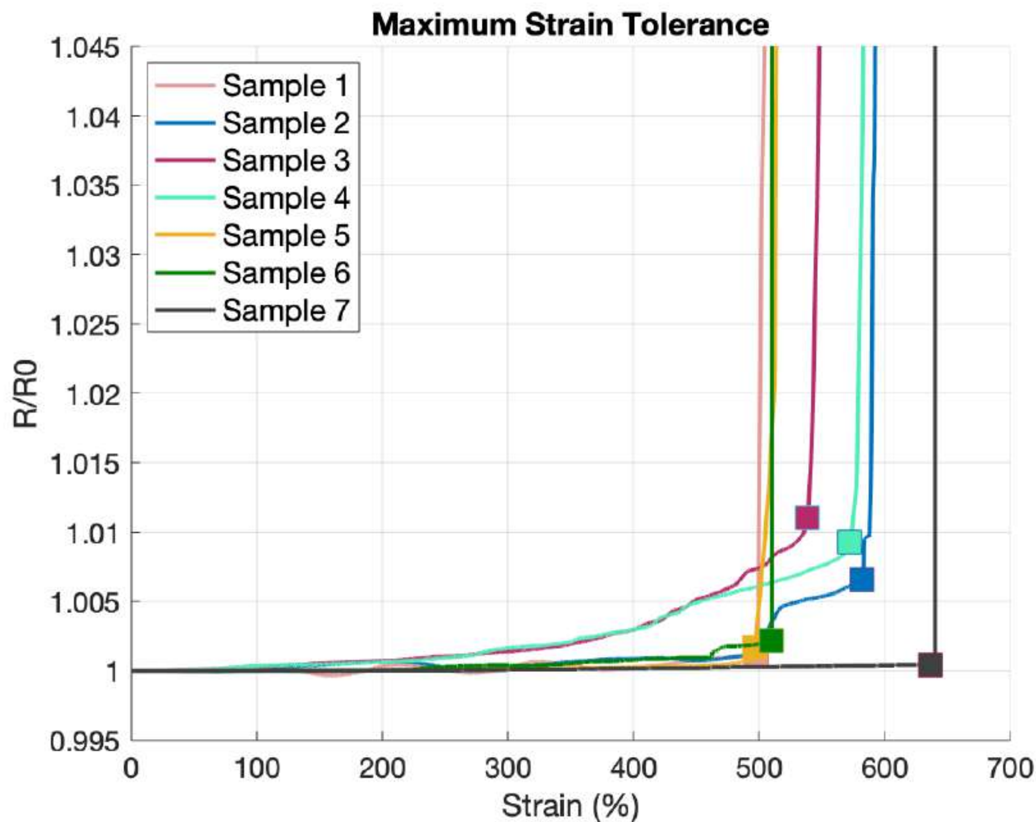

Figure 4.1: Results of the uniaxial tension test performed at a constant rate of 100 mm/min for each individual sample. The electrical resistance was normalized as R/R_0. Each sample is represented by a different color for better comprehension of the graphic. A square was used to mark the point correspondent to electrical failure in each of the samples.

The percent elongation at break for the set of samples tested was 550 ± 52%, with sample 7 showing the highest recorded elongation, at ~650%. The great attachment evidenced by the results is due to the SIS surrounding the resistors and the components piercing through the soft structures during the vapor treatment (later proved in detail in Section 4.2). Electrical failure occurs due to component detachment for all the tested samples.

Small holes start appearing on the stress zones of the samples at around 200% displacement (Figure 4.2a) and grow increasingly larger with strain (Figure 4.2b). These tears are most definitely facilitated by the low thickness of the substrate and the penetration ability of the rigid components during the treatment. In spite of this, the appearance of the holes is not responsible for the immediate failure of the system.

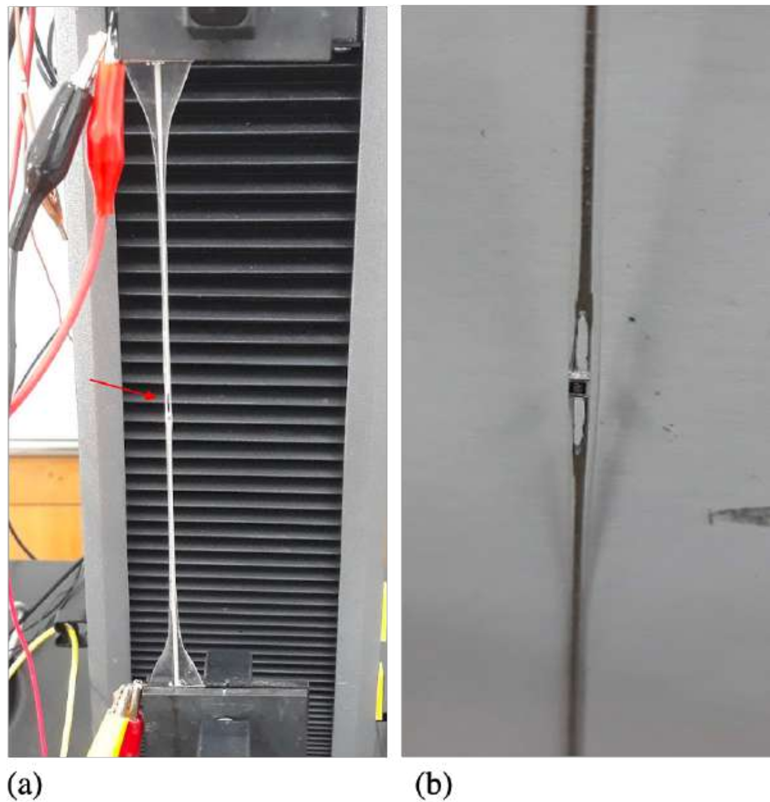

Figure 4.2: Tears appear on the samples during the uniaxial tensile loading tests. (a) Sample stretched to 200% strain. Small gaps start appearing on the SIS at this strain (red arrow). (b) Closeup of sample stretched to 500% strain. The holes progressively increase in size with the amount of strain.

Figure 4.3 compares the obtained result with other recent works on the subject. As can be seen, the average maximum displacement obtained through this method (550%) is 2.75× higher than the highest value presented in previous works (200%). It is important to note that the result obtained by Hu et al. [81] relies on an anisotropic conductor and specific micropatterning for each individual rigid component, which adds to the complexity of the fabrication process. Likewise, many other results displayed on the graph are only achievable through very complicated setups. The presented method, in comparison, does not require as many steps nor the deposition of additional material. Elimination of one or more fabrication steps is beneficial for

lowering fabrication costs, especially when large-scale fabrication is intended.

It is also worth mentioning that all the results exhibited in Figure 4.3 were achieved using circuits sealed with encapsulation layers, which help reaching superior values of maximum strain but at the cost of an additional fabrication step. The proposed method does not have an encapsulation layer and the results were still very much superior to those achieved with other state-of-the-art techniques.

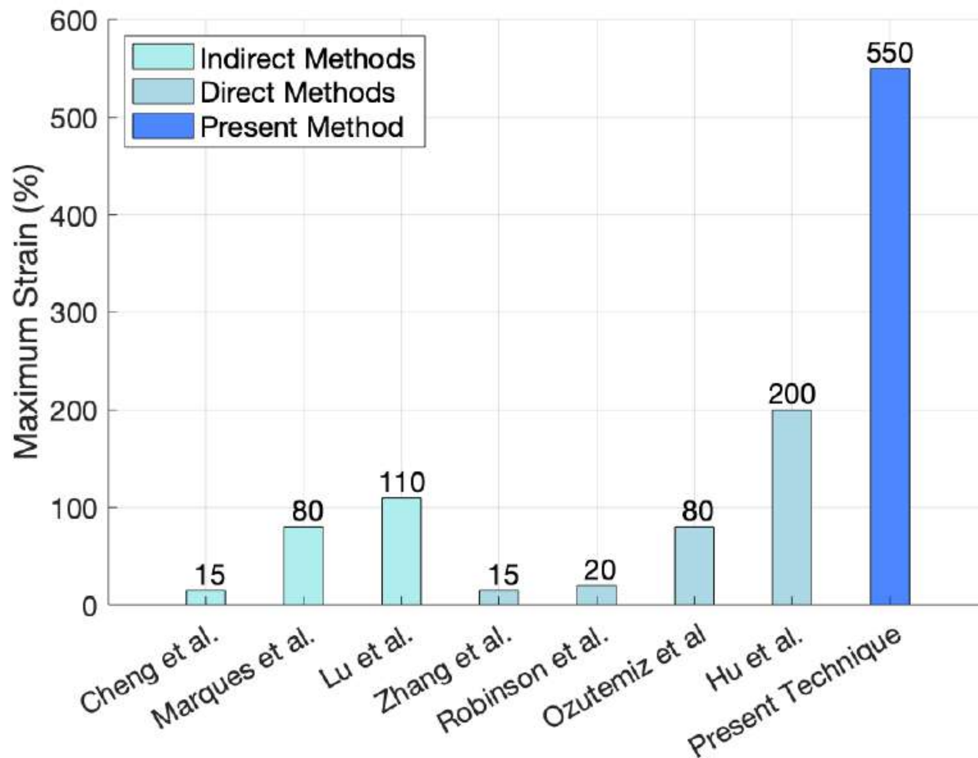

Figure 4.3: Maximum stretchability comparison between results obtained with the developed method and other techniques by Cheng et al. [79], Zhang et al. [82], Ronbinson et al. [80], Ozutemizet et al. [84], Marques et al. [32], Lu et al. [63], Hu et al. [81]. In all the methods except for the present technique, the circuits were sealed with encapsulation layers, which helps in achieving superior amounts of maximum strain.

b) Cyclic Loading Tests

Resistance to mechanical and electrical degradation is crucial for any stretchable device in the medical field as materials are often stretched numerous times in each singular application.

It is, then, important to understand if the attachment of the resistor interfaced through toluene vapor exposure is strong and reliable enough to withstand repeated

deformation. To verify if the fabricated circuit remains functional under various loading conditions, the electrical behavior for a specimen loaded 1000 cycles between 0% and 40% strain was examined. The maximum strain of 40% was chosen by using a safety factor of 2 over the minimum displacement for over-the-skin applications (20%).

A 10 Ω resistor (±0.5%, 0805, 2.0 mm×1.2mm×0.45mm) was used in the tests and the primary focus was the attachment and electrical stability of this component throughout the whole procedure. During the experiments, it was found that a substrate made of a 400 μm SIS was inadequate for the test, as it would tear along the lines of the track. Because of this, a substrate with 800 μm was employed in the fabrication of the sample for this test. The results of the cyclic loading test can be seen in Figure 4.4.

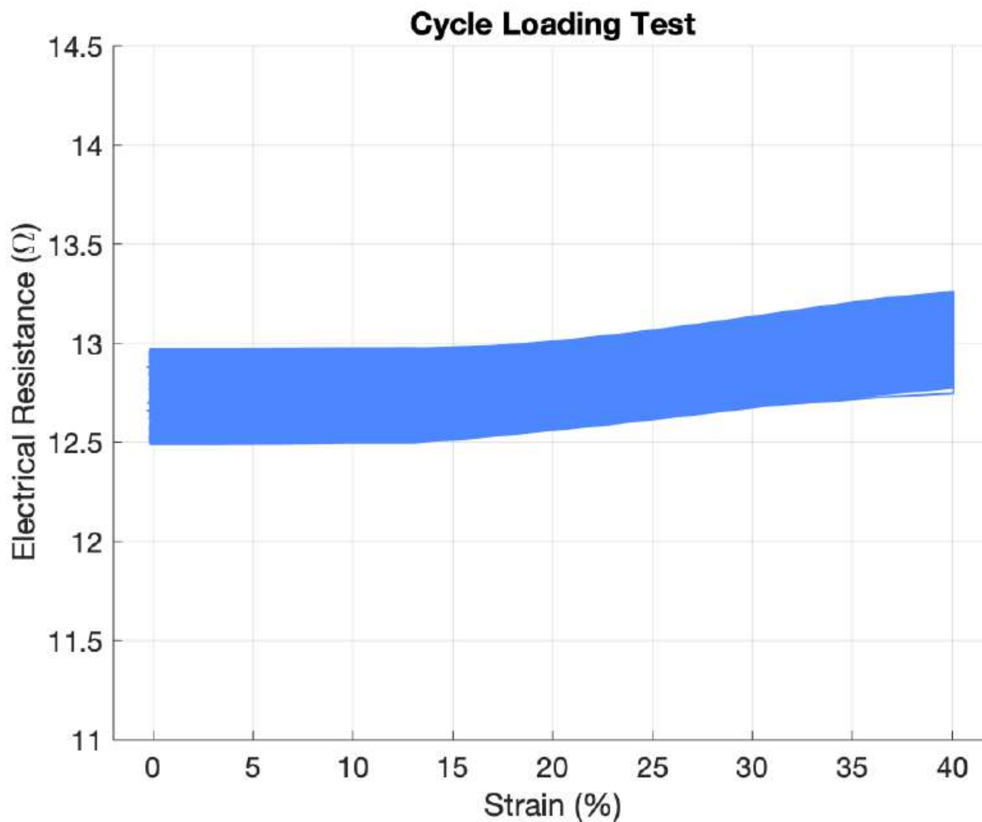

Figure 4.4: Cyclic loading test carried out with a 10 Ω resistor, interfaced with the circuit through the toluene vapor method. The graphic represents the electrical resistance of the samples during the 1000 cycles loading up to 40% strain at a cycle rate of 1.8 cycles/min.

As it can been seen on the graph of Figure 4.4, the interface created with the vapor method could withstand 1000 cycles of mechanical loading up to 40% strain. In addition, only a small variation of around 0.5 Ω is measured between the maximum and minimum values across all strain values. This change in electrical resistance is negligible enough to not interfere with the functionality of most digital circuits.

The graphs from Figure 4.5 were elaborated to better understand the variation of the electrical resistance over the cycles. From cycles 0 to 20, the resistance gradually decreases as the LM cracks inside the conductive interconnect. Then, it progressively increases due to a combination of ink fatigue and substrate degradation, which leads to small tears under the printed trace. However, the performance of the system can be considered stable all throughout the test. In the last 10 displacement cycles, the changes in electrical resistance are extremely predictable and consistent. Overall, the test was considered successful as the sample was able to maintain a stable electrical performance over 1000 displacement cycles.

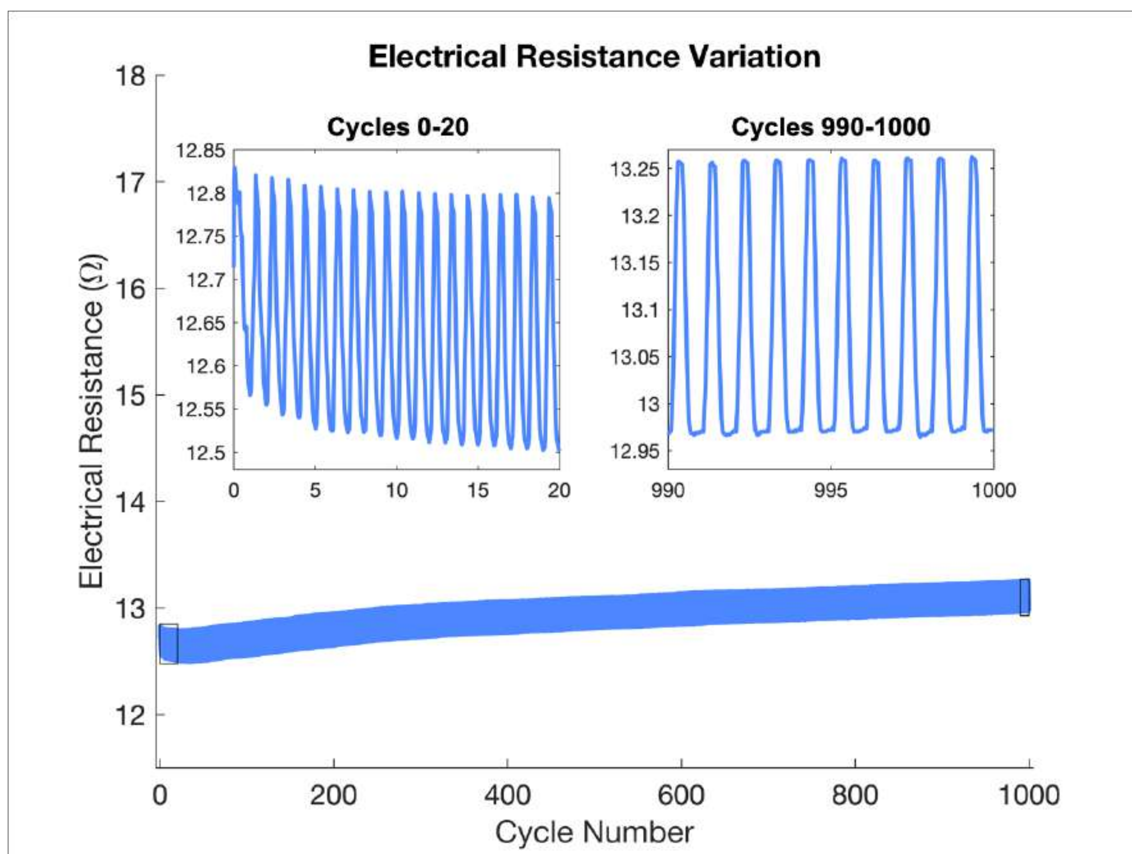

Figure 4.5: Representation of electrical resistance variation over the displacement cycles. The smaller windows correspond to zooms from cycles 0-20 and 990-1000.

4.2 Interface Microscopy

After identifying the potential of the technique through the electromechanical characterization tests, it became important to exactly understand the underlying process that leads to immobilization of the SMD components in the soft system. To achieve this, a resistor (0805, 2.0 mm $\times$ 1.2 mm $\times$ 0.45 mm) was interfaced over a 1 mm gap in an ink track through a 45 minute vapor treatment. The integration was inspected with top (Figure 4.6), side (Figure 4.7) and bottom (Figure 4.8) microscopic pictures, taken before and after the vapor treatment. A 400 μm thick substrate was used for the top and side pictures, while a sample with 200 μm in thickness was used for the bottom ones.

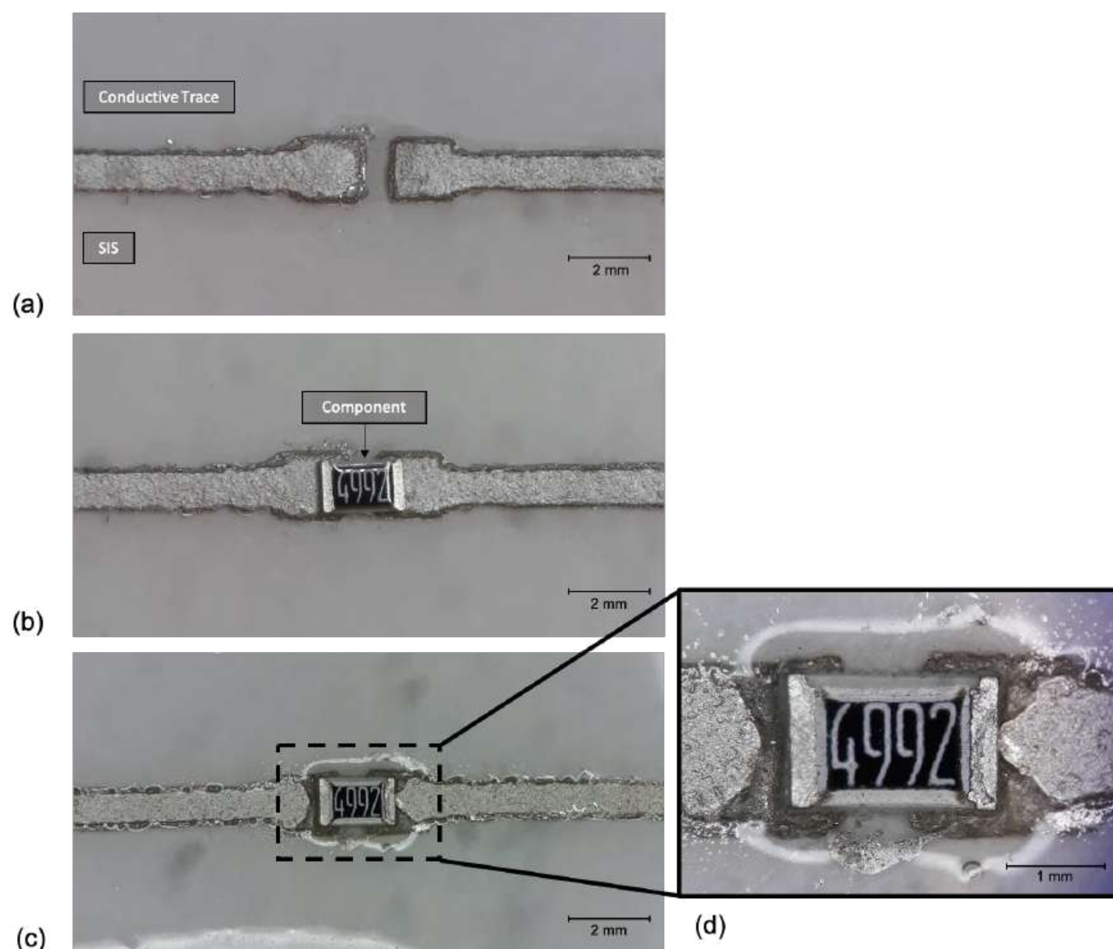

Figure 4.6: Top pictures of the process for integration of a surface-mount 49.9k in a sample. (a) Conductive trace printed on the SIS substrate. (b) Component placed on top of the pads of the interconnect (before treatment). (c) Aspect of the system after integration of the rigid component through the vapor treatment. (d) Closeup of the previous picture at the interfacing site.

The provided microscopic pictures clearly prove the concept explained earlier in section 3.2.2. Because the SIS elastomer softens during the treatment, the weight of the rigid component is able to push the pads of the conductive interconnect down during the vapor treatment, causing SIS to overflow the region. This is visible in the images from Figure 4.6.

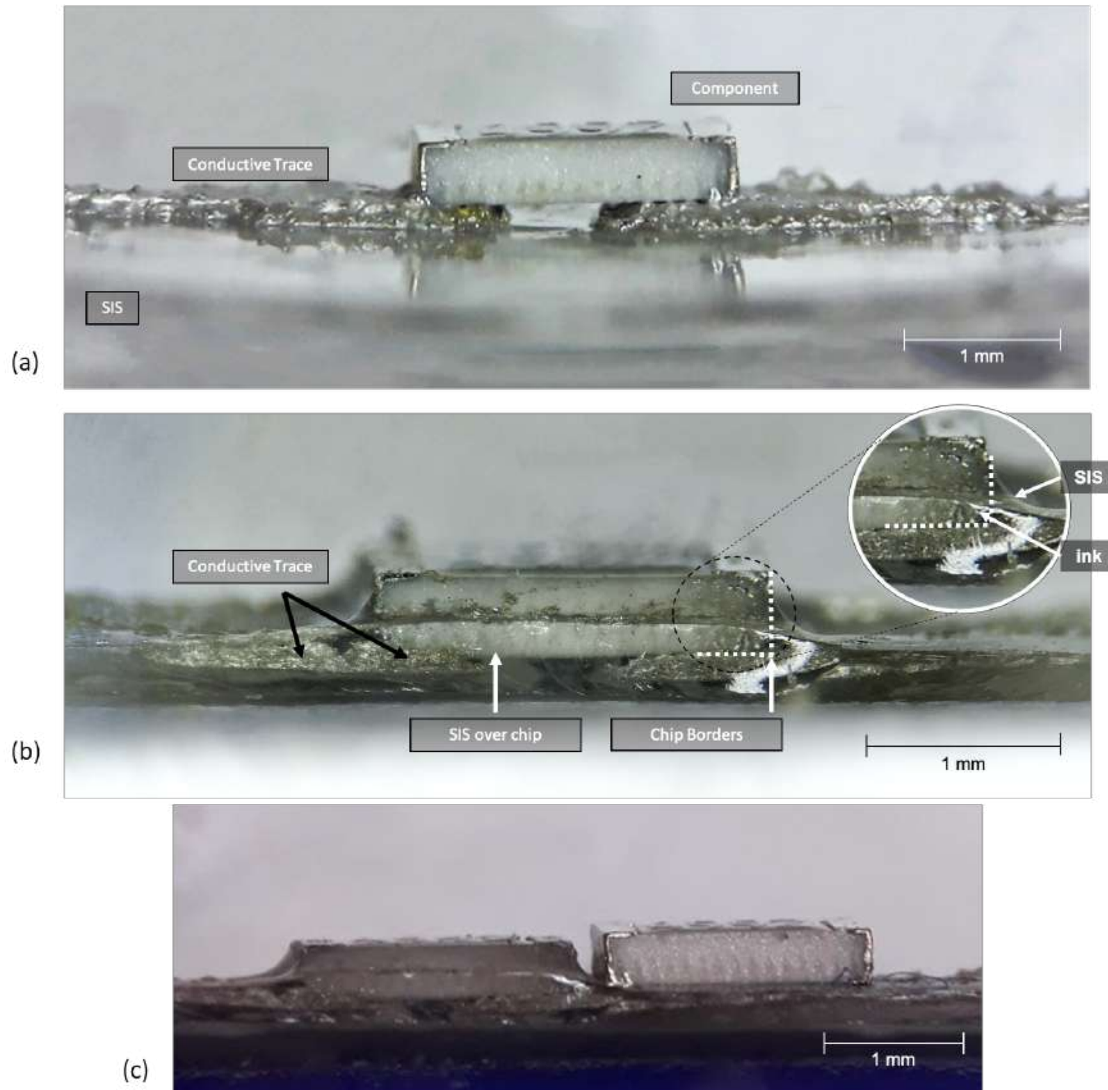

Figure 4.7: Side-view pictures of the process for integration of a surface-mount 49.9k in a sample. (a) Component placed on top of the pads of the interconnect (before treatment) – equivalent to Figure 4.6b. (b) Aspect of the system after integration of the rigid component through the vapor treatment – equivalent to Figure 4.6c/d. (c) Integrated component and similar resistor (not integrated) placed side-by-side.

The integration phenomenon is even more evident in the side-view pictures. Before toluene exposure (Figure 4.7a), the whole component sits on top of the conductive trace. However, after the treatment (Figure 4.7b), more than half of the resistor is encompassed in SIS. It is also evident that the pads of the conductive trace are absolutely encapsulated in the elastomer. Because the ink is composed of SIS, it also softens during the treatment which causes the resistor to slightly penetrate the interconnect. After the treatment, the whole system is left for curing and, due to the adhesive nature of SIS, the attachment becomes extremely strong and reliable. The integration of the chip is even more visually striking when a similar resistor (not integrated) is placed right next to it (Figure 4.7c).

A sample with a different substrate thickness (200 μm) was used to inspect the bottom part of the circuit. The captured images can be seen in Figure 4.8. Because the substrate has a lower thickness, a portion of the resistor coated with ink actually appears on the bottom side of the sample, further proving the "sinking" concept. This means that during the treatment the component is able to penetrate more than 200 μm in ink and SIS.

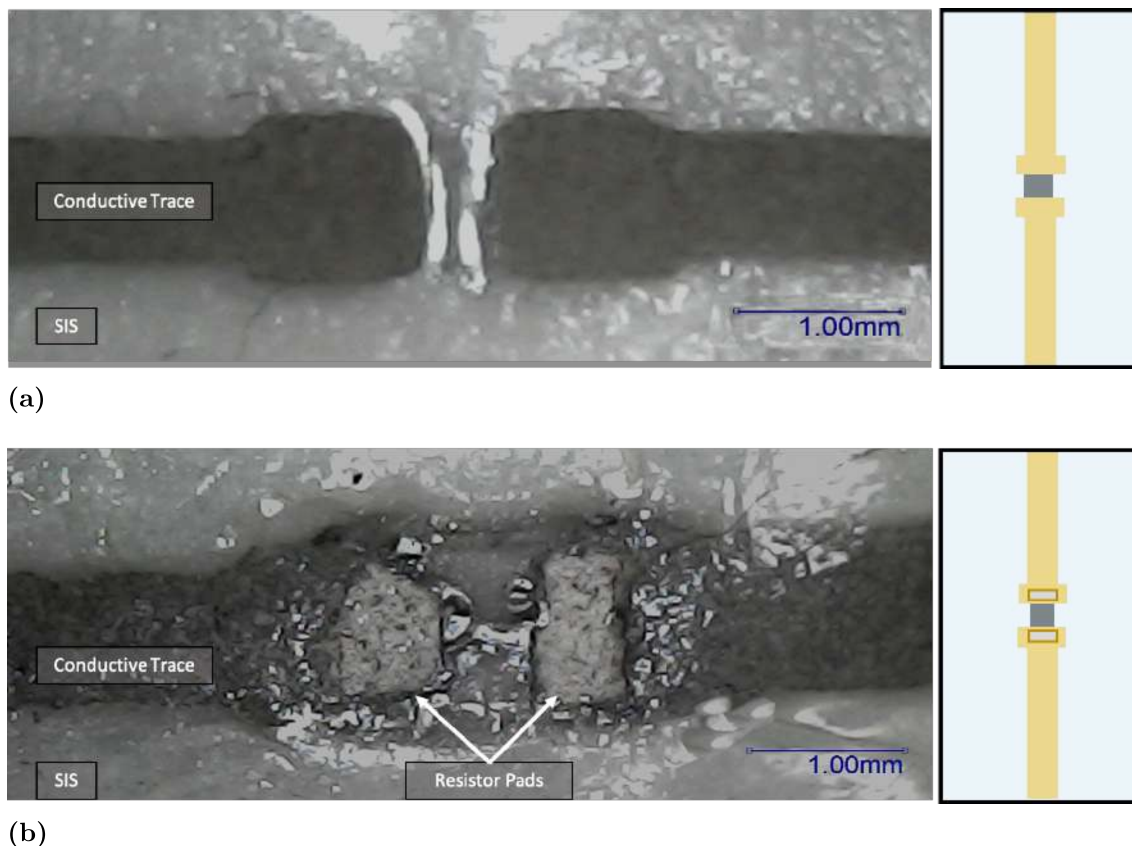

Figure 4.8: Bottom pictures and schematics of a sample with a surface-mount 49.9k resistor integrated in a stretchable circuit. (a) Sample before the treatment. (b) Sample after the treatment.

If the toluene treatment is performed for more than 45 minutes, the rigid chip and conductive interconnect will have more time to penetrate the SIS substrate. This is demonstrated in Figure 4.9, which depicts a component that was left for more than 1h30m in toluene treatment. It can be seen that the SIS engulfs almost completely the chip from all sides. With longer treatment times, the SIS becomes even softer and the conductive interconnect drops below the elastomer, becoming totally coated by it.

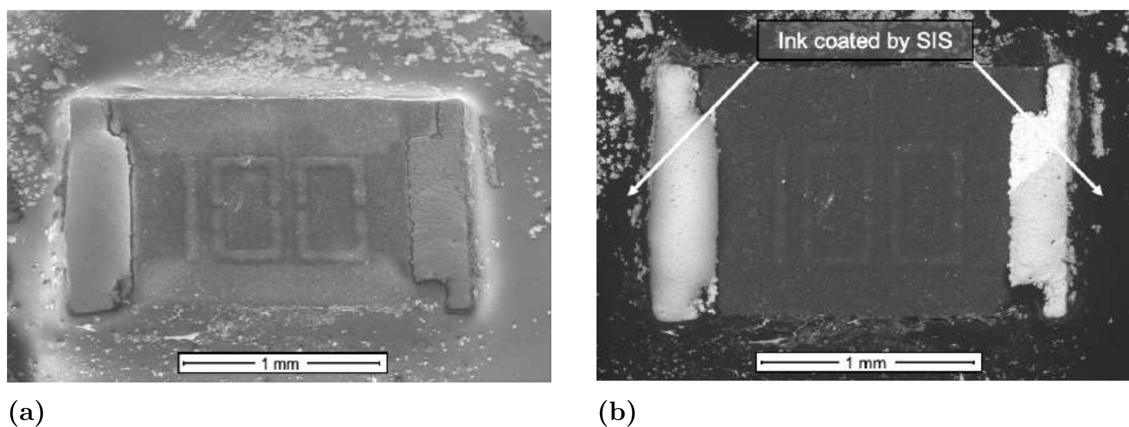

(a) **(b)**

Figure 4.9: Top images of the integration site after an extreme toluene treatment. (a) Image produced using secondary electrons (SE). The rigid component is totally encompassed in SIS. (b) Image produced using back-scattered electrons (BSE). SIS (black in the picture) coats the conductive interconnect (it would have a metallic color if it was visible).

4.3 Printed Circuit Characterization

This section focuses on the evaluation of the changes in properties and microstructure of the materials that compose the stretchable circuit, namely of the conductive ink and SIS, after toluene treatment. Likewise, the results from the tests performed to assess variations in electrical conductivity and maximum strain tolerance will be presented and associated with the microstructural rearrangement observed in the referred materials.

4.3.1 Improvement of Electrical Conductivity After Treatment

During the execution of the project, it was discovered that toluene vapor might not only be used for interfacing rigid components, but also to improve the electrical resistance of the printed traces. In order to characterize this change in resistance, 6 samples without a resistor and with double-layer continuous ink track were placed inside the toluene chamber for 45 minutes. Their conductivity was measured before and after the toluene treatment, as well as after 5 displacement cycles loading up from 0% to 40%. The mean value of the resistance measured in the 6 samples in each of the described moments is displayed on the graph in Figure 4.10.

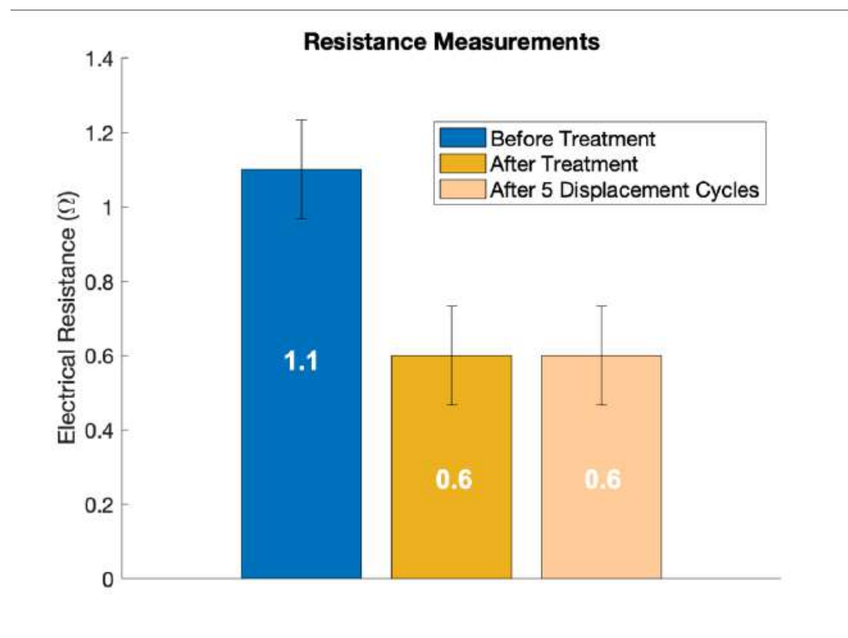

Figure 4.10: Resistance measurements of the samples tested in the electrical characterization. The mean value is exhibited in the middle of the bars, for each of the moments when electrical resistance was measured.

It can be seen that the toluene vapor improves the performance of the ink tracks by lowering their electrical resistance by half. The resistance remains even after 5 full displacement cycles, which suggests that the ink treated with toluene is stable after a low number of displacement cycles. The microstructure of the conductive ink, before and after toluene exposure, was analyzed to understand this drop in electrical resistance. To do this, samples consisting of ink deposited over a SIS surface were prepared and some of them were exposed to toluene vapor. Then, treated and untreated samples were examined under SEM and the resulting images are represented in Figures 4.12, 4.13, and 4.14.

Concerning the morphology of the ink's microstructure, one of the most striking differences is the rearrangement of the components into cluster structures after vapor exposure. This is visible when comparing images from Figure 4.12. For each individual cluster, the silver flakes and LM appear to be more compact and the SIS (black in the pictures) that makes up the ink composite seems to have almost disappeared. This is more visible when an ultrathin layer of ink is applied using spray coating, as can be seen in Figure 4.12. However, it can also be seen to a lesser extent in samples in which a thicker layer of the ink is applied using a stencil, like the one represented in 4.13a,b. These results suggest that the toluene treatment increases the percolation of the metallic fillers present in the conductive ink.

The components of the ink seem not only to rearrange spatially, but also chemically. As it can be seen in Figure 4.13c, there were barely any $AgIn_2$ particles before the toluene vapor treatment. However, it appears that, during the treatment, the silver flakes interact with the LM, resulting in very abundant $AgIn_2$ particles surrounded by Ga-rich film (4.13d,f).

The explanation for the previously described phenomena might lie on the findings provided by the cross-section images of the ink composite. As it can be seen in Figure 4.14, SIS seems to be common throughout the composite before the procedure. After the treatment, SIS appears to have migrated to the surface of the conductive interconnect and formed a very thin layer. Some of the elastomer might have also gone below the ink. Besides, $AgIn_2$ particles at the surface of the composite became more numerous after the treatment.

These discoveries suggest that, as the toluene starts acting on the ink, SIS leaves the composite to surrounding areas which compacts the rest of the ink's components. This increases the percolation of the metallic fillers in the composite (Figure 4.11), resulting in the rearrangement of the components in blackberry-like clusters (Figure 4.12b) and the coating of the Ag particles by the In (Figure 4.13b). These phenom-

ena can be considered responsible for the drop in electrical resistance when the ink samples undergo toluene exposure.

It was also found that the thickness of the ink composite decreased during the toluene vapor treatment, as is evidenced in Figure 4.7a,b. This can also be attributed to migration of SIS to regions above and below the interconnect.

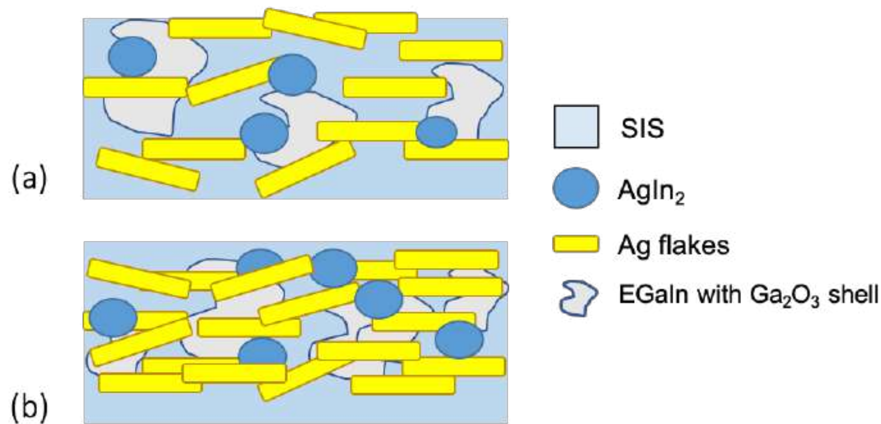

Figure 4.11: Cross-section schematics showing the rearrangement of the composite's components during the toluene treatment. (a) Before toluene exposure. The particles are spread over the trace. (b) After toluene exposure. SIS migrates to the top and bottom of the conductive trace. Components become more compacted, leading to a spatial rearrangement and increased percolation of the metallic components. $AgIn_2$ particles become more numerous.

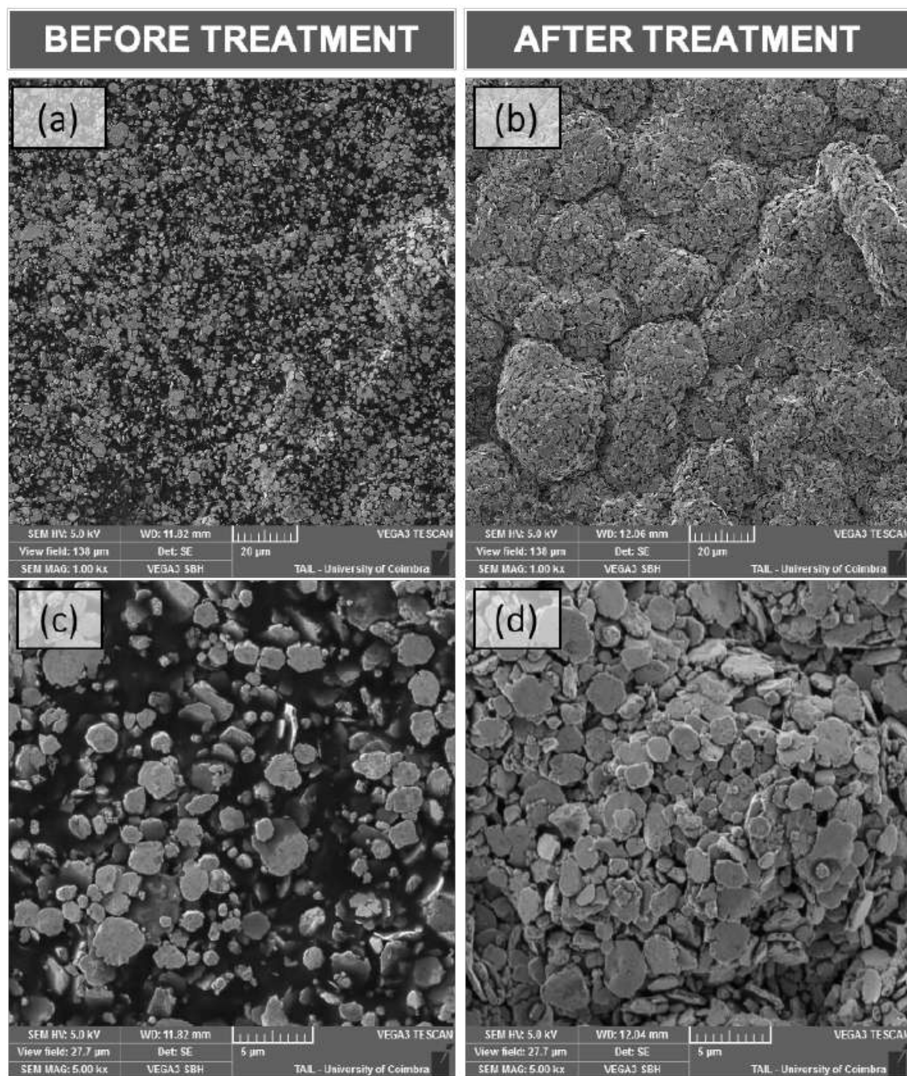

Figure 4.12: Images of a thin layer of ink deposited through spray coating, before and after toluene vapor treatment. (a) Secondary-Electrons (SE); Magnification: 1000x. (b) SE; Magnification: 1000x. (c) SE; Magnification: 5000x. (d) SE; Magnification: 5000x.

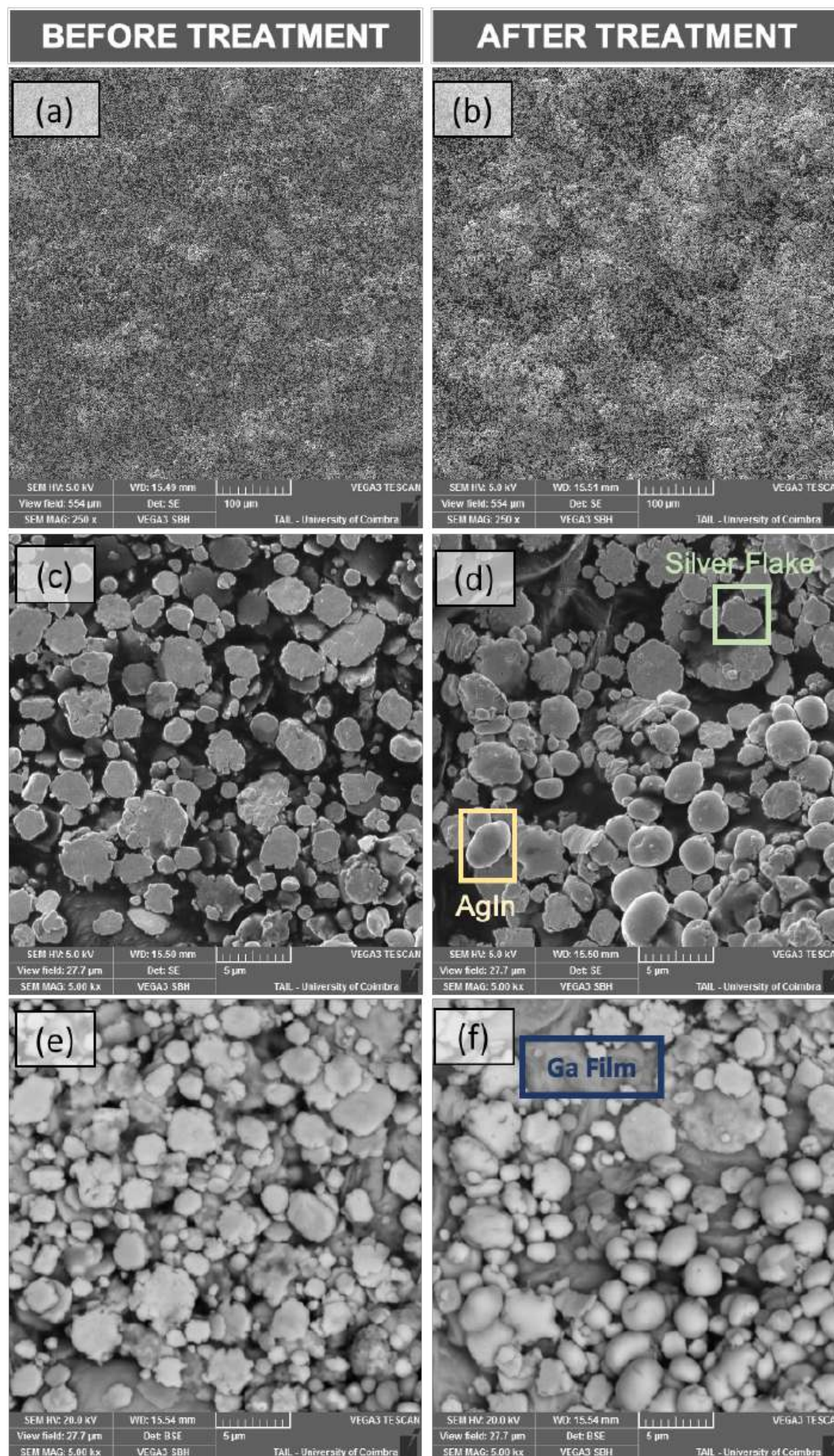

Figure 4.13: Images of a layer of ink deposited through stencil printing, before and after toluene vapor treatment. $AgIn_2$ particles are characterized by their rounder shape compared to that of silver flakes. (a) SE; Magnification: 250x. (b) SE; Magnification: 250x. (c) SE; Magnification: 5000x. (d) SE; Magnification: 5000x. (e) BSE; Magnification: 5000x. (f) BSE; Magnification: 5000x.

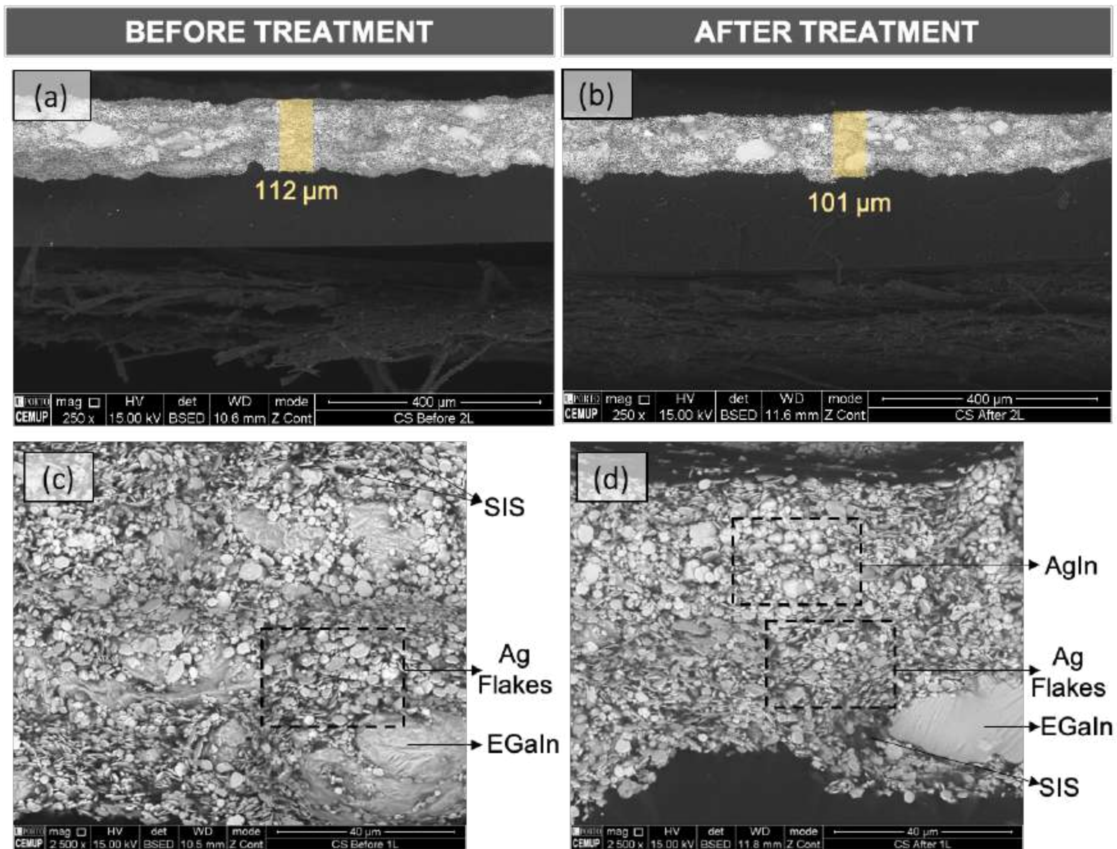

Figure 4.14: Cross-section images of a layer of ink deposited through stencil printing, before and after toluene vapor treatment. (a) SE; Magnification: 250x.; Thickness of the layer: 112 μm. (b) SE; Magnification: 250x; Thickness of the layer: 101 μm. (c) BSE; Magnification: 2500x. (d) BSE; Magnification: 2500x.

The resistance measurements in Figure 4.10 and the thickness calculation in Figure 4.14 made it possible to determine the conductivity of the conductive traces before and after the toluene treatment through Equation 4.1.

$$\sigma = \frac{\ell}{RA} \tag{4.1}$$

Where σ is the conductivity of the trace, ℓ is the length of the specimen (5 mm), R is the electrical resistance of the trace, and A is the cross-sectional area of the specimen – thickness × line width (1 mm).

The conductivity was calculated according to the trace measurements shown in Figure 3.11. By analysing Figure 4.15, it can be seen that the conductivity of the traces after the toluene vapor treatment is more than twice higher than the conductivity measured prior to the procedure. This is explained by the drop in electrical resistance and the decrease in the trace's thickness that occurs during the vapor treatment.

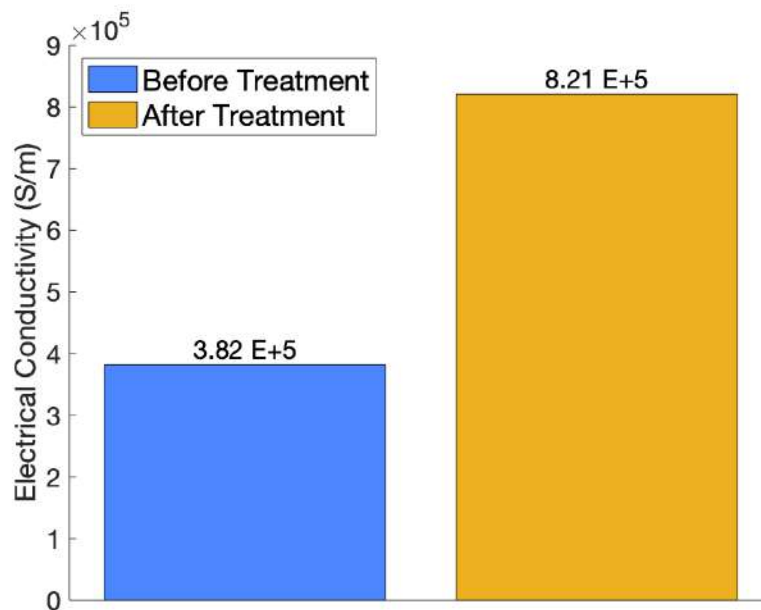

Figure 4.15: Conductivity calculations from previously determined resistances. **Before Treatment:** Thickness = 112 μm; Electrical Resistance = 1.1 Ω. **After Treatment:** Thickness = 101 μm; Electrical Resistance = 0.6 Ω.

To understand the behavior of the ink without a component and to verify it was similar to that demonstrated in the cycling loading test, a similar test was carried out with only 5 displacement cycles going from 0% to 40% strain. The results are exhibited in Figure 4.16. It can be seen that the electrical resistance of the conductive ink remains stable during the 5 displacement cycles.

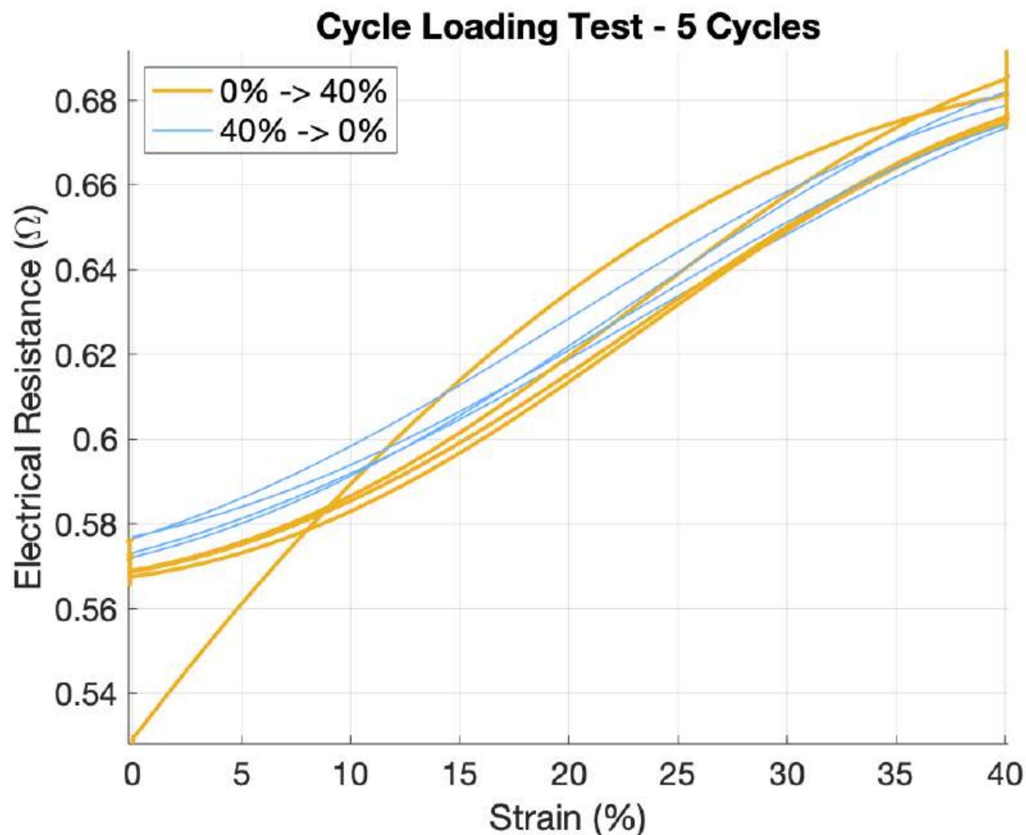

Figure 4.16: Cyclic loading test of 5 cycles without a rigid component. The performance of the ink is stable, with only negligible increases in electrical resistance.

Overall, it can be said that the toluene vapor treatment improves the conductivity of the printed traces tested by triggering a reorganization in the microstructure of the conductive composite. Furthermore, the performance of the ink after vapor exposure was considered to be extremely stable during repeated use.

4.3.2 Improvement of Strain Tolerance of the Stretchable Circuit After Treatment

It is known that the toluene vapor leads to a macroscopic change in the SIS substrate. To understand if it has any impact in the maximum strain that can be reached by the elastomer substrate, samples (without a rigid component) were treated and stretched until failure. The same test was done for their untreated equivalents, and the results can be seen in Figure 4.17, where the yellow lines represent untreated samples and the blue plots represent treated specimens.

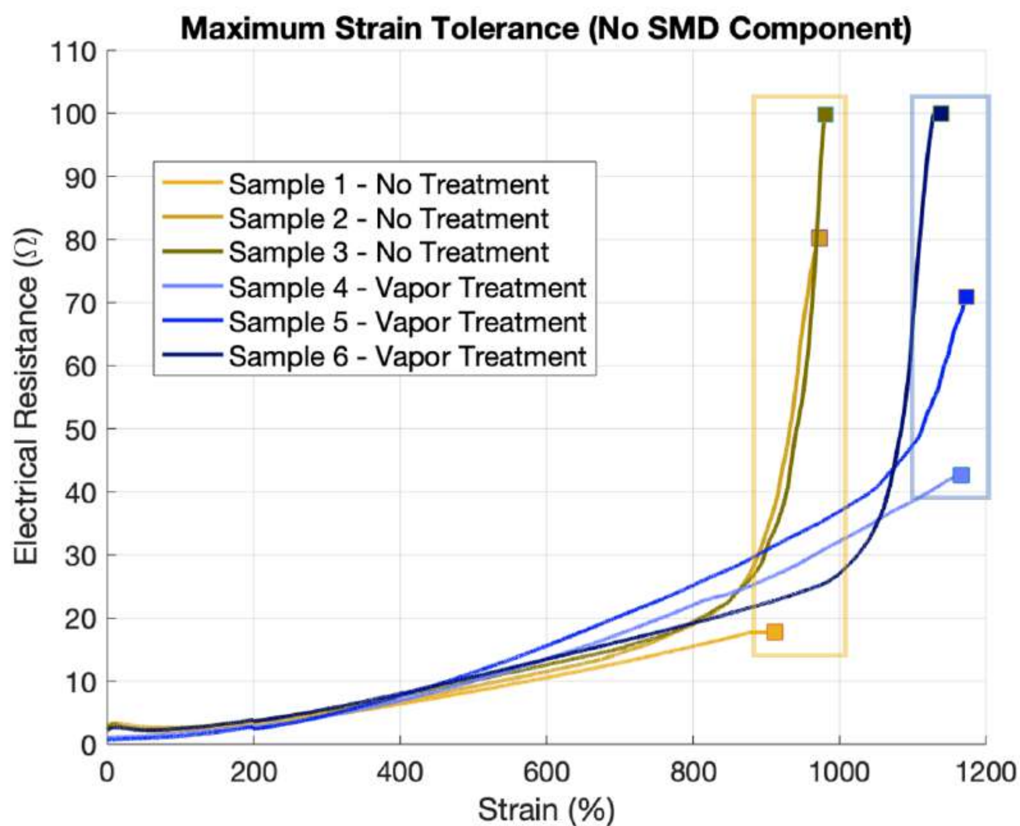

Figure 4.17: Results of the uniaxial tension test performed to treated and untreated samples. Yellow lines represent untreated samples while blue plots represent the treated ones.

Some interesting conclusions can be drawn from the results obtained. As expected, the treated samples start with a lower value of electrical resistance when compared with the batch of untreated samples, which is consistent with the previous findings. In addition, while performing the break tests, it became noticeable that the treated samples could withstand larger displacements before the substrate finally ruptured. In Figure 4.17, it can be seen that the untreated samples withstand 900% strain

(consistent with the literature [90]), but treated specimens can withstand more than 1100% strain.

To explain this interesting and unexpected finding, treated and untreated SIS samples were examined under SEM. The resulting images can be seen in Figure 4.18.

The differences between the before and after micrographs are apparent. Before the toluene treatment, the surface of the SIS substrate appears to be more heterogeneous. Unsolved SIS (identifiable due to the crystal arrangement of materials seen in Figure 4.18a) can be found scattered around the surface of the elastomer. After the treatment, these elements seem to have disappeared. Vapor exposure dissolves the elastomer during the treatment and ensures that the fraction of SIS that was left undissolved combines with the rest of the substrate.

Perhaps the most important change in the elastomer, though, is the healing of small micro-cracks in the substrate through the effect of the toluene vapor. These micro-fissures can be seen in Figure 4.18a,c. After the treatment, the SIS surface is much more homogeneous and without any sign of cracks. This suggests that during vapor exposure the SIS softens and fills in any remaining voids, evening out the surface and making it smoother.

Therefore, it can be said that the improvement in strain tolerance seen in Figure 4.17 is attributed to vapor exposure as it has the ability to heal small fissures in the SIS substrate. This is an extremely advantageous by-product of the treatment because it prevents micro-fissures from growing larger with increased strain or repeated use, which would eventually lead to early failure of the system due to substrate rupture.

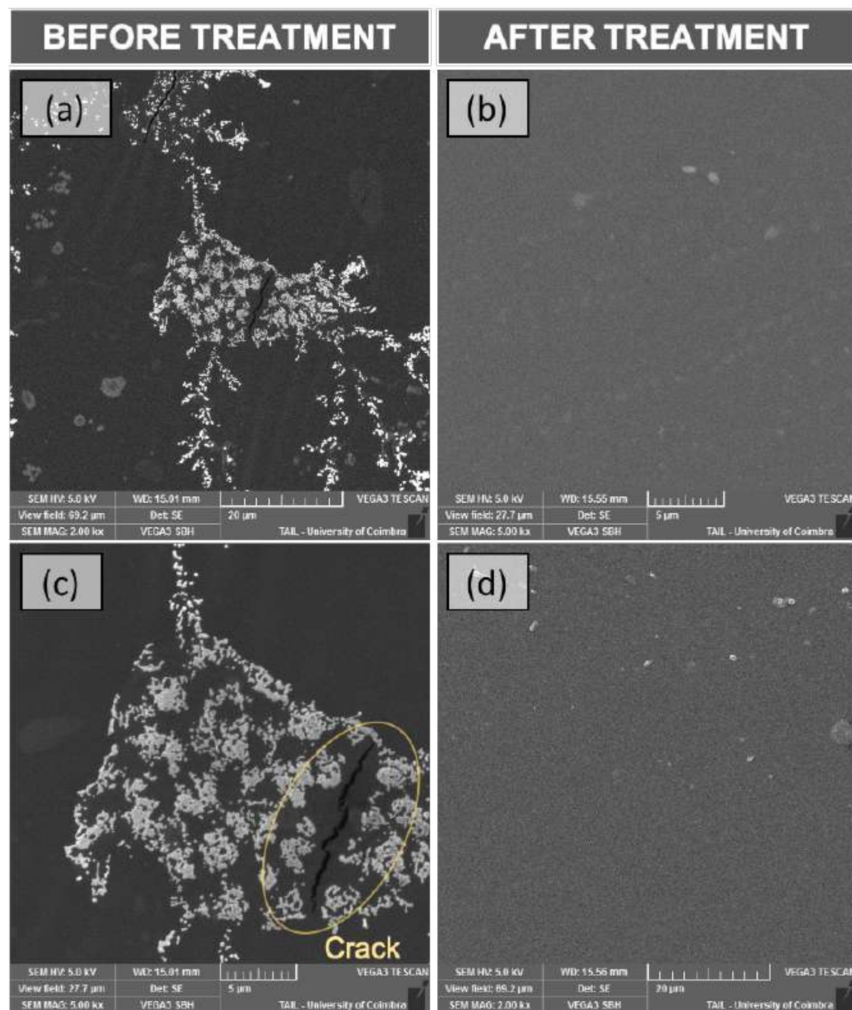

Figure 4.18: Images of a SIS layer (400 μm) deposited using a thin film applicator, before and after toluene vapor treatment. (a) SE; Magnification: 2000x. (b) SE; Magnification: 2000x. (c) SE; Magnification: 5000x. (d) SE; Magnification: 5000x.

5

Case Studies

The objective of this chapter is to show that the developed interfacing method can be used to fabricate fully functional stretchable circuits. This was demonstrated through the development of a soft temperature patch that can be directly applied on the skin or transferred to a stretchable textile that allows for the fabrication of complex e-textile circuits for wearable monitoring.

5.1 Stretchable Temperature Patch

A stretchable temperature patch was built with the described interfacing method with the goal of understanding if components of very different sizes and architectures could be integrated to produce an individual functional system.

The system is composed of a rigid temperature sensor, SMD LEDs, and a microprocessor (CY8C4014SXS-421). The sensor measures the temperature of the environment it is placed in and converts the input data to electronic data. This component is connected to the microprocessor for signal processing and subsequent temperature display. The output of the microprocessor is linked to the SMD LEDs, which are divided in two different groups: one lights up to permanently show the 3 digit, while the other displays digits 0-9 depending on the information given by the microprocessor. Therefore, the stretchable patch can display temperatures in the range of 30-39 °C as a visible number through the LEDs. If the sensor measures a temperature out of range (40 °C, for example), the second group of LEDs does not light up.

The fabrication of the patch was very similar to the procedure described in Section 3.2. First, a 400 μm SIS film was prepared with the thin film applicator. The Voltera^{TM} V-One Extrusion Printer was employed to print the conductive ink on the surface of the SIS (Figure 5.1a) as this equipment allows for printing in higher resolutions when compared to stencil printing. Laser ablation could have also been

used but this technique is more likely to produce short-circuits in the conductive traces due to leftover LM that the laser might not be able remove. All the rigid components were placed on their respective connection sites using a pick and place machine. (Figure 5.1b). The circuit was exposed to toluene vapor for around 45 minutes to assemble the chips into the system. Then, the circuit was placed in the oven for 10 minutes to ensure full solvent evaporation. Finally, the SIS substrate is peeled from the glass and the prototype is ready to use.

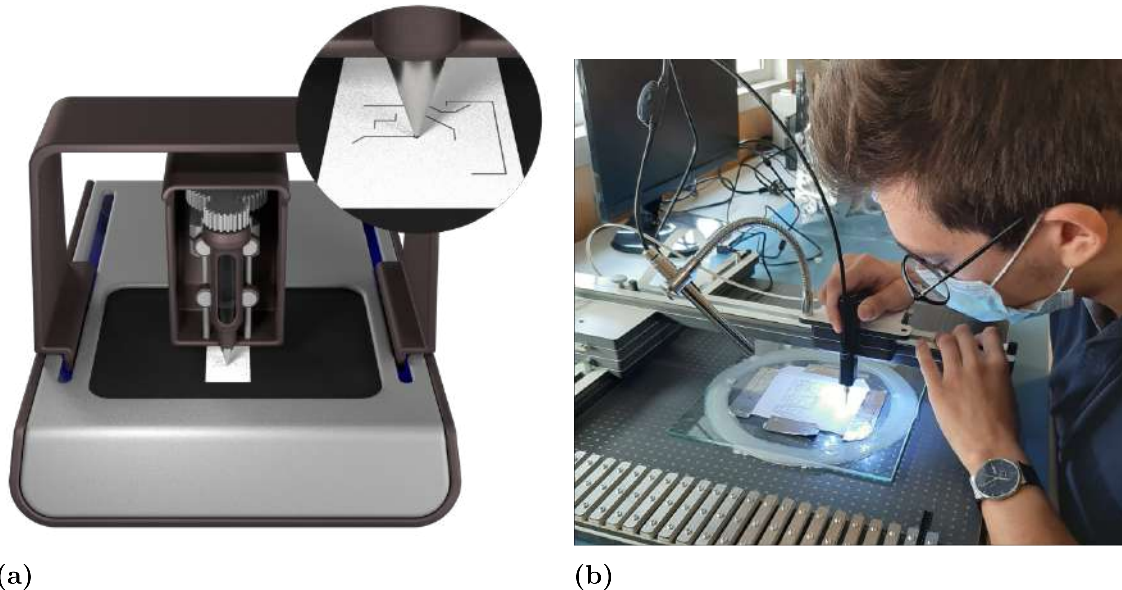

(a) **(b)**

Figure 5.1: Machines used in the fabrication process of the stretchable temperature patch. (a) Voltera used to deposit the conductive ink on SIS through printing extrusion. (b) Pick and place machine used for placing the rigid chips on their exact positions in the circuit.

The patch can be stretched and deformed without any signs of loss of conductivity and maintaining its temperature reading and display functions (Figure 5.2). The circuit was placed on the forearm to measure the skin temperature, like it can be seen in Figure 5.3.

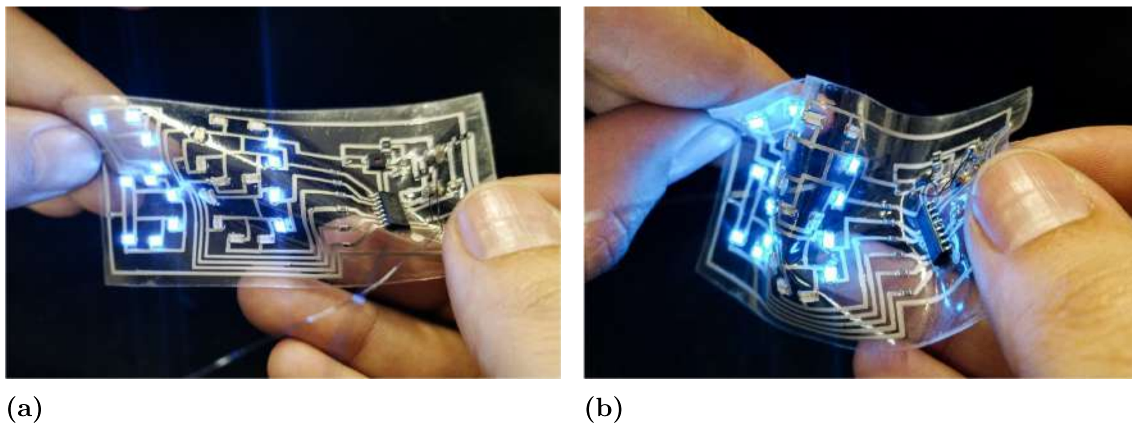

(a) (b)

Figure 5.2: The circuit can (a) withstand some strain and can also be (b) deformed without loss of conductivity and function.

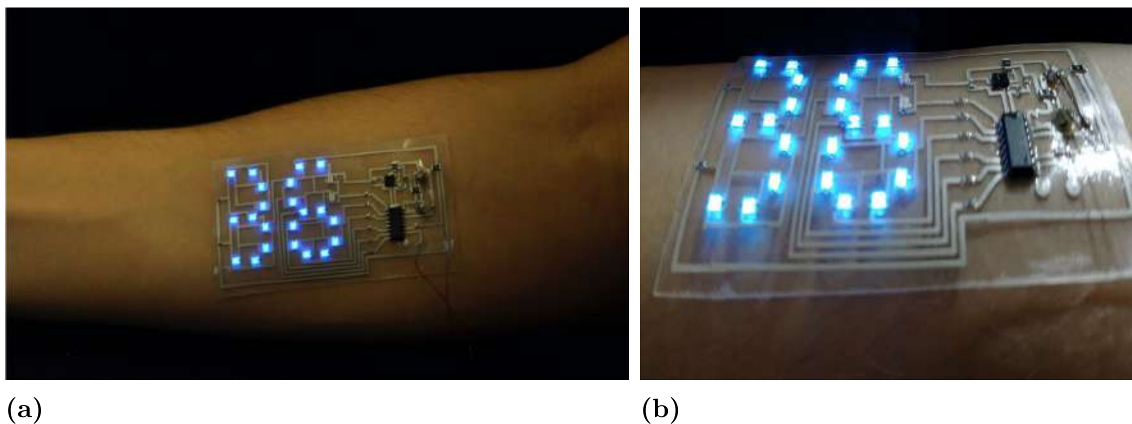

(a) (b)

Figure 5.3: Stretchable temperature patch placed over the forearm. (a) The system is able to directly display the body temperature with the SMD LEDs. (b) Close-up of the components of the stretchable circuit.

To test the ability to be transferred to substrates, the stretchable patch was attached to a cloth mask. To do this, we took advantage SIS substrate's properties: stretchability and adhesiveness. Stretchability is a crucial factor for transference to textiles, as the electronic system needs to endure considerable deformation. To add the least amount of steps possible to the transference process, the circuit was placed on the surface of the mask and this system was left in the toluene vapor chamber for 1 hour. During the process, the SIS became softer and penetrated the porous textile (Figure 5.4), ensuring a successful attachment to the surface of the mask due to the adhesive nature of the elastomer. Then, the mask was left to dry in open air for 1 day to make sure that all the toluene evaporated from the circuit and from the textile.

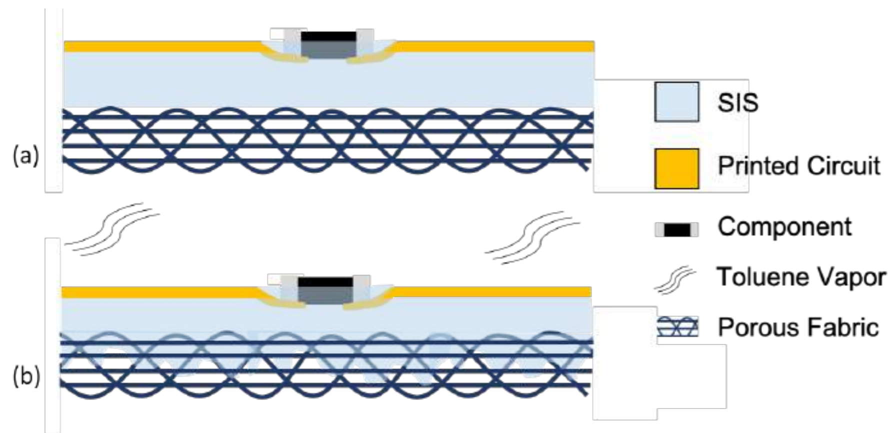

Figure 5.4: Side-view schematics of the transference process to the cloth mask through the toluene vapor treatment. (a) Stretchable circuit is placed on the fabric's surface. (b) The system is exposed to toluene vapor, which leads to the infiltration of the soft SIS into the porous fabric. After drying the SIS remains glued to the textile.

The mask with the integrated circuit can be seen in Figure 5.5. The system was successfully used for temperature acquisition and subsequent display. Besides, the prototype was fairly easy to produce, which demonstrates the versatility and effectiveness of the developed interfacing method. Therefore, it can be said that the toluene exposure technique, combined with the pick-and-place and automatic printing techniques, shows potential for mass-production and industrial scalability which was one of the main objectives of the this work.

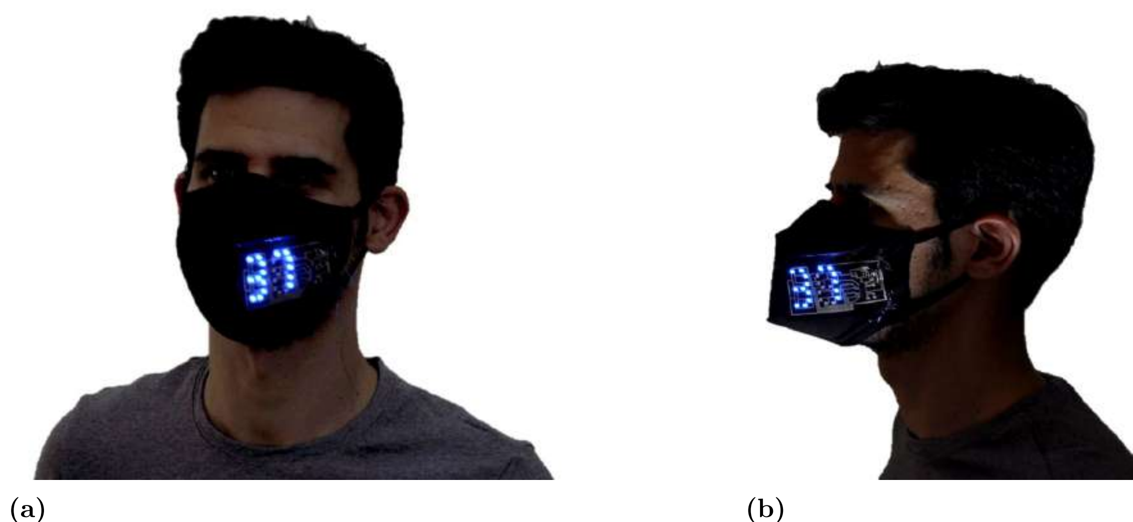

(a) **(b)**

Figure 5.5: Mask with attached temperature system. The patch is able to read the temperature of the user and display it accordingly through the SMD LEDs. (a) Front-view of the circuit. (b) Side-view of the circuit.

Introducing the developed mask with the integrated circuit could be an interesting step for tackling the Covid-19 pandemic. This way, any person would be able visually identify the temperature of the user without breaching safety distancing. Widespread use could, therefore, reduce contact between people and overall contribute to a reduction in active cases.

6

Conclusions

In this project, we developed and characterized a novel technique for interfacing rigid chips with soft stretchable circuits. The method consisted in provoking a rigid-soft transition in the printed ink and substrate, which leads to a seamless integration of SMD chips into the stretchable circuit.

This work presents, for the first time, an interfacing technique capable of producing electronic systems that withstand more than 500% uniaxial strain, well above any previously reported results. The samples are also able to resist to 1000 displacement cycles loading up from 0% to 40% strain without any signs of electrical or mechanical damage. The toluene vapor technique is easy and fast to reproduce, and also compatible with chips of very different sizes and architectures.

In addition to being very mechanically robust, the samples treated with toluene vapor also showed improved electromechanical properties. The procedure is able to increase the conductivity of the conductive printed traces by more than twice. Besides, the treatment is able to heal any cracks that exist on the SIS substrate and make it more robust by withstanding 200% more strain than untreated samples. The underlying mechanisms of action that led to the emergence of these electromechanical properties were explained through SEM analysis.

Finally, the potential of the technique was demonstrated with the fabrication of a stretchable temperature sensor that could be worn on the skin or embedded in a textile (a mask, in this case). This system proved that the technique can be used to fabricate fully functional electronic systems.

Overall, the developed toluene vapor technique is considered to be promising as its favorable set of properties and simplicity make it the ideal procedure for ”soldering” rigid components to stretchable circuits.

6.1 Limitations and Future Work

Even though the developed interfacing technique already shows great potential, there is definitely room for improvement. When using the treatment, sometimes the printed conductive circuit would drift away in the SIS, originating broken traces and short-circuits. This seems to be related with the leveling and flatness of the surface below the substrate during the treatment. Because the component and ink descend into the substrate due to the gravity force, an uneven surface can cause a slight motion of the circuit in other directions. Nevertheless, this is a technical challenge that should be easily addressable by development of an ad hoc vapor exposure chamber.

It is also not yet understood if the treatment can be used in bigger and more complex circuits. A priority for the future will be the determination of the best combination of toluene concentration, chamber volume, and exposure time to achieve generally consistent results.

Although the present work demonstrates a maximum strain tolerance of over 500%, it is well accepted in the literature that encapsulation can improve the maximum strain limit. However, initial efforts to encapsulate these circuits using PDMS and SIS, led to delamination. To our surprise, during toluene vapor exposure we observed a self-coating phenomenon that occurred in some of the samples. As the ink and component descend into the SIS substrate, sometimes a thin-layer of the substrate covers the printed circuit. This seems to be a function of the circuit geometry, areal density, component mass, exposure time, and substrate thickness. This is a subject that should be further studied, as fine tuning of these parameters might lead to self-coating of the whole circuit.

The technique can be used as it is with excellent results. However, tackling the aforementioned limitations will be important for introducing vapor treatment in the scalable and industrial production of stretchable electronic systems.

Publications

The presented dissertation is under preparation for registration of an international patent titled "Method for Integration of Silicon Microchips into Printed Stretchable Circuit".

Appendices

A

Substrate Choice

Toluene vapor is not usually employed in the development of stretchable electronic systems. Therefore, the interaction between the vapor and several popular substrates is relatively unknown and had to be determined beforehand.

Stretchable circuits are typically built by incorporating stretchable interconnects on a polymer matrix like PDMS. As was mentioned before, the materials employed in the construction of the system must not react with toluene in a way the hinders the whole interfacing process. Achieving this required a complete overhaul of the initial plan.

Latex was initially used as the polymeric substrate, but it was quickly discarded as an option due to swelling in toluene vapor, a phenomenon that can be observed in Figure A.1a. Even though the swelling could be reversed by evaporating the solvent, the movement of the substrate prevented the attachment of the rigid components to the ink. Additionally, as the latex expanded it cracked the ink and prevented the creation of a functional circuit (Figure A.1b). Besides, latex became extremely fragile and brittle after the treatment, often breaking even with careful handling. These problems associated with the elastomer made latex an impractical choice.

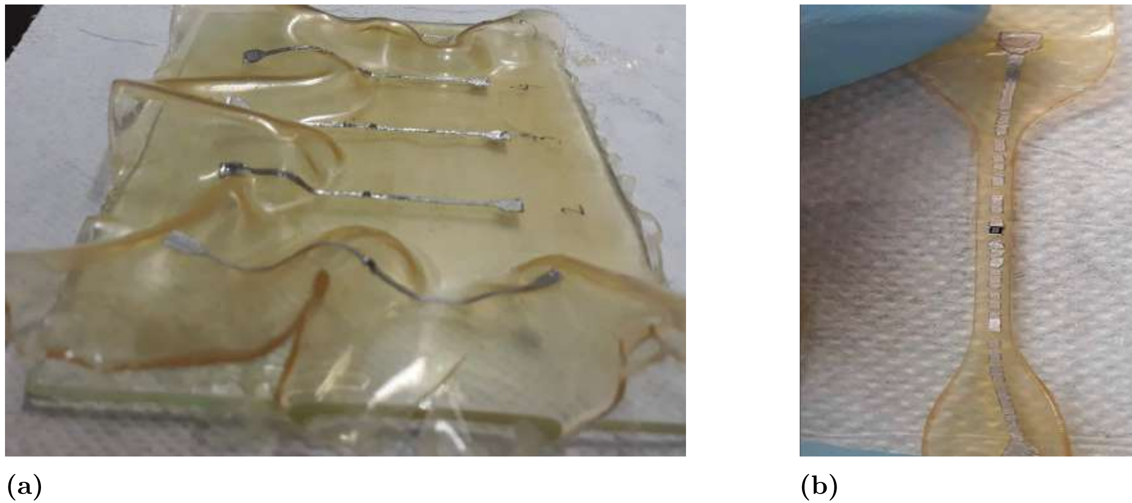

(a) (b)

Figure A.1: Pictures of latex substrate after toluene treatment. (a) Extreme swelling caused by the reaction between the polymer and toluene. (b) Ink cracking due to swelling of the elastomer.

In order to determine if any extensible polymer could be used as a substrate, strips of PDMS, Ecoflex^{TM} 00-30, PMC^{TM}-744, and Dragon Skin^{TM} were placed inside a desiccator with paper soaked with 50 mL of toluene for 24 hours. A vacuum was applied to the chamber to be certain the final results were due to the vapor. PDMS was already known to swell with non-polar solvents like toluene [91], but it was still tested to visually compare its behaviour with that of the other elastomers.

The initial substrates and the results after this time period can be seen in Figure A.2. As can be seen on the pictures, Ecoflex^{TM} 00-30 was the only substrate that did not show any macroscopic swelling, while Dragon Skin ^{TM} showed minimal expansion.

However, it was found that reactiveness to toluene was a key factor for superior ink adhesion to the substrates. Therefore, even though Ecoflex^{TM} 00-30 and Dragon Skin^{TM} are able to resist the toluene treatment, they are challenging to print on, and the ink can easily be peeled from the substrates due to poor adhesion. With this being said, a more unconventional alternative for a substrate had to be considered.

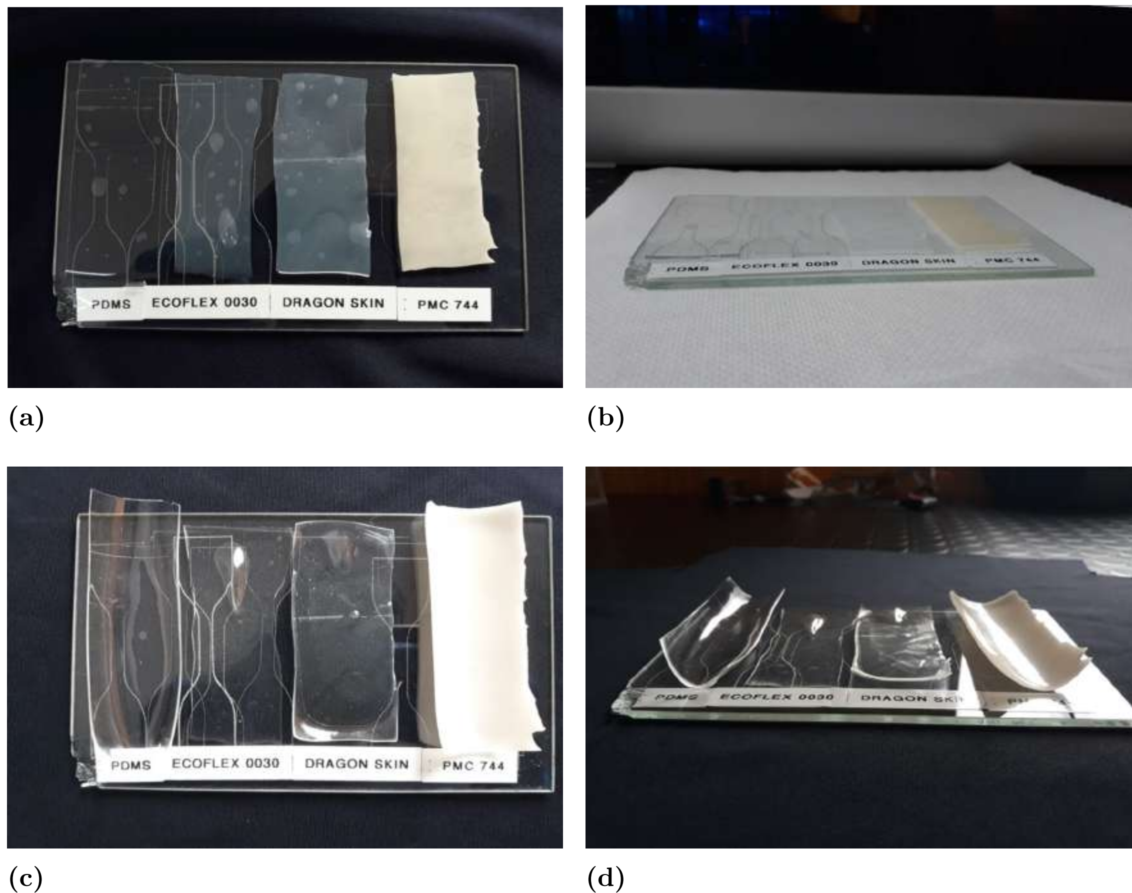

Figure A.2: Substrate samples before and after toluene treatment. (a) Top view of the substrates used – PDMS, Ecoflex^{TM} 00-30, Dragon Skin^{TM}, and PMC^{TM}-744 (from left to right). (b) Side-view of the substrates before the toluene treatment, showing their flat surface. (c) Top view of the substrates after the toluene treatment. (d) Side-view of the substrates after the toluene treatment, showing their swelled state.

The ink is composed of a SIS polymer matrix and it does not show any signs of swelling under vapor treatment. SIS is typically not used as a substrate because thicker layers (>1000 μm) cure very unevenly. Furthermore, building several layers of SIS is resource expensive and time-consuming due to the evaporation of a significant portion of the initial solution.

Nonetheless, thin layers of SIS make up for great substrates as they do not swell. Cured SIS softens as the toluene vapor acts on its surface, but this phenomenon turned out to be beneficial for the interfacing method by strongly gluing rigid components to the substrate.

The elastomer easily regains its consistency by curing it at 60°C for a few minutes or by just leaving it to cure at room temperature. Because the SIS layer is extremely

thin (about 400 μm thick) it might need to be transferred to a thicker and more robust substrate depending on the application. This is generally not a problem as SIS can be smoothly transferred and encapsulated in polymeric substrates like PDMS.

For all these reasons, SIS makes up an excellent intermediary substrate in the interfacing method.

Bibliography

[1] Y. Liu, M. Pharr, and G. A. Salvatore, "Lab-on-skin: a review of flexible and stretchable electronics for wearable health monitoring," *ACS nano*, vol. 11, no. 10, pp. 9614–9635, 2017.

[2] D.-H. Kim, R. Ghaffari, N. Lu, and J. A. Rogers, "Flexible and stretchable electronics for biointegrated devices," *Annual review of biomedical engineering*, vol. 14, pp. 113–128, 2012.

[3] H. Li, S. Lv, and Y. Fang, "Bio-inspired micro/nanostructures for flexible and stretchable electronics," *Nano Research*, pp. 1–9, 2020.

[4] D. F. Fernandes, C. Majidi, and M. Tavakoli, "Digitally printed stretchable electronics: a review," *Journal of Materials Chemistry C*, vol. 7, no. 45, pp. 14035–14068, 2019.

[5] W. Wu, "Stretchable electronics: functional materials, fabrication strategies and applications," *Science and Technology of Advanced Materials*, vol. 20, no. 1, pp. 187–224, 2019.

[6] J. Nam, B. Seo, Y. Lee, D.-H. Kim, and S. Jo, "Cross-buckled structures for stretchable and compressible thin film silicon solar cells," *Scientific reports*, vol. 7, no. 1, pp. 1–8, 2017.

[7] J. Zang, C. Cao, Y. Feng, J. Liu, and X. Zhao, "Stretchable and high-performance supercapacitors with crumpled graphene papers," *Scientific reports*, vol. 4, no. 1, pp. 1–7, 2014.

[8] S. Xu, Y. Zhang, J. Cho, J. Lee, X. Huang, L. Jia, J. A. Fan, Y. Su, J. Su, H. Zhang, *et al.*, "Stretchable batteries with self-similar serpentine interconnects and integrated wireless recharging systems," *Nature communications*, vol. 4, no. 1, pp. 1–8, 2013.

[9] T. Yamada, Y. Hayamizu, Y. Yamamoto, Y. Yomogida, A. Izadi-Najafabadi, D. N. Futaba, and K. Hata, "A stretchable carbon nanotube strain sensor for human-motion detection," *Nature nanotechnology*, vol. 6, no. 5, p. 296, 2011.

[10] S. Yao, J. Cui, Z. Cui, and Y. Zhu, "Soft electrothermal actuators using silver nanowire heaters," *Nanoscale*, vol. 9, no. 11, pp. 3797–3805, 2017.

[11] D. Janczak, M. Zych, T. Raczyński, Ł. Dybowska-Sarapuk, A. Pepłowski, J. Krzemiński, A. Sosna-Głebska, K. Znajdek, M. Sibiński, and M. Jakubowska, "Stretchable and washable electroluminescent display screen-printed on textile," *Nanomaterials*, vol. 9, no. 9, p. 1276, 2019.

[12] "IDTechEx stretchable and conformal electronics 2019-2029." `https://www.idtechex.com/fr/research-report/stretchable-and-conformal-electronics-2019-2029/636`. Accessed: 2020-03-10.

[13] C. Leal, P. Alhais Lopes, A. Serra, J. F. Coelho, A. T. de Almeida, and M. Tavakoli, "Untethered disposable health monitoring electronic patches with integrated ag2o-zn battery, aginga current collector and hydrogel electrodes," *ACS Applied Materials & Interfaces*, 2019.

[14] W.-D. Huang, H. Cao, S. Deb, M. Chiao, and J.-C. Chiao, "A flexible ph sensor based on the iridium oxide sensing film," *Sensors and Actuators A: Physical*, vol. 169, no. 1, pp. 1–11, 2011.

[15] C. Li, P.-M. Wu, J. Han, and C. H. Ahn, "A flexible polymer tube lab-chip integrated with microsensors for smart microcatheter," *Biomedical microdevices*, vol. 10, no. 5, pp. 671–679, 2008.

[16] J. J. Norton, D. S. Lee, J. W. Lee, W. Lee, O. Kwon, P. Won, S.-Y. Jung, H. Cheng, J.-W. Jeong, A. Akce, *et al.*, "Soft, curved electrode systems capable of integration on the auricle as a persistent brain–computer interface," *Proceedings of the National Academy of Sciences*, vol. 112, no. 13, pp. 3920–3925, 2015.

[17] Y. Liu, J. J. Norton, R. Qazi, Z. Zou, K. R. Ammann, H. Liu, L. Yan, P. L. Tran, K.-I. Jang, J. W. Lee, *et al.*, "Epidermal mechano-acoustic sensing electronics for cardiovascular diagnostics and human-machine interfaces," *Science Advances*, vol. 2, no. 11, p. e1601185, 2016.

[18] N. Kim, T. Lim, K. Song, S. Yang, and J. Lee, "Stretchable multichannel electromyography sensor array covering large area for controlling home electronics

with distinguishable signals from multiple muscles," *ACS applied materials & interfaces*, vol. 8, no. 32, pp. 21070–21076, 2016.

[19] C. Pang, G.-Y. Lee, T.-i. Kim, S. M. Kim, H. N. Kim, S.-H. Ahn, and K.-Y. Suh, "A flexible and highly sensitive strain-gauge sensor using reversible interlocking of nanofibres," *Nature materials*, vol. 11, no. 9, pp. 795–801, 2012.

[20] R. Rocha, P. Lopes, A. T. de Almeida, M. Tavakoli, and C. Majidi, "Soft-matter sensor for proximity, tactile and pressure detection," in *2017 IEEE/RSJ International Conference on Intelligent Robots and Systems (IROS)*, pp. 3734–3738, IEEE, 2017.

[21] S. C. Mannsfeld, B. C. Tee, R. M. Stoltenberg, C. V. H. Chen, S. Barman, B. V. Muir, A. N. Sokolov, C. Reese, and Z. Bao, "Highly sensitive flexible pressure sensors with microstructured rubber dielectric layers," *Nature materials*, vol. 9, no. 10, pp. 859–864, 2010.

[22] C. Yan, J. Wang, and P. S. Lee, "Stretchable graphene thermistor with tunable thermal index," *ACS nano*, vol. 9, no. 2, pp. 2130–2137, 2015.

[23] Y. Hattori, L. Falgout, W. Lee, S.-Y. Jung, E. Poon, J. W. Lee, I. Na, A. Geisler, D. Sadhwani, Y. Zhang, *et al.*, "Multifunctional skin-like electronics for quantitative, clinical monitoring of cutaneous wound healing," *Advanced healthcare materials*, vol. 3, no. 10, pp. 1597–1607, 2014.

[24] M. Tavakoli, R. P. Rocha, J. Lourenço, T. Lu, and C. Majidi, "Soft bionics hands with a sense of touch through an electronic skin," in *Soft Robotics: Trends, Applications and Challenges*, pp. 5–10, Springer, 2017.

[25] T. Pickering, J. M. Hamm, A. F. Page, S. Wuestner, and O. Hess, "Cavity-free plasmonic nanolasing enabled by dispersionless stopped light," *Nature communications*, vol. 5, p. 4972, 2014.

[26] P. A. Lopes, H. Paisana, A. T. De Almeida, C. Majidi, and M. Tavakoli, "Hydroprinted electronics: ultrathin stretchable ag–in–ga e-skin for bioelectronics and human–machine interaction," *ACS applied materials & interfaces*, vol. 10, no. 45, pp. 38760–38768, 2018.

[27] C. Dagdeviren, B. D. Yang, Y. Su, P. L. Tran, P. Joe, E. Anderson, J. Xia, V. Doraiswamy, B. Dehdashti, X. Feng, *et al.*, "Conformal piezoelectric energy harvesting and storage from motions of the heart, lung, and diaphragm," *Proceedings of the National Academy of Sciences*, vol. 111, no. 5, pp. 1927–1932, 2014.

[28] I. R. Minev, P. Musienko, A. Hirsch, Q. Barraud, N. Wenger, E. M. Moraud, J. Gandar, M. Capogrosso, T. Milekovic, L. Asboth, *et al.*, "Electronic dura mater for long-term multimodal neural interfaces," *Science*, vol. 347, no. 6218, pp. 159–163, 2015.

[29] M. Vosgueritchian, J. B.-H. Tok, and Z. Bao, "Stretchable leds: Light-emitting electronic skin," *Nature Photonics*, vol. 7, no. 10, p. 769, 2013.

[30] H. Wang, M. Yang, Q. Tang, X. Zhao, Y. Tong, and Y. Liu, "Flexible, conformal organic synaptic transistors on elastomer for biomedical applications," *Advanced Functional Materials*, vol. 29, no. 19, p. 1901107, 2019.

[31] S. Park, H. Lee, Y.-J. Kim, and P. S. Lee, "Fully laser-patterned stretchable microsupercapacitors integrated with soft electronic circuit components," *NPG Asia Materials*, vol. 10, no. 10, pp. 959–969, 2018.

[32] D. G. Marques, P. A. Lopes, A. T. de Almeida, C. Majidi, and M. Tavakoli, "Reliable interfaces for egain multi-layer stretchable circuits and microelectronics," *Lab on a Chip*, vol. 19, no. 5, pp. 897–906, 2019.

[33] M. P. Wolf, G. B. Salieb-Beugelaar, and P. Hunziker, "Pdms with designer functionalities—properties, modifications strategies, and applications," *Progress in Polymer Science*, vol. 83, pp. 97–134, 2018.

[34] M. L. Hammock, A. Chortos, B. C.-K. Tee, J. B.-H. Tok, and Z. Bao, "25th anniversary article: the evolution of electronic skin (e-skin): a brief history, design considerations, and recent progress," *Advanced materials*, vol. 25, no. 42, pp. 5997–6038, 2013.

[35] S. Wagner and S. Bauer, "Materials for stretchable electronics," *Mrs Bulletin*, vol. 37, no. 3, pp. 207–213, 2012.

[36] V. Rao and J. Johns, "Mechanical properties of thermoplastic elastomeric blends of chitosan and natural rubber latex," *Journal of applied polymer science*, vol. 107, no. 4, pp. 2217–2223, 2008.

[37] "Ecoflex™ 00-30 Product Information." `https://www.smooth-on.com/products/ecoflex-00-30/`. Accessed: 2020-03-10.

[38] P. Boonvisut and M. C. Çavuşoğlu, "Estimation of soft tissue mechanical parameters from robotic manipulation data," *IEEE/ASME Transactions on Mechatronics*, vol. 18, no. 5, pp. 1602–1611, 2012.

[39] J.-S. Noh, "Conductive elastomers for stretchable electronics, sensors and energy harvesters," *Polymers*, vol. 8, no. 4, p. 123, 2016.

[40] S. H. Jeong, S. Zhang, K. Hjort, J. Hilborn, and Z. Wu, "Pdms-based elastomer tuned soft, stretchable, and sticky for epidermal electronics," *Advanced Materials*, vol. 28, no. 28, pp. 5830–5836, 2016.

[41] R. Moser, G. Kettlgruber, C. M. Siket, M. Drack, I. M. Graz, U. Cakmak, Z. Major, M. Kaltenbrunner, and S. Bauer, "From playroom to lab: Tough stretchable electronics analyzed with a tabletop tensile tester made from toy-bricks," *Advanced Science*, vol. 3, no. 4, p. 1500396, 2016.

[42] N. Lu and D.-H. Kim, "Flexible and stretchable electronics paving the way for soft robotics," *Soft Robotics*, vol. 1, no. 1, pp. 53–62, 2014.

[43] R. Niu, G. Liu, X. Ding, and J. Sun, "Ductility of metal thin films in flexible electronics," *Science in China Series E: Technological Sciences*, vol. 51, no. 11, pp. 1971–1979, 2008.

[44] K. Kim, J. Kim, B. G. Hyun, S. Ji, S.-Y. Kim, S. Kim, B. W. An, and J.-U. Park, "Stretchable and transparent electrodes based on in-plane structures," *Nanoscale*, vol. 7, no. 35, pp. 14577–14594, 2015.

[45] X. Wang, H. Hu, Y. Shen, X. Zhou, and Z. Zheng, "Stretchable conductors with ultrahigh tensile strain and stable metallic conductance enabled by prestrained polyelectrolyte nanoplatforms," *Advanced Materials*, vol. 23, no. 27, pp. 3090–3094, 2011.

[46] Y. Iwata and E. Iwase, "Stress-free stretchable electronic device using folding deformation," in *2017 IEEE 30th International Conference on Micro Electro Mechanical Systems (MEMS)*, pp. 231–234, IEEE, 2017.

[47] M. Gonzalez, F. Axisa, M. V. Bulcke, D. Brosteaux, B. Vandevelde, and J. Vanfleteren, "Design of metal interconnects for stretchable electronic circuits," *Microelectronics Reliability*, vol. 48, no. 6, pp. 825–832, 2008.

[48] D. Brosteaux, F. Axisa, M. Gonzalez, and J. Vanfleteren, "Design and fabrication of elastic interconnections for stretchable electronic circuits," *IEEE Electron Device Letters*, vol. 28, no. 7, pp. 552–554, 2007.

[49] N. Matsuhisa, X. Chen, Z. Bao, and T. Someya, "Materials and structural designs of stretchable conductors," *Chemical Society Reviews*, vol. 48, no. 11, pp. 2946–2966, 2019.

[50] M. D. Dickey, "Stretchable and soft electronics using liquid metals," *Advanced Materials*, vol. 29, no. 27, p. 1606425, 2017.

[51] I. D. Joshipura, H. R. Ayers, C. Majidi, and M. D. Dickey, "Methods to pattern liquid metals," *Journal of materials chemistry c*, vol. 3, no. 16, pp. 3834–3841, 2015.

[52] M. D. Dickey, R. C. Chiechi, R. J. Larsen, E. A. Weiss, D. A. Weitz, and G. M. Whitesides, "Eutectic gallium-indium (egain): a liquid metal alloy for the formation of stable structures in microchannels at room temperature," *Advanced functional materials*, vol. 18, no. 7, pp. 1097–1104, 2008.

[53] E. Davis and S. Ndao, "On the wetting states of low melting point metal galinstan® on silicon microstructured surfaces," *Advanced Engineering Materials*, vol. 20, no. 3, p. 1700829, 2018.

[54] K. P. Mineart, Y. Lin, S. C. Desai, A. S. Krishnan, R. J. Spontak, and M. D. Dickey, "Ultrastretchable, cyclable and recyclable 1-and 2-dimensional conductors based on physically cross-linked thermoplastic elastomer gels," *Soft Matter*, vol. 9, no. 32, pp. 7695–7700, 2013.

[55] Q. Zhang, J. Liang, Y. Huang, H. Chen, and R. Ma, "Intrinsically stretchable conductors and interconnects for electronic applications," *Materials Chemistry Frontiers*, vol. 3, no. 6, pp. 1032–1051, 2019.

[56] C. Ladd, J.-H. So, J. Muth, and M. D. Dickey, "3d printing of free standing liquid metal microstructures," *Advanced Materials*, vol. 25, no. 36, pp. 5081–5085, 2013.

[57] Y.-L. Park, B.-R. Chen, and R. J. Wood, "Design and fabrication of soft artificial skin using embedded microchannels and liquid conductors," *IEEE Sensors journal*, vol. 12, no. 8, pp. 2711–2718, 2012.

[58] L. Cai, S. Zhang, J. Miao, Z. Yu, and C. Wang, "Fully printed stretchable thin-film transistors and integrated logic circuits," *Acs Nano*, vol. 10, no. 12, pp. 11459–11468, 2016.

[59] N. Matsuhisa, D. Inoue, P. Zalar, H. Jin, Y. Matsuba, A. Itoh, T. Yokota, D. Hashizume, and T. Someya, "Printable elastic conductors by in situ formation of silver nanoparticles from silver flakes," *Nature materials*, vol. 16, no. 8, pp. 834–840, 2017.

[60] S. Choi, S. I. Han, D. Jung, H. J. Hwang, C. Lim, S. Bae, O. K. Park, C. M. Tschabrunn, M. Lee, S. Y. Bae, *et al.*, "Highly conductive, stretchable and biocompatible ag–au core–sheath nanowire composite for wearable and implantable bioelectronics," *Nature nanotechnology*, vol. 13, no. 11, pp. 1048–1056, 2018.

[61] R. Taherian, "Development of an equation to model electrical conductivity of polymer-based carbon nanocomposites," *ECS Journal of Solid State Science and Technology*, vol. 3, no. 6, p. M26, 2014.

[62] M. H. Malakooti, M. R. Bockstaller, K. Matyjaszewski, and C. Majidi, "Liquid metal nanocomposites," *Nanoscale Advances*, 2020.

[63] T. Lu, J. Wissman, and C. Majidi, "Soft anisotropic conductors as electric vias for ga-based liquid metal circuits," *ACS applied materials & interfaces*, vol. 7, no. 48, pp. 26923–26929, 2015.

[64] X. X. Gong, G. T. Fei, W. B. Fu, M. Fang, X. D. Gao, B. N. Zhong, and L. De Zhang, "Flexible strain sensor with high performance based on pani/pdms films," *Organic Electronics*, vol. 47, pp. 51–56, 2017.

[65] M. D. Dickey, "Emerging applications of liquid metals featuring surface oxides," *ACS applied materials & interfaces*, vol. 6, no. 21, pp. 18369–18379, 2014.

[66] T. Lu, L. Finkenauer, J. Wissman, and C. Majidi, "Rapid prototyping for soft-matter electronics," *Advanced Functional Materials*, vol. 24, no. 22, pp. 3351–3356, 2014.

[67] Y. Zheng, Z.-Z. He, J. Yang, and J. Liu, "Personal electronics printing via tapping mode composite liquid metal ink delivery and adhesion mechanism," *Scientific reports*, vol. 4, p. 4588, 2014.

[68] A. Tabatabai, A. Fassler, C. Usiak, and C. Majidi, "Liquid-phase gallium–indium alloy electronics with microcontact printing," *Langmuir*, vol. 29, no. 20, pp. 6194–6200, 2013.

[69] A. F. Silva, H. Paisana, T. Fernandes, J. Góis, A. Serra, J. F. Coelho, A. T. de Almeida, C. Majidi, and M. Tavakoli, "High resolution soft and stretchable circuits with pva/liquid-metal mediated printing," *Advanced Materials Technologies*, p. 2000343, 2020.

[70] C. W. Park, Y. G. Moon, H. Seong, S. W. Jung, J.-Y. Oh, B. S. Na, N.-M. Park, S. S. Lee, S. G. Im, and J. B. Koo, "Photolithography-based patterning

of liquid metal interconnects for monolithically integrated stretchable circuits," *ACS applied materials & interfaces*, vol. 8, no. 24, pp. 15459–15465, 2016.

[71] A. Fassler and C. Majidi, "3d structures of liquid-phase gain alloy embedded in pdms with freeze casting," *Lab on a Chip*, vol. 13, no. 22, pp. 4442–4450, 2013.

[72] R. K. Kramer, C. Majidi, and R. J. Wood, "Masked deposition of gallium-indium alloys for liquid-embedded elastomer conductors," *Advanced functional materials*, vol. 23, no. 42, pp. 5292–5296, 2013.

[73] N. B. Jaafar and R. Damalerio, "Challenges of wirebonding with polyimide flexible printed circuit board (fpcb)," in *2017 IEEE 19th Electronics Packaging Technology Conference (EPTC)*, pp. 1–5, IEEE, 2017.

[74] V. Dixit, H. Davis, and M. Clark, "Wire bonding considerations: Design tips for performance and reliability," *Advanced Packaging*, vol. 15, no. 6, p. 28, 2006.

[75] P. Elenius and L. Levine, "Comparing flip-chip and wire-bond interconnection technologies," *Chip Scale Review*, vol. 4, no. 6, 2000.

[76] T. Loher, R. Vieroth, M. Seckel, A. Ostmann, and H. Reichl, "Stretchable electronic systems for wearable and textile applications," in *2008 IEEE 9th VLSI Packaging Workshop of Japan*, pp. 9–12, IEEE, 2008.

[77] "3D Insider electrically conductive adhesives: What it is and where to buy." `https://3dinsider.com/electrically-conductive-adhesives/`. Accessed: 2020-08-21.

[78] J. Vanfleteren, M. Gonzalez, F. Bossuyt, Y.-Y. Hsu, T. Vervust, I. De Wolf, and M. Jablonski, "Printed circuit board technology inspired stretchable circuits," *MRS bulletin*, vol. 37, no. 3, pp. 254–260, 2012.

[79] S. Cheng and Z. Wu, "Microfluidic stretchable rf electronics," *Lab on a Chip*, vol. 10, no. 23, pp. 3227–3234, 2010.

[80] A. Robinson, A. Aziz, Q. Liu, Z. Suo, and S. Lacour, "Hybrid stretchable circuits on silicone substrate," *Journal of Applied Physics*, vol. 115, no. 14, p. 143511, 2014.

[81] X. Hu, P. Krull, B. De Graff, K. Dowling, J. A. Rogers, and W. J. Arora, "Stretchable inorganic-semiconductor electronic systems," *Advanced Materials*, vol. 23, no. 26, pp. 2933–2936, 2011.

[82] B. Zhang, Q. Dong, C. E. Korman, Z. Li, and M. E. Zaghloul, "Flexible packaging of solid-state integrated circuit chips with elastomeric microfluidics," *Scientific reports*, vol. 3, p. 1098, 2013.

[83] Q. Wang, Y. Yu, J. Yang, and J. Liu, "Fast fabrication of flexible functional circuits based on liquid metal dual-trans printing," *Advanced Materials*, vol. 27, no. 44, pp. 7109–7116, 2015.

[84] K. B. Ozutemiz, J. Wissman, O. B. Ozdoganlar, and C. Majidi, "Egain–metal interfacing for liquid metal circuitry and microelectronics integration," *Advanced Materials Interfaces*, vol. 5, no. 10, p. 1701596, 2018.

[85] M. Tavakoli, H. Paisana, A. T. De Almeida, and C. Majidi, "Liquid metal fusion with conductive inks and pastes," July 9 2020. US Patent App. 16/647,083.

[86] W. Zhang and Y. Xu, *Mechanical Properties of Polycarbonate: Experiment and Modeling for Aeronautical and Aerospace Applications.* Elsevier, 2019.

[87] A. International, "Standard test methods for vulcanized rubber and thermoplastic elastomers-tension," 2008.

[88] M. Tavakoli, M. H. Malakooti, H. Paisana, Y. Ohm, D. Green Marques, P. Alhais Lopes, A. P. Piedade, A. T. de Almeida, and C. Majidi, "Egain-assisted room-temperature sintering of silver nanoparticles for stretchable, inkjet-printed, thin-film electronics," *Advanced Materials*, vol. 30, no. 29, p. 1801852, 2018.

[89] A. Eberle, S. Mikula, R. Schalek, J. Lichtman, M. K. Tate, and D. Zeidler, "High-resolution, high-throughput imaging with a multibeam scanning electron microscope," *Journal of microscopy*, vol. 259, no. 2, pp. 114–120, 2015.

[90] P. Ghioca, L. Iancu, B. Spurcaciu, R. M. Grigorescu, A.-R. Gabor, and C.-A. Nicolae, "Accelerated natural aging of styrene-isoprene block-copolymers," *MATERIALE PLASTICE*, vol. 50, no. 3, pp. 188–191, 2013.

[91] S. H. Yoo, C. Cohen, and C.-Y. Hui, "Mechanical and swelling properties of pdms interpenetrating polymer networks," *Polymer*, vol. 47, no. 17, pp. 6226–6235, 2006.